KfK 3180 B
Juni 1981

The Basic Concept of the SNQ Linear Accelerator

Editor: J. E. Vetter
Institut für Kernphysik
Projekt Spallations-Neutronenquelle

Kernforschungszentrum Karlsruhe

KERNFORSCHUNGSZENTRUM KARLSRUHE
Institut für Kernphysik

Projekt Spallations-Neutronenquelle

KfK 3180 B

The Basic Concept of the SNQ Linear Accelerator

Translation from the SNQ project study, prepared in collaboration of the nuclear research centers of Jülich and Karlsruhe

J. E. Vetter

Editor

Kernforschungszentrum Karlsruhe GmbH, Karlsruhe

Kernforschungszentrum Karlsruhe GmbH
ISSN 0303-4003

Das Konzept des Linearbeschleunigers für die Spallations-Neutronenquelle (SNQ)

Zusammenfassung

Der vorliegende Bericht ist eine Übersetzung eines Auszugs aus der SNQ-Realisierungsstudie. In ihm sind die wissenschaftlich-technischen Grundlagen zusammengefaßt, die den Entwurf des Beschleunigers begründen.

Abstract

This report is a translation of an excerpt from the SNQ project study. Basic considerations are summarized, which justify the design of the linear accelerator.

Foreword

The SNQ study report will be issued in June 1981. It will consist of 3 parts. Part I is a project summary with emphasis on the scientific motivation. Part II contains the scientific and technical basis of the project. Detailed technical information can be found in the laboratory notes compiled as part III. The following contributions are an excerpt of part II. It is intended, to explain design aspects and choice of parameters rather than discussing the aspects of engineering, construction and operation which are contained in chapter B of part II.

References in this report include internal notes from laboratories, which have participated to the SNQ-study. In case of unclear copyrights, these references were designated as unpublished reports or as private communications.

Within the SNQ cooperation, the accelerator design was worked out by the KfK linear accelerator development group. We are grateful to our consultants and guests, especially from CERN, CRNL, GSI and LANL and from industry for their valuable contributions. The proposal was prepared by members of the KfK-staff, whose work and cooperation is thankfully acknowledged.

Our readers are cordially invited to comment on the proposed design and to contact the authors or the editor for information from the parts of the proposal which could not yet be translated.

J.E. Vetter
KfK, April 1981

KfK LINAC GROUP

K. Bongardt+
P. Budig
G. Dammertz
P. Grundel
R. Hietschold
G. Hochschild
M. Hochstrate
A. Hornung+
W. Kühn
R. Lehmann
K. Mittag
N. Münch
H. Oppermann
M. Pabst+
G. Redemann
D. Sanitz
P. Schlick
D. Schulze
H. Schweickert
J.E. Vetter

+ University of Karlsruhe

Consultants and guests

E. Boltezar / CERN
K. Goebel / CERN
D. Warner / CERN
M. Weiß / CERN
S. Schriber / CRNL
M. Shubaly / CRNL
K. Crandall / LASL
H. Hereward
G. Schaffer

Contents

Contents

A 1 The Linear Accelerator

1.1 Basic Concept

1.1.1 Requirements and Discussion of Main Parameters

The Spallation Neutron Source (SNQ), under study in W.-Germany, is proposed as an intense source of slow (meV) neutrons. Neutron fluxes are produced by spallation of high energy protons on a heavy metal target and subsequent moderation. Peak fluxes, more than one order of magnitude higher than in high flux reactors are the essential advantage of the SNQ; these fluxes can be generated with a time structure optimized to the needs of the experiments.

Concerning the requirements of high time average and peak neutron fluxes (7×10^{14} / cm^2s and $> 10^{16}$ / cm^2s thermal neutron flux) an rf-linear accelerator is considered as the only practicable source of high energy protons.

Synchrotons are unable to produce beam currents of at least several mA time averaged. Cyclotrons are, in principle, capable of accelerating the time averaged currents required, but not the peak currents. For the purpose discussed here, induction linacs seem feasible, but will still need fundamental development.

Requirements for the main application, neutron scattering research with slow neutrons, are listed in table A 1.1-1. The parameters chosen for the linac will be briefly outlined below, a more detailed discussion can be found in the following chapters.

	requirements	parameters chosen	options
particles	p, H^-	p	H^-
output energies	350 MeV, 1 GeV	350 MeV, 1.1 GeV	
beam current			
- time average	5 mA	5 mA	10 mA
- peak	the highest possible	100 mA	
time structure			
- beam pulse duration	500 µs	500 µs	1 ms
- repetition frequency	100 Hz	single pulses to 100 Hz	

Table A 1.1-1: Requirements and parameters chosen for the SNQ-Linac

Protons were chosen as particles to be accelerated. Operation with H^--ions was considered, but was rejected for immediate realization, as ion sources of the required intensity are not available at present. Acceleration of H^- has the difficulty of stripping in residual gas and high magnetic fields. The layout chosen does take into account H^--operation at a later time. Deuterons were proposed in studies for electro-breeders. They offer up to 30 % higher neutron production yields compared to protons /1/. As deuterons activate accelerator components from very low energies on (d-d-reaction), the final choice was made in favour of protons.

From the linac point of view, the final energy is a question of length and cost. The high energy part of the accelerator consists of modules of nearly identical geometry. No new effects or technical problems are encountered with higher linac energy within the range discussed here (600 to 1200 MeV). With the output energy of 1100 MeV chosen, the linac pulses can be further increased in peak intensity by an optional compressor ring /2/. The choice of a high proton energy was supported by target considerations.

A time average beam current of 5 mA (option 10 mA) was required to produce a neutron flux comparable to a high flux reactor.

For the majority of scattering experiments with thermal neutrons, proton beam pulses of 500 µs duration and a repetition frequency of 100 Hz are the optimum compromise. As a result, the peak current of the proton pulse is $\hat{I}$ = 100 mA. Pulse currents are a critical quantity for an rf-linac. The higher $\hat{I}$, the more beam dynamics and rf parameters are influenced by beam loading and space charge effects.

As discussed in A 1.2, space charge forces have to be considered in the choice of injection energies and operation frequencies of the rf accelerator and in the design of components for beam optics. Taking into account possible beam loss and cosidering further the difficulty to produce the high pulse power, the peak beam current was limited to 100 mA.

A linear accelerator with the properties mentioned, is a powerful source of protons, fast neutrons, mesons and neutrinos. The proton beam can be split by fast switching and sent into different target areas. The time structure of the beam fragments can be chosen according to the experiments in the respective area (see ch. A 1.5).

machine/ laboratory	particle	final energy/ MeV	peak beam current/mA	duty factor of the beam	status
new Linac CERN	p	50	150	10^{-4}	operat.
p-Linac, FNAL	p H^-	200	300 46	10^{-4} 10^{-3}	operat.
LAMPF, LANL	p, H^-	800	12, 0.1	6...12 %	operat.
Unilac, GSI	schwere Ionen	10 MeV/ Nukleon	µ A	25 %	operat.
FMIT,HEDL/ LANL	d	40	100	100 %	conc. design, proto-typing
Electro-breeder, CRNL	p	1000	300	100 %	study, proto-typing
Proton Linac, New England Nuclear	p	45	60	10 %	constr.
SNQ-Linac	p (H^-)	1100	100	5 (10) %	study

Table A 1.1-2: Linear Accelerators with high Intensities or high Duty Factors as compared to the SNQ-Linac

1.1.2 Experience, State of the Art

Proton linear accelerators have been built since about 15 years all over the world as injectors for synchrotrons. These machines, two examples are listed in table A 1.1-2, accelerate high peak beam currents to energies of up to 200 MeV. Beam pulses of several hundred μs duration and intensities up to 300 mA were demonstrated and correspond to the requirements of the SNQ. The repitition frequency is, however, limited in these machines as the following synchrotrons operate in slow cycles of typically 1 Hz.

Routine operation of these facilities demonstrates that production and transport of particle beams with strong space charge influence is within current practice. Design principles and methods of calculation have been applied to the SNQ design. Although, the average beam current and hence the average beam power are comparatively small in these injector machines.

In the early fifties proton and deuteron beams of 50 mA cm current had been accelerated to several MeV with the aim to develop an electro-breeder at Livermore, USA /3/. Several designs were recently worked out for linear accelerators with high time averaged beam currents. These efforts were stimulated by growing interest in applications for isotope production, materials irradiation, electro-breeding, and inertial confinement fusion with heavy ions. Prototype work is done at present for electro-breeding and inertial fusion. Beam currents of several hundred mA are proposed for accelerator breeders. Design and component tests for the FMIT accelerator are in an advanced state /4/. FMIT is an accelerator-based intense neutron source for irradiation of materials relevant for fusion. 100 mA of deuterons are accelerated to 40 MeV by the FMIT-linac. Another linear accelerator is under construction for commercial isotope production /5/. 5 mA of average proton current and a final energy of 45 MeV are specified for this project. In all accelerators mentioned so far, the particles are accelerated to their final energy by an Alvarez structure.

At energies higher than $\sim$ 100 MeV the Alvarez structure can be replaced by more efficient types of structure. Multi-stage accelerators are state of the art as e.g. demonstrated by the GSI-linac "Unilac". This machine is a further example of high duty factor operation (25 %). Cavity loss at reasonable field strengths and at a duty cycle of 10 %, as proposed for the SNQ, is therefore not considered as a major problem.

Among the existing accelerators, the LAMPF machine, in operation at LANL, Los Alamos, USA, offers most of applicable experience for this study. Proton beam currents of 1.1 mA average, 12 mA peak can be accelerated to 800 MeV. Compared to LAMPF, the following conclusion can be drawn for the SNQ:

- The final energy of the SNQ is only modestly higher.

- The SNQ peak beam intensity is higher by a factor of 8, the average intensity is increased by a factor of 5.

- The duty cycle is comparable.

The LAMPF accelerator has been developed to a very reliable machine. Initial problems with beam handling and -loss and beam power loading are understood and widely managed /6/. Experience gained in development of operation of LAMPF could be favourably applied to the SNQ design.

It can be therefore concluded from comparison with existing facilities that the SNQ requirements correspond to the state of the art in accelerator development.

1.1.3 Design Aspects

Linear accelerators are built out of a large quantity of components in a serial arrangement. High reliability of the single component is mandatory to obtain a high availability of the overall system. The SNQ-linac is scheduled for 6000 h of operation per year, i.e. 68 % of the total time.

Components should be built within the state of the art, development should be restricted to such cases where essential improvements of function or considerable savings can be made. This applies to the klystrons, the accelerator structure in the high energy part and to the fast kicker systems. The availability can be increased by careful inspection procedures, early recognition of developing defects and preventive replacement within scheduled service periods. Even in very complex accelerator systems, as e.g. CERN or FNAL, operation time exceeds 90 % of scheduled time, which proves, that very high availability can be obtained.

Operating personnel has to be protected from hazards by either spontaneous radiation or remanent activity. In addition, machine components have to be protected against impact of beam energy and excessive radiation. These considerations have strongly influenced the design of buildings, cooling circuits, air conditioning systems and controls, as reported elsewhere in this study /7/.

Beam spill was considered as the highest possible risk for operation of the accelerator. Excessive beam loss may cause local heating at low energies, where the proton range is short. At higher energies, secondary radiation is produced, which requires extensive shielding, in particular against fast neutrons. Permanent radiation will activate machine components, radiation damage has to be minimized by proper choice of materials. Among these effects, remanent activity merits particular attention.

The activity produced in air and water is short lived and can be handled easily, whereas isotopes, building up in copper and steel, have long lifetimes. Service and repair can be difficult, if no provisions were made in the design to cope with this situation.

Beam loss can be of different origin. The values of geometry, accelerating field strengths and focusing fields can be predicted with uncertainties, machining and mounting tolerances will add to these deviations. Most errors can be cured in a particular start-up program without and with beam. This procedure will require special instrumentation (see ch. A 1.3).

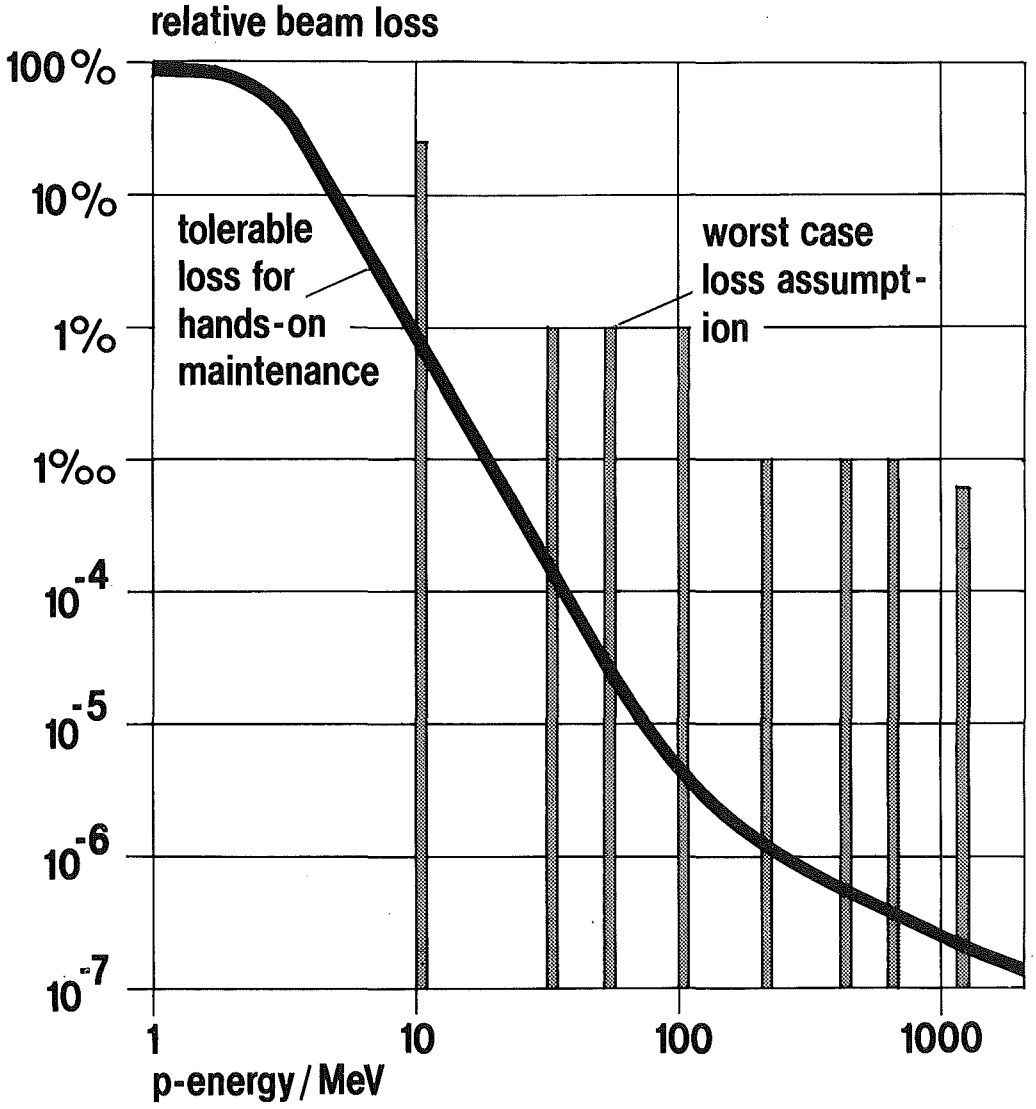

Fig. A 1.1-1: Tolerable beam loss per m length of the accelerator to maintain unlimited access to the machine after shut down are shown as the curve. For the design of buildings and utilities as well as for the choice of materials, higher losses were assumed. As a worst case assumption, point sources were placed at the upper end of an energy interval, as shown above.

Dynamic deviations from preset values are corrected by control mechanisms or by adjustment within periodically repeated test phases.

Particular attention is required for stabilization of amplitude and phase of the rf-field in the accelerator sections. It was shown in measurements at the CERN new linac, that transient effects from beam loading contribute to beam loss. These can be reduced by the control system proposed in ch. A 1.7.

The beam loss, which can be expected, can be roughly estimated from experience: Beam loss in the LAMPF-linac allows for unlimited access to the accelerator after shut down, including the high energy part. Peak and average currents of SNQ are higher by a factor of 6 to 8 compared to LAMPF. With the experience accessible today, and making use of important improvements in methods of calculation and experimental techniques, it can be expected, that operation conditions as favourable as at LAMPF can be obtained.

For the design of the SNQ accelerator, however, higher losses were anticipated. Loss assumptions are shown in fig. A 1.1-1 together with the limit for hands-on-maintenance. Design of buildings, layout of shielding, choice of materials, maintenace concept and design of utilities were based on these assumptions /8/. Local shielding and handling equipment will be installed only if required. It adds only a few percent on the accelerator cost.

Economic arguments play an important role in the design of a large accelerator system. Part of these arguments hold for linacs in general. The energy gain per meter of accelerator length, for example, is chosen by optimizing capital and operation costs (fig. A 1.1-2).

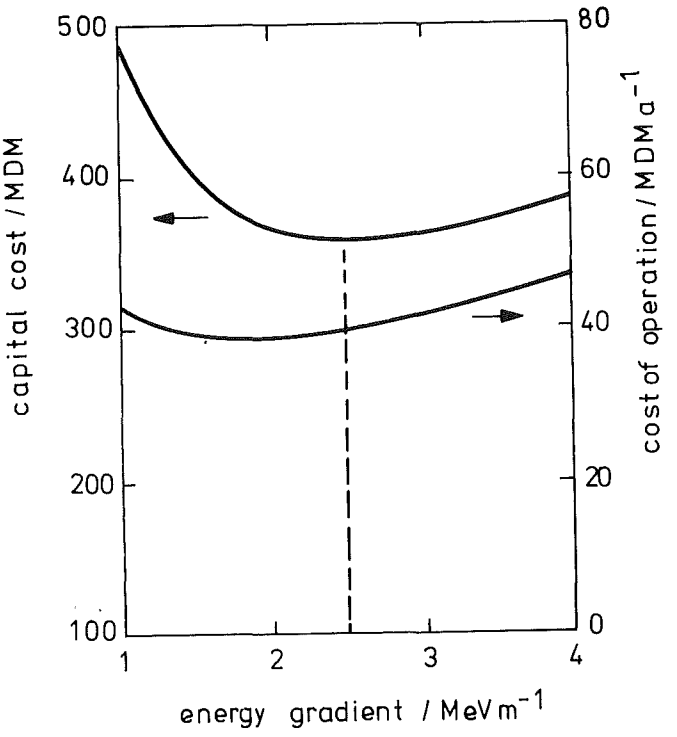

Fig. A 1.1-2: Capital and operation cost for the DAW-accelerator as function of the energy gradient (energy gain per m of technical length, including the intertank spaces). The gradient chosen is 2.5 MeV/m.

Operation cost consists of expenditures for repair and maintenance, salaries and electrical power. Only a weak dependence on the gradient is seen. An upper limit for the gradient due to sparking in the resonators should be taken into account. A peak field of 18 MV/m was therefore assumed for the design which corresponds to 2.5 MeV/m average acceleration rate, sufficiently close to the economical optimum.

In an accelerator with a beam power of many MW, particular attention has to be paid to minimize power consumption in various parts of the machine. Power flow is shown in fig. A 1.1-3. One quarter of the mains power is consumed by injection, beam transport, instrumentation, air conditioning and cooling installations.

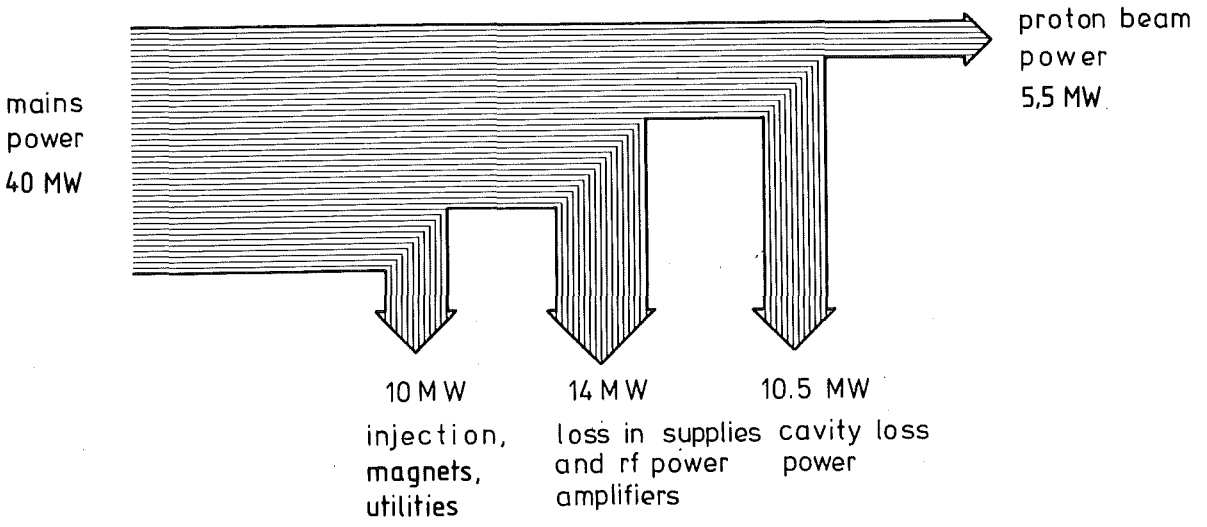

Fig. A 1.1-3: Power flow in the SNQ-linac

About 30 MW are transfered to the power supplies of the rf-system. The conversion efficiency of dc- into rf-power was optimized in the design by choice of high efficiency klystrons and appropriate modulation systems (see ch. A 1.7).

A major fraction of the power fed into the accelerator sections is spent as wall losses. A high shunt impedance is therefore required. This argument is important for the choice of accelerating structures, operation frequencies and the energy of transition into a high velocity structure (see ch. A 1.5).

The linear accelerator consists of injection, Alvarez- and Disk-and-Washer-accelerator parts and the high energy beam transport. Proton current is extracted from a pulsed magnetic multipole ion source and preaccelerated to an energy of 450 KeV. Beam pulses are formed precisely by an ultrafast chopper system (<10 ns rise-time) and transverse emittance is limited in the low energy beam transport. Microstructure, as required for rf acceleration, is formed by a 3-gap buncher system.

About 85 % of the particles injected are accelerated in the Alvarez structure to a final energy of 105 MeV. Operation frequency of the Alvarez part amounts to 108 MHz. Rf power is generated by 14 tetrode amplifiers, each delivering 1.75 MW of peak power. Beam properties are measured and beam parameters are matched in the beam matching setion preceding the high energy part of the accelerator. 57 tanks of Disk-and-Washer structure accelerate the beam to the final energy of 1100 MeV. Tanks are separated by intermediate sections containing a quadrupole doublet for transverse focusing and, where required, beam diagnostics and steering elements. A total number of 89 pulse power klystron amplifiers of 3.75 MW saturation power each are installed to feed the necessary rf power into the structures at a frequency of 324 MHz, three times the Alvarez frequency.

The main beam is guided to the neutron target. Fractions of the beam can be switched into separate target areas at 350 and 1100 MeV for nuclear physics and medicine experiments. Future addition of a compressor ring is considered in the design, further up-grading or completion can be planned in prolongation of the accelerator axis.

Only part of the rf-pulse can be used for beam acceleration. During build-up time of the accelerating fields, "waste power" is spent. The design of the rf-system took care of optimizing the filling procedure and to stabilize the accelerating fields in phase and amplitude during the beam pulse (ch. A 1.7).

Description of the Concept chosen

The following description of the concept chosen shall facilitate the understanding of the following chapters. A more complete description is contained elsewhere in the study (chapter B), parameters are compiled in A 1.8.

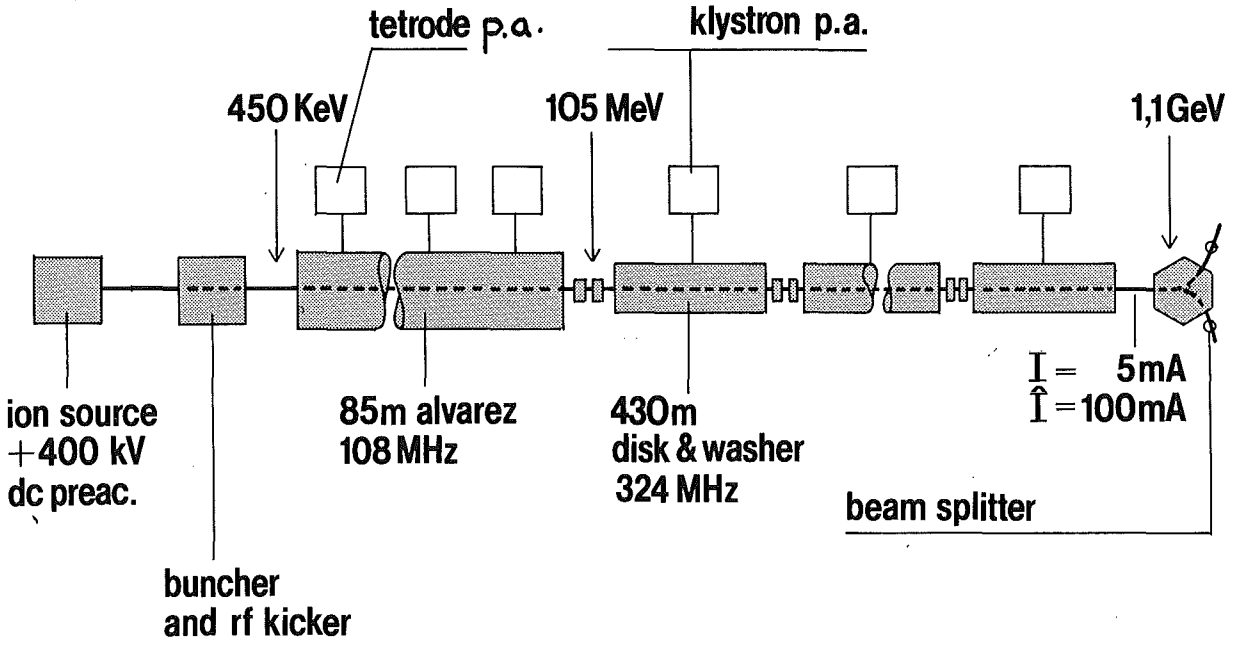

Fig. A 1.1-4: Principle Arrangement of the SNQ-linac

References

/1/ C.M. van Atta, J.D. Lee, W. Heckrotte: "The Electronuclear Conversion of Fertile to Fissile Material", UCRL-52144, Lawrence Livermore Lab., Oct. 11, 1976

/2/ The SNQ project study report, Part II, ch. D, KFA Jülich - KfK Karlsruhe, June 1981, unpublished

/3/ C.M. van Atta: "A Brief History of the MTA Project, in Proc. an Information Meeting on Accelerator-Breeding", BNL, Jan. 18, 1977, CONF-770107, p. 9

/4/ Proc. of the 1979 Linear Accelerator Conference, Brookhaven, BNL 51 134, p. 21-24

/5/ ibid., p. 32-36

/6/ ibid., p. 78-82

/7/ The SNQ project study report, Part II, ch. B, KFA Jülich - KfK Karlsruhe, June 1981, unpublished

/8/ K. Goebel: "Strahlenschutzprobleme beim Betrieb eines Hochstrom-linearbeschleunigers", Kernforschungszentrum Karlsruhe, 1980, unpublished report

/9/ J.E. Vetter: "Optimierung des Energiegewinns im DAW-Beschleuniger nach Kostengesichtspunkten", SNQ project study report, Part III, Volume A1, KFA Jülich - KfK Karlsruhe, June 1981, unpublished

Contents

A 1.2 Beam Dynamics

1.2 Beam Dynamics

1.2.1 Introduction

In a linear accelerator a radiofrequency wave is generated whose electric field is mainly in the direction of the accelerator axis. The wave velocity is chosen to be equal to the average velocity of the particles to be accelerated. The fictitious particle moving with this velocity is called the synchronous particle. The difference between the rf phase of the synchronous particle and the phase of the maximum of the rf wave is the synchronous phase. It is chosen such that particles trailing the synchronous particle experience a higher accelerating field, hence their velocity increases relatively faster. They overtake the synchronous particle, and are then effected by a relatively smaller accelerating field. In this manner the longitudinal phase oscillations develop: the accelerating electric wave focuses the protons longitudinally towards the synchronous phase. So the proton bunch (micropulse) is kept longitudinally together. This longitudinal focusing force is linear in first approximation. The bunches follow one another at the Alvarez frequency. Ideally there are no protons in between the bunches. For the SNQ a macropulse consists of about 10^5 micropulses.

Also the transverse bunch extension is finite. The accelerating electric wave has a radial component off axis, increasing approximately linearly with distance from the axis. For phase stable longitudinal acceleration this radial rf force is always defocusing, and has to be counteracted by focusing external forces. In the Alvarez accelerator this is achieved by magnetic quadrupole lenses in the drift tubes. Their action is "strong focusing" in both transverse directions by having alternating polarities in consecutive quadrupoles. In the disk-and-washer accelerator magnetic quadrupole doublets are installed between the accelerator tanks for transverse focusing. An important parameter of a periodic focusing system is the tune. It measures what fraction of an oscillation a particle experiences in a single focusing period. The square of the tune is approximately proportional to the algebraic sum of the gradients of all focusing and defocusing forces averaged over a focusing period.

Focusing is necessary even without the action of defocusing forces, since all particles in the bunch move on different trajectories, as the bunch has a finite emittance. The phase volume spanned by the three space and the three momentum coordinates of all particles always has a finite size. The projections on the two-dimensional space-momentum phase spaces are constants of the motion, if coupling between them can be neglected. The normalized emittances are proportional to these projections (e.g. $E_{xn} = \pi\beta\gamma\Delta x\Delta x'$ with β = proton velocity/light velocity, γ = relativistic mass/rest mass, Δx = space, and $\Delta x'$ = angle deviation).

At high beam current the Coulomb repulsion between the protons has to be included in the balance of focusing and defocusing forces. A major problem is the determination of the density distribution of the protons inside the bunch, since also the six-dimensional phase space distribution is not known exactly. Normally measurements can only reveal two-dimensional projections. Self consistent solutions of the differential equation for the distribution function (Vlasov-equation) are possible only for special cases. Hence the treatment of the space charge forces has to be based on models which are supported by theoretical calculations, as well as by emittance measurements on real beams. In this connection the concept of the rms- (root mean square) emittance is of importance. It is obtained by a proper quadratic average of the phase space coordinates of all particles, and describes the behavior of the bunch kernel. It was shown both theoretically /1/ and experimentally /2/ that beam dynamics calculations including space charge forces based on the rms-emittance concept yield results that are nearly independent of the actual phase space distribution.

During acceleration the transverse dimensions of the bunch remain constant in first approximation. Tne geometrical bunch length slowly increases. On the other hand, the proton velocity increases relatively faster, such that the bunch time extent measured in rf phase width decreases rapidly. This longitudinal phase damping allows the transition in operating frequencies between the Alvarez- and the disk-and-washer accelerator.

In the following paragraphs the accelerator design is discussed from the beam dynamics standpoint. In comparison to the existing proton linear

accelerators the SNQ linac has a high average beam current. Beam spill can cause unwanted activation especially in the high energy part of the machine. Hence the major guide line for the parameter choice was to minimize paricle loss at high energies.

1.2.2 Choice of the Beam Current, the Injection Energies and the Operating Frequencies for the Alvarez- and the Disk-and-Washer Accelerators

The choice of the parameters beam current, operating frequencies, and injection energies is influenced by numerous different arguments concerning injection, beam dynamics, accelerating structures, and rf engineering, which are summarized in this section. Although these parameters are correlated they will be treated one after the other for clarity.

Peak beam current

The peak beam current (beam current averaged over a macropulse) has been fixed to 100 mA. It should be as high as possible for the majority of the neutron experiments. The accelerator efficiency rises with the peak beam current, as the power delivered to the beam increases relatively to the fixed rf losses in the accelerator. On the other hand the installation of additional rf pulsed power requires further investments for the rf sources.

For peak beam currents of much more than 100 mA the beam dynamics in the Alvarez accelerator would be dominated by the space charge forces which are known only approximately. Theoretical predictions would become uncertain. The beam matching between consecutative accelerator sections would depend sensitively on the real density distribution in the bunch especially at low energies. Resulting beam mismatches could cause large emittance increases, and consequently also higher beam loss. The longitudinal acceptance would decrease towards zero, the phase focusing would become highly non-linear /3/. The consequence would be a large longitudinal emittance increase, a reduced longitudinal phase damping resulting in increased proton losses after the transition to the disk-and-washer

accelerator. Further, the probability would increase for transverse emittance growth due to parametric space charge instabilities, and due to space charge induced coupling between the longitudinal and the transverse motion.

Quantitatively the space charge influence on the beam dynamics can be described by space charge factors μ_l and μ_t for each space direction, which are the ratio of space charge force to the sum of the external forces. The space charge factors are shown in Fig. A 1.2-1,2 for 100 mA peak beam current at injection into the Alvarez accelerator as functions of the injection energy, and the normalized transverse emittance lying typically in the 1 to 3 π mm mrad range. The space charge factors increase with the peak beam current, the value of 1 is the stability limit for the particle motion. On the other hand, the focusing forces cannot be increased much above the values on which the figures are based: An increased transverse focusing leads for an 108 MHz Alvarez frequency to parametric instabilities of the transverse motion. At 200 MHz the quadrupole focusing is unsufficient for injection energies smaller than 750 keV, as there is not space in the short drift tubes for strong enough quadrupoles. The longitudinal focusing force is proportional to the accelerating field, hence it is limited by sparking in between the drift tubes.

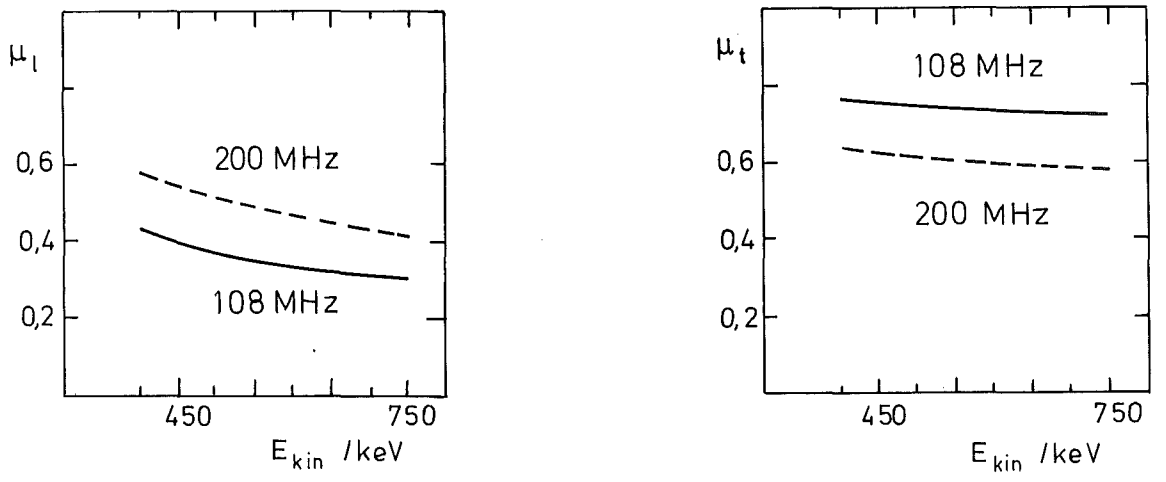

Fig. A 1.2 - 1: Longitudinal (μ_l) and transverse (μ_t) space charge factor as a function of injection energy E_{kin} (normalized emittance here 3 π mm mrad, peak beam current 100 mA; parameter is the Alvarez frequency)

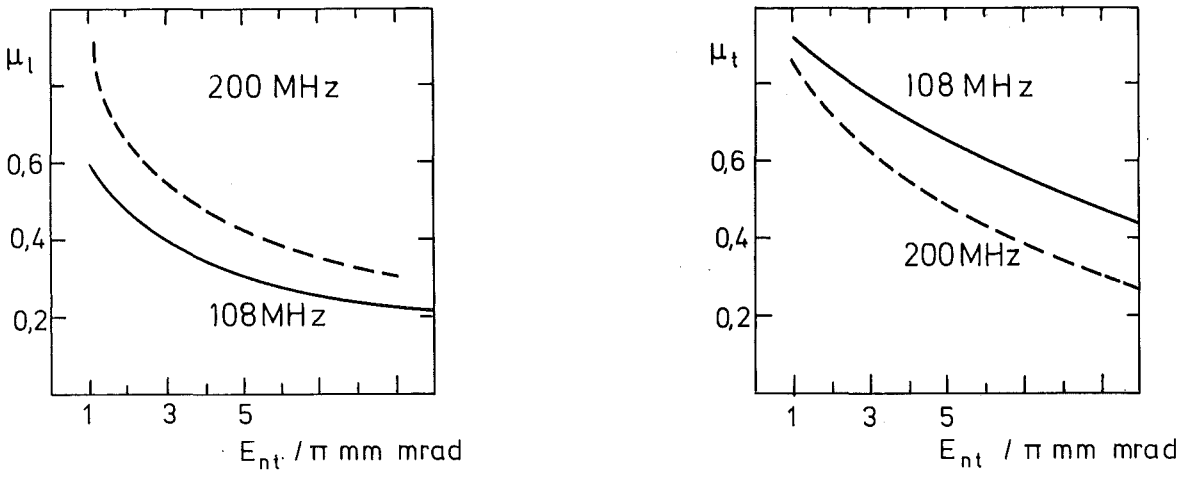

Fig. A 1.2 - 2: Longitudinal (μ_l) and transverse (μ_t) space charge factor as a function of the normalized transverse emittance E_{nt} (injection energy here 500 keV, peak beam current 100 mA; parameter is the Alvarez frequency)

A comparison is given in Tab. A 1.2-1 between the beam current chosen for the SNQ, and beam currents achieved in operating proton linear accelerators. With the 800 MeV-accelerator in Los Alamos a 12 mA peak beam current and a 1.1 mA average beam current is obtained /4/. This is the only existing proton linac in which there is a transition in operating frequency between the Alvarez and the high energy part, and where special attention has to be given to the longitudinal phase damping in the Alvarez part. Other proton machines, as the new CERN-linac or the ones in Brookhaven (BNL) or Argonne (FNAL), achieve between 150 and 300 mA peak beam current at final energies in the 50 to 200 MeV range, but at a comparatively much smaller average beam current. Hence the beam spill problem is much relaxed at these machines.

Summarizing: the choice of 100 mA peak beam current is a good compromise between user demands, feasibility in the near future, and cost arguments; the value chosen does not represent a sharp physical limit. However, a peak beam current increase as an improvement program after realization of the machine is difficult and would require high additional investments especially in rf power sources. Therefore, this proposal has not been considered for further machine options.

Proton linear accelerator	SNQ	LAMPF	FNAL-Linac	BNL-Linac	new CERN-Linac
final energy / MeV					
- Alvarez accelerator	100	100	200	200	50
- high energy accelerator	1100	800	--	--	--
beam current during macropulse / mA	100	12	300[c]	220	150
average beam current / mA	5[a]	1,1[b]	0,046	0,44	0,015
operating frequency / MHz					
- Alvarez accelerator	108	201	201	200	202
- high energy accelerator	324	805	--	--	--
injection energy for the Alvarez accelerator/keV	450	750	750	750	750

a) option: 10 mA, b) the limitation for operation to 0.6 mA results from the capability of the meson target, c) short pulses, at present the machine accelerates H^--ions

Tab. A 1.2 - 1: SNQ-linear accelerator parameters in comparison to similar machines /4,5,6/

Injection energy

The injection energy was chosen to be 450 keV with consideration of the high average beam current in the injector /7/. This choice reflects the state of this technique (see Chap. A 1.4).

A higher injection energy would doubtlessly have been chosen by considering solely beam dynamics arguments. Both the longitudinal and the transverse acceptance get larger with increasing injection energy. This is shown in

Fig. A 1.2-3. Here the longitudinally accepted beam current and the normalized transverse acceptance are plotted as a function of the injection energy. This estimate is based on the analytic formula which assumes constant focusing parameters and velocity, from which there result too small values for the longitudinally accepted beam current and also for the transverse acceptance; however, the parameter dependences obtained are correct.

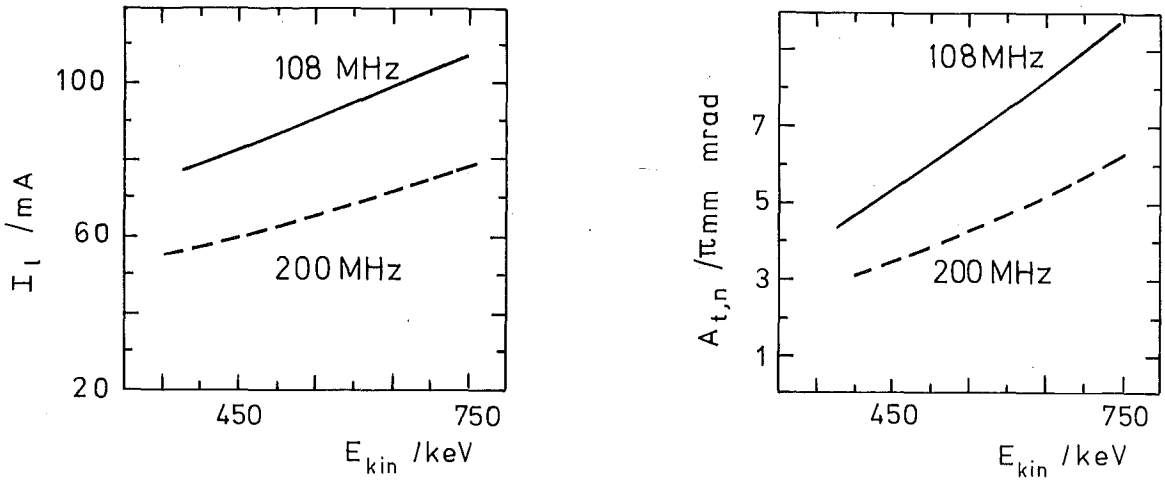

Fig. A 1.2 - 3: Longitudinally accepted beam current I_l and normalized transverse acceptance A_{tn} as a function of the Alvarez injection energy E_{kin} (assumed normalized emittance here 3 π mm mrad; parameter is the Alvarez frequency; analytical estimate, higher beam currents can be accelerated in practice)

The drift tubes and the accelerating gaps at the beginning of the Alvarez accelerator would be a lesser problem at a higher injection energy. Also, the quadrupole strength required for sufficient transverse focusing could realized more easily, especially so for a 200 MHz Alvarez frequency. Further, the coupling decreases between the radial and the longitudinal motion, hence also the associated emittance growth would be less.

The rf quadrupole structure (RFQ) /8/ is studied as an alternative to the dc-preinjector. The proton beam would be injected into the RFQ with only 50 keV energy. The RFQ then takes the protons up to about 2 MeV energy

over about 2 m length. At this injection energy into the Alvarez accelerator the beam dynamics problems are reduced considerably. The rf quadrupole field on the RFQ axis is so shaped that it focuses the beam both transversely and longitudinally, and in addition accelerates the beam. Hence, the RFQ not only replaces the dc injector but also the bunching system. Therefore, it looks very promising. Nevertheless, the described reference concept does not include a RFQ since its development is not finished as yet. Also, the problem of generating gaps in the macropulse with about nanosecond risetime would still have to be solved (see Chap. A 1.6). This could probably not be achieved by a fast kicker system in combination with slots at the 50 keV energy level, as the non-space charge neutralized beam would diverge too much between the deflector and the slot. A fast kicker system after the RFQ would have the disadvantage that the bunches leaving the RFQ would diverge too much both in the longitudinal and in the transverse direction. Further beam optics elements as rebunchers and quadrupoles would be required for a rematching of the beam.

The beam current accepted by the RFQ decreases with increasing frequency; according to present knowledge 100 mA peak beam current can be realized at 108 MHz, but would be difficult at 200 MHz because of larger space charge forces /9/.

Operating frequencies for the Alvarez and the disk-and-washer accelerator

The operating frequency for the Alvarez accelerator (108 MHz) and for the disk-and-washer accelerator were chosen regarding the following arguments /7,10,11/: The investment costs for the rf installation are lower for the chosen frequencies than for the also considered alternative 200 MHz/600 MHz (see Chap. A 1.7). The efficiency of the rf accelerating structures (shunt impedance) increases with frequency; the resulting saving of the total rf power would be about 20 % at a factor of two higher frequency, since a constant part is taken by the beam power. The structure construction cost did not show a strong frequency dependence (see Chap. A 1.5). The handling of the rf tubes, the klystrons, and the accelerating

structures would be easier at a higher frequency because of their smaller size. In total, the smaller investment costs for the rf power installation is the dominating argument.

Next, the problems at the 450 keV injection into the Alvarez accelerator are compared between the 108 MHz and the more common 200 MHz solution. At the higher frequency the lengths and gaps of the first drift tubes would be rather small causing construction problems. The quadrupole gradients achievable with cooled electromagnetic quadrupoles would not be sufficient. Consequently, the transverse particle motion would be too close to the stability limit resulting in a strong transverse emittance growth due to the phase dependence of the rf defocusing force. Permanent quadrupoles generate large enough gradients; however, just at the beginning of the accelerator the quadrupoles should have changeable gradients to achieve an optimum matching between the buncher system and the Alvarez accelerator during operation.

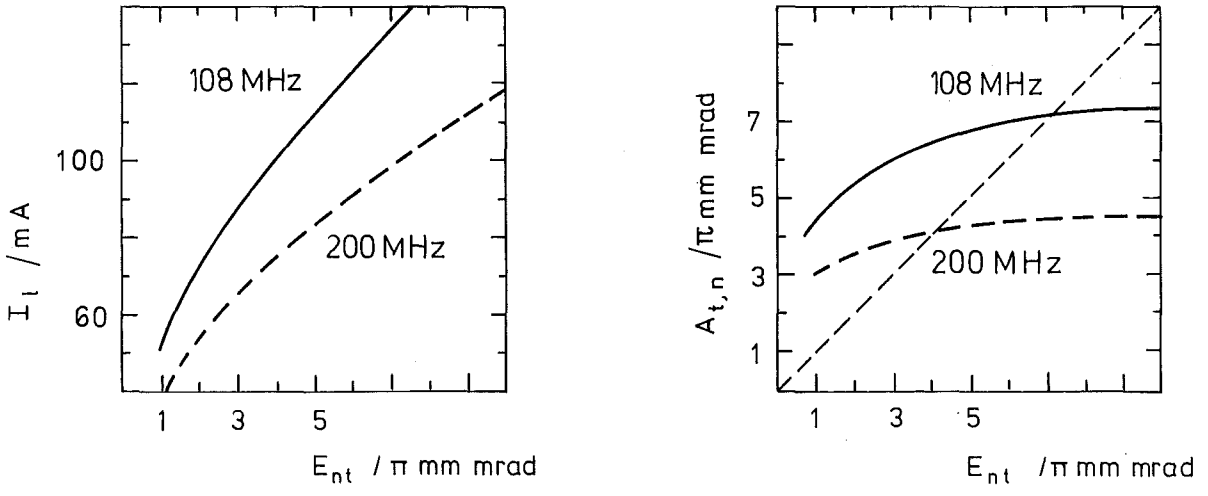

Fig. A 1.2 - 4: Longitudinally accepted beam current I_l and normalized transverse acceptance A_{tn} as a function of the normalized transverse emittance E_{tn} (assumed injection energy here 500 keV; parameter is the Alvarez frequency; analytical estimate, higher beam currents can be accelerated in practice)

The longitudinal and transverse acceptances are more favourable at the lower frequency (Fig. A 1.2-3,4), and the influence of the longitudinal space charge force is smaller (Fig. A 1.2-1,2). The latter is also true for the bunching system, which would be more difficult to realize at 450 keV and 200 MHz /10/. On the other hand, the transverse space charge forces are more severe at the smaller frequency.

Summarizing: the problems at injection into the Alvarez accelerator are easier to solve at 108 MHz than at 200 MHz. Analytical estimates show that several parameters of a 108 MHz/450 keV solution are similar to those of the more common 200 MHz/750 keV on /10/.

Next the particle motion in the accelerator after the injection is dealt with /7,10,11/. The acceptances both longitudinally and transversely are larger at the smaller frequency. Hence there is more clearance available to accept particles outside the major part of the bunch.

The phase damping is independent of frequency if the accelerating gradient and the synchronous phase are comparable, and if space charge forces can be neglected. The longitudinal space charge forces counteract the phase damping. The longitudinal space charge factor μ_l increases along the Alvarez accelerator, since the longitudinal focusing rf force decreases faster with increasing proton velocity than the longitudinal space charge force. If μ_l approaches the value 1, the nonlinearity of the longitudinal focusing gains in importance: protons trailing the synchronous particle experience only small or even no longitudinal focusing force any more; their phase damping gets smaller than without space charge. This effect is more severe at a higher frequency, for which higher proton beam spill would therefore be expected after the transition to the disk-and-washer accelerator.

Things are different for the transverse particle motion, as the transverse space charge factor μ_t is smaller at the higher frequency. It follows that the difference between the incoherent transverse tune μ (equals the single particle tune) and the coherent tune μ_o (equals the tune of the bunch center e.g. at a transverse beam displacement = single

particle tune without space charge) is larger at the smaller frequency. In order to avoid transverse parametric envelope resonances μ_o has to be chosen smaller than 90° /12/. Transverse instabilities of third order can be excited if $\mu < 60°$ but $\mu_o > 60°$ holds /12,13/. For a 200 MHz Alvarez accelerator one would chose about $\mu = 35°$, resulting in a μ_o close to 60° for 100 mA peak beam current, so that the excitation of this instability would be highly improbable. On the other hand, the 108 MHz SNQ Alvarez accelerator has a $\mu = 40°$ and a μ_o of about 80°, so that the appearance of the third order instability is possible in principle.

Also, the transverse emittance growth caused by the phase dependence of the transverse rf defocusing force is more pronounced at the lower than at the higher frequency /10/. Detailed multiparticle simulations show for the SNQ Alvarez accelerator only small transverse emittance growth and no excitation of instabilities (see below).

In summary: For the Alvarez accelerator the 108 MHz frequency is preferred over that of 200 MHz because of the relatively small 450 keV injection energy. At a 750 keV injection energy or more the advantages would not be so unequivocal. An accelerator of higher frequency is more suitable to produce beams of high transverse brightness /14/. However, an accelerator of a lower frequency can yield a rather higher peak beam current at the expense of a smaller brightness. This statement is the more true if a frequency transition is required between different accelerator parts, as is the case for the SNQ. The reserve in acceptance is larger when lower frequencies are chosen, resulting in smaller beam spill and activation of the accelerator.

Transition energy and frequency ratio between the Alvarez and the disk-and-washer accelerator

The shunt impedance of the Alvarez structure decreases rapidly for proton energies beyond 100 MeV (Chap. A 1.5). Therefore, a transition to an accelerator type more efficient at higher proton velocities has to take place in this energy range. This high energy accelerator could operate at a three to five times higher frequency than the Alvarez accelerator. As

an example, at the LAMPF accelerator the frequency is increased by a factor of 4. At this transition the phase damping in the Alvarez accelerator must have progressed so far that all protons can be longitudinally accepted by the disk-and-washer accelerator. At first, this problem was studied analytically to resolve the parameter dependencies /7,11/. The result is that in the energy ranges from 70 to 100 MeV and from 100 to 200 MeV the phase width decreases by about 10 % each. The phase acceptance decreases with increasing energy due to the more and more dominating longitudinal space charge force relative to the phase focusing. The influence of non-linearities increases as well as the probability of longitudinal emittance growth. Therefore, a 105 MeV transition energy was chosen, at which the shuntimpedances of the Alvarez and disk-and-washer structures are about equal. Besides, 105 MeV conveniently fits a practical solution consisting of seven Alvarez tanks.

The disk-and-washer frequency was chosen to be a factor of three higher than the Alvarez one. To justify this choice the bunch phase width at the Alvarez exit has to be compared with the disk-and-washer phase acceptance. Multiparticle simulations yielded 18^{o} phase width (measured at 108 MHz) at the Alvarez output. Choosing a -30^{o} synchronous phase for the disk-and-washer part its phase acceptance is about 54^{o} at 324 MHz taking space charge effects into account. This corresponds to 18^{o} at 108 MHz which is equal to the bunch phase width. In the case of a factor of four higher frequency the acceptance would be reduced to 13^{o}, for a factor of five to 11^{o} measured again at 108 MHz. Between the two accelerators there is a beam matching section (see below). This contains two rebunchers by which the bunch phase width could be further reduced, and a possible longitudinal emittance growth in the Alvarez part could be dealt with. The transverse acceptance is largest at the smallest frequency. A large acceptance reserve is favourable in any case to be able to also transport the beam halo which develops in the cause of the acceleration. These arguments are supported by cost estimates for the rf installation.

1.2.3 H^--Acceleration

A beam of H^--ions could be accelerated simultaneously with the protons /15/ if they were displaced 180° in phase. A low intensity H^--beam would represent no additional load to the rf sources, and it could be separated from the proton beam by simple bending magnets. In case of a high H^--beam quality this concept would be especially suited to feed nuclear physics experiments e.g. at 350 MeV.

The advantages of increased flexibility for the applications is in contrast to major limitations for the operation. The difficulties start at the funneling section for the two bunches, 180° displaced in phase. The two beams differ considerably in emittance and space charge density. Therefore, they put different requirements to the beam transport, especially also they have different matching parameters. There exists no solution for the longitudinal and transverse matching to the Alvarez accelerator which is optimal for both beams. Further matching difficulties exist between Alvarez tanks, and between the Alvarez and the disk-and-washer accelerator. Additional emittance growth and increased beam spill would be the consequence.

Another problem originates from the fact that steering errors act differently on particles of opposite charge. Steering elements acting independently on both beams would be required in the disk-and-washer accelerator which are difficult to realize. A further difficulty consists in diagnosing the parasitic H^--beam in the presence of the high intensity H^+-one.

Simultaneous acceleration of H^+- and H^--beams has been achieved at LASL. The experience reported indicate major problems: "The general problem of matching simultaneously H^+- and H^--beams is one of the major limitations in machine performance" /16/. It is concluded that for the SNQ project a simultaneous H^+-/H^--acceleration can only be achieved after having gained sufficient operating experience.

On the other hand, it would be feasible to change the operation from H^+- to H^--ions keeping the beam specification. H^--ions offer considerable advantages for the improvement of the SNQ: The beam switching to several targets can be of especially simple design (Chap. A 1.6); H^--beams can more easily be collimated, and hence they can yield a better beam quality. Finally, the injection into an accumulator ring can be achieved by charge exchange (Chap. D 2). However, care has to be taken not to lose the electron weakly bonded to the hydrogen atom by rest gas scattering or by high magnetic fields (Lorentz stripping), because the neutral atom would be lost from the beam causing activation. An accelerator designed to also handle a H^--beam therefore has to allow for good vacuum conditions, and the guiding magnetic fields have to be kept below certain levels. These aspects have been incorporated in the SNQ-design, such that the machine can be switched to H^--operation at a later date.

1.2.4 Low Energy Beam Transport System and Beam Matching to the Alvarez Accelerator

The low energy beam transport system /17,18/ (Fig. A 1.2-5) has to fullfill several tasks: First, the beam has to be transported from the dc-injector to the Alvarez accelerator. Quadrupole triplets produce the required transverse focusing, keeping the beam cross section as circular as possible to minimize space charge effects. A 75 cm drift space lies between the 45 cm long triplets. This choice of spacing has been a compromise between two counteracting design criteria: first, the drift space should be as large as possible to allow for plenty of diagnostic and beam handling equipment; second, the drift space should be as short as possible to yield a small average beam diameter, and thereby obtaining beam optics dominated by finite emittance rather than space charge effects; for the lengths chosen 1/3 of the defocusing stems from the finite emittance, 2/3 from the space charge influence. The average transverse tune of the triplet system is about 20^o, the beam diameter varies between 22 and 4 mm. The transverse beam envelope is sketched in Fig. A 1.2-5.

It is of great importance for a stable and predictable beam transport to exclude uncertainties about the degree of neutralization. This requires a vacuum of

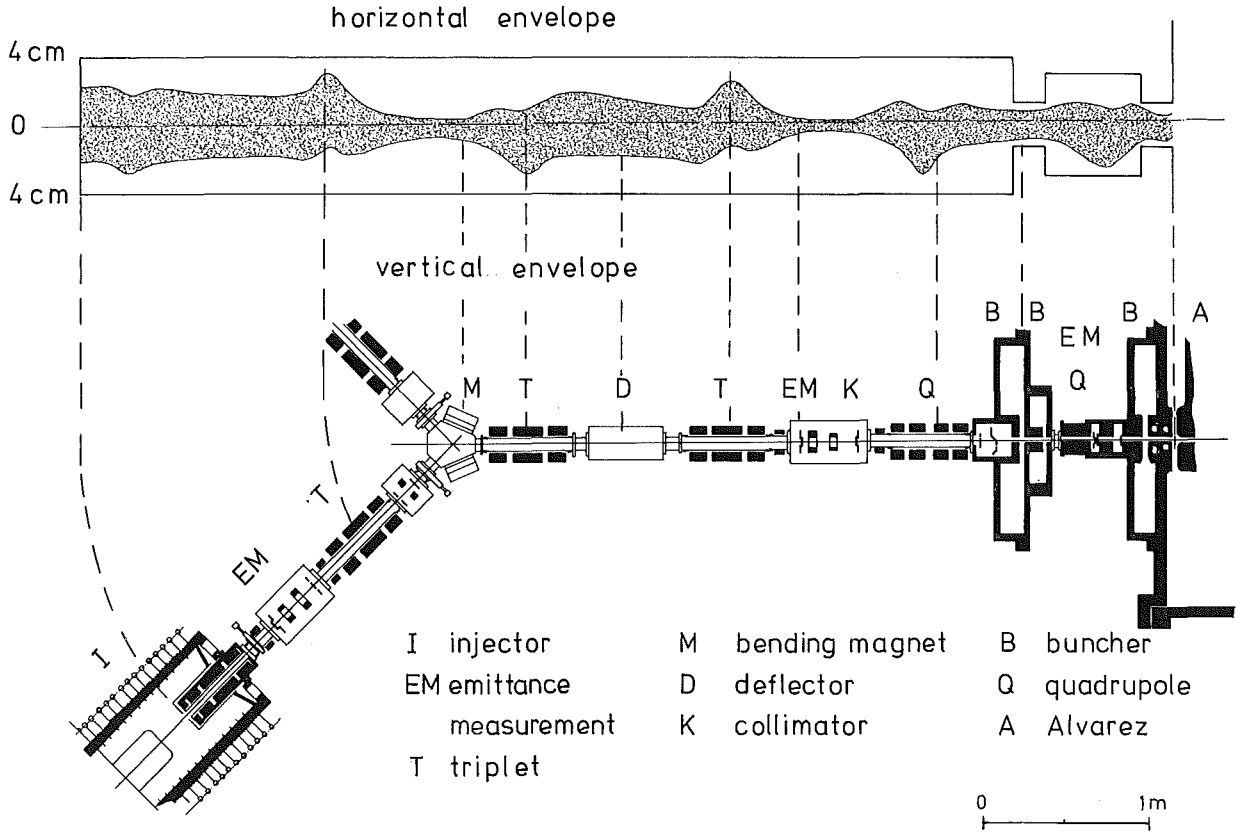

Fig. A 1.2 - 5: Low energy beam transport system

about 10^{-10} bar yielding a neutralisation below 1 % in the 500 µs long macropulse presenting no problem. This vacuum also would be adequate for H^--ions causing a negligible loss rate.

The following elements are positioned between the triplets (Fig. A 1.2-5): The beam switch allows to use either of both injectors. A fast deflector in combination with a slot makes the ends of the macropulse sharp and creates gaps in the macropulse (Chap. A 1.6). Transverse emittance measurement devices exist between the injector and the bending magnet, in front of the buncher system, and between the second and the third buncher. The transverse emittances can be limited by collimators /18,19/. Further elements are beam current monitors, electron traps, and steering magnets to correct the transverse beam position.

Directly in front of the Alvarez accelerator the beam is matched both longitudinally and transversely in about 1 m length. Matching means that for all of the three beam emittances (xx', yy', φ W) the axis ratios, and their directions in the phase spaces have to correspond to the respective acceptance values. Hence there are two parameters to be matched for each space direction. This is achieved by four magnetic quadrupoles for the two transverse directions. The longitudinal beam matching is considerably more complex, as the continuous beam has to be bunched to micropulses: A first 108 MHz buncher produces a velocity modulation on the longitudinal particle distribution, its amplitude being determined by the matching requirements. Shortly thereafter a 216 MHz buncher takes care that the particle distribution in the longitudinal phase space is as homogeneous as possible to minimize space charge effects. The third 108 MHz buncher directly in front of the Alvarez gives an additional energy kick to the particles lying outside the longitudinal acceptance, such that they will be lost at a low energy in the Alvarez accelerator. This is of special importance for a machine with a high average beam current to keep the activation low. The distance between the first buncher and the Alvarez accelerator has been chosen such that the longitudinal focus is about at the first accelerating gap. In front of the third buncher the beam density modulation can be detected by a fast beam monitor.

The design and the calculation of the low energy transport system was guided by a similar one operating successfully at CERN /2,17,18/. The check of the design by the multiparticle simulation code BUNCH predicts a longitudinal trapping efficiency between 82 and 87 % depending on the emittance analysis. The emittances thus calculated are included in Fig. A 1.2-6 (plots at 0.45 MeV).

At the first glance this bunching scheme seems to be rather sophisticated. However, its function as well as its high reliability was proven by operating experience at CERN. Due to the use of computer control its operation presents no special problem despite of the many parameters independently adjustable.

1.2.5 Beam Dynamics in the Alvarez Accelerator

After the bunching system the 450 keV beam is injected into the Alvarez accelerator which takes it up to an energy of 105 MeV. The calculations for the beam dynamics were done using computer codes of CERN origin /20,21/, which were supplemented and further improved. The major parameters for the beam dynamics in the Alvarez accelerator are compiled in Tab. A 1.2-2. In the following sections only those topics are discussed which are of special importance for a high peak and high average beam current linear accelerator. Additional information is collected in the reports /3,7,10,11,13,19,22,23/.

peak beam current/mA	100	
frequency/MHz	108	
energy/MeV	0,45	105
average axial electric field E/MV m^{-1}	2	2
transit time factor T	0,7	0.87
synchron. phase φ_s/°	-35	-35
longitudinal tune/°	28	2,5
transverse tune at 100 mA (μ)/°	40	40
transverse tune at 0 mA (μ_o)/°	83	65
drift tube beam hole diameter/cm	2,8	6,6
100 % beam diameter in the quadrupole/cm	1,8	4,0
95 % beam diameter in the quadrupole/cm	1,4	1,5
rms - beam diameter in the quadrupole/cm	0,6	0,7
100 % normalized transverse emittance/ π mm mrad	3	6
rms - normalized transverse emittance/ π mm mrad	0,6	1,2
100 % phase width/°	150	18
95 % phase width/°	74	11
rms - phase width/°	41	6
100 % energy spread/MeV	0,12	1,4
95 % energy spread/MeV	0,10	0,8
rms - energy spread/MeV	0,05	0,35

Tab. A 1.2-2: Beam dynamics parameters of the Alvarez accelerator (results of multiparticle simulation, only accepted particles taken into account)

The drift tube beam hole diameter and the ratio of accelerating gap length to cell length was chosen such that the transit time factor T is larger than 0.7 all over the Alvarez. A smaller factor would result in a too low accelerator efficiency, and the longitudinal acceptance would be reduced. The influence of higher order transit time factors would increase, resulting in a less accurate theoretical prediction. The drift tube beam hole diameter is increased along the Alvarez accelerator roughly proportional to the third root of the velocity increase in order to take into account a beam diameter increase due to transverse emittance growth, beam displacement resulting from alignment errors, and beam cross section modulations caused by beam mismatches.

The synchronous phase φ_s is kept constant (-35^o) along the Alvarez accelerator for the reference concept to ensure a large longitudinal acceptance. A decrease of the synchronous phase towards the Alvarez end might result from a further optimization.

All beam dynamic parameters should vary smoothly along the Alvarez accelerator so that the emittances can adiabatically adjust to the new acceptances. All discontinuous parameter changes lead to beam envelope oscillations about the matched solutions resulting in emittance growth. This holds especially for the quantities ET and φ_s (E = average axial electric field). Also the Alvarez intertank sections should be as short as possible, because the built-up of a longitudinal mismatch can scarcely be compensated by another parameter choice. First estimates require not more than half a cell length intertank spacing.

Fixing the transverse focusing parameters one especially has to take care that, first, the focusing is strong enough to keep small the transverse emittance growth due to the phase dependence of the rf defocusing /10/, and, second, that the focusing is not so strong as to cause transverse instabilities by the onset of parametric resonances /12/. Keeping the tune μ at full beam current as a fixed parameter, the phase dependence of the rf defocusing does not depend on the transverse emittance in first approximation. Hence at first $\mu = 40^o$ was chosen for the synchronous particle such that the bunch head is just stable transversely. Next, the tune μ_o

for negligible beam current was calculated by the computer code ADAPT as a function of the transverse emittance; μ_o has to be smaller than 90° to surely avoid the second order parametric resonance (envelope resonance) /12,24/. The result is for μ = 40° a μ_o = 83° for a 3 π mm mrad emittance. As μ cannot be chosen smaller because of the phase dependence of the rf defocusing it follows that the transverse emittance at the Alvarez entrance should not be much smaller than 3 π mm mrad.

The next dangerous third order parametric resonance can built up if $\mu < 60°$ but $\mu_o > 60°$ /12/. This instability region cannot be avoided for a 108 MHz Alvarez frequency choice. Analytically the two most important properties of this resonance were estimated /13/: the amplification factor is such that at resonance a space charge density modulation will be enhanced by a factor e in about eight Alvarez cells causing a large emittance growth; the resonance width is relatively sharp namely $\pm$ 4.5° around the 60° center. A relatively small tune variation could therefore avoid this instability. This conclusion indicates that for a high peak beam current linear accelerator the quadrupoles gradients must undoubtedly be variable to allow an optimum setting of machine parameters to minimize beam spill.

Multiparticle simulations were carried through to check the Alvarez design. A major problem in such calculations is the modelling of the space charge forces by macroparticles carrying about 3 x 10^6 proton charges for the SNQ case. Thereby the probability for the occurance of close collisions between macroparticles is enhanced by the same factor compared to the proton beam, and the computer results can get doubtful. In existing computer codes the close collisions between macroparticles are avoided by limiting the forces at small distances more or less arbitraryly. In the calculations reported here, the macroparticle occupies a finite volume over which its charge is assumed to be distributed homogeneously. This volume is chosen such that the sum of all macroparticle volumes equals the bunch volume. Test runs showed that the results based on this model depend only weakly on the model parameters such as the number of macroparticles and the macroparticle volume.

In general symmetry assumptions for the space charge forces are made for such calculations to save computing time. This is not allowed when looking for instabilities depending strongly on asymmetries as is the case e.g. for the parametric third order instability. No symmetries were assumed for the calculations presented below. However, the beam at injection is assumed to be ideally on the accelerator axis.

The results of the multiparticle simulations by the code MAPRO are shown in Fig. A 1.2-6 to 9. The initial distribution at injection into the Alvarez accelerator was obtained from the program BUNCH using parameters of the bunching system /17,18/. The initial distribution at the beginning of the bunching system was assumed to be ellipsoidal and homogeneous in the four-dimensional transverse phase space.

Two-dimensional phase space projections for the accepted particles are shown in Fig. A 1.2-6 for different energies along the Alvarez accelerator. The longitudinal phase damping can clearly be seen in the upper series, the beam profile in the real space is presented in the lowest series. The built-up of the beam halo is obvious; however, its extension is small relative to the apertures which are off scale in these pictures. This holds especially also for the phase, so that no special problems are to be expected at the frequency transition to the disk-and-washer accelerator. No transverse instabilities are detected. The other pictures show the decrease of the non-normalized emittances xx' and yy', and also of the angles x'y' due to the proton velocity increase along the accelerator.

The normalized rms-emittances along the Alvarez accelerator are shown in Fig. A 1.2-7 calculated from the accepted particles only. The transverse emittance increase is largest at low energies being relatively small beyond 20 MeV; longitudinally the situation is reversed which can be understood by the extremely small longitudinal tune towards the Alvarez end. The oscillations can be related to mismatches. One cause of mismatch is that the Alvarez parameters were optimized for a 100 mA peak beam current; however, for the calculations reported a 125 mA beam was injected into the Alvarez accelerator to allow for bunching losses; from this 112 mA were accepted and accelerated in the simulation.

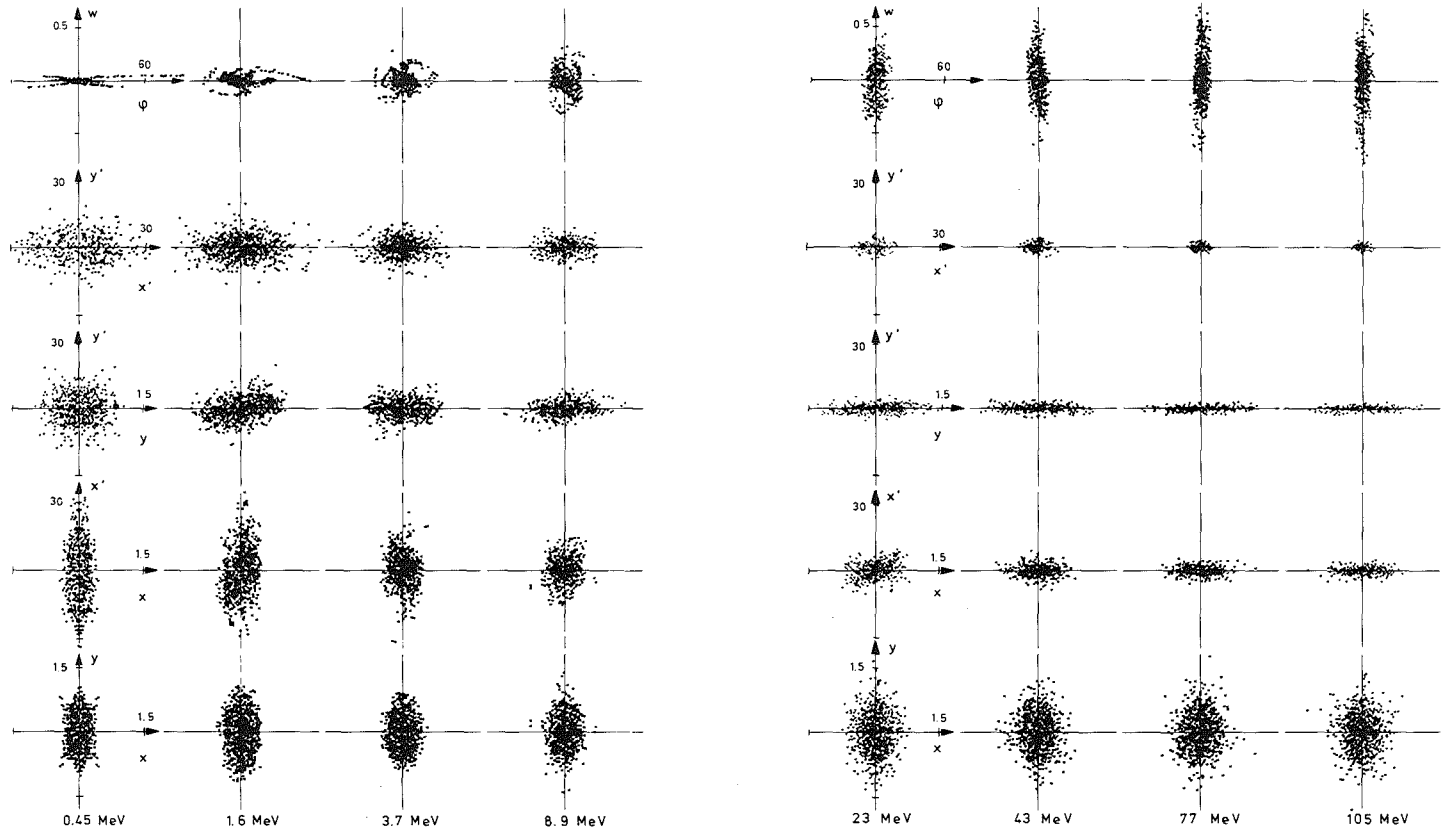

Fig. A1.2-6: Particle coordinates projections for various proton energies along the Alvarez accelerator (simulation with 2000 macro particles; from those lying closely together only one is plotted; x,y = transverse space coordinates, x',y' = transverse angles, ϕ = phase, w = energy; all coordinates relative to the bunch center)

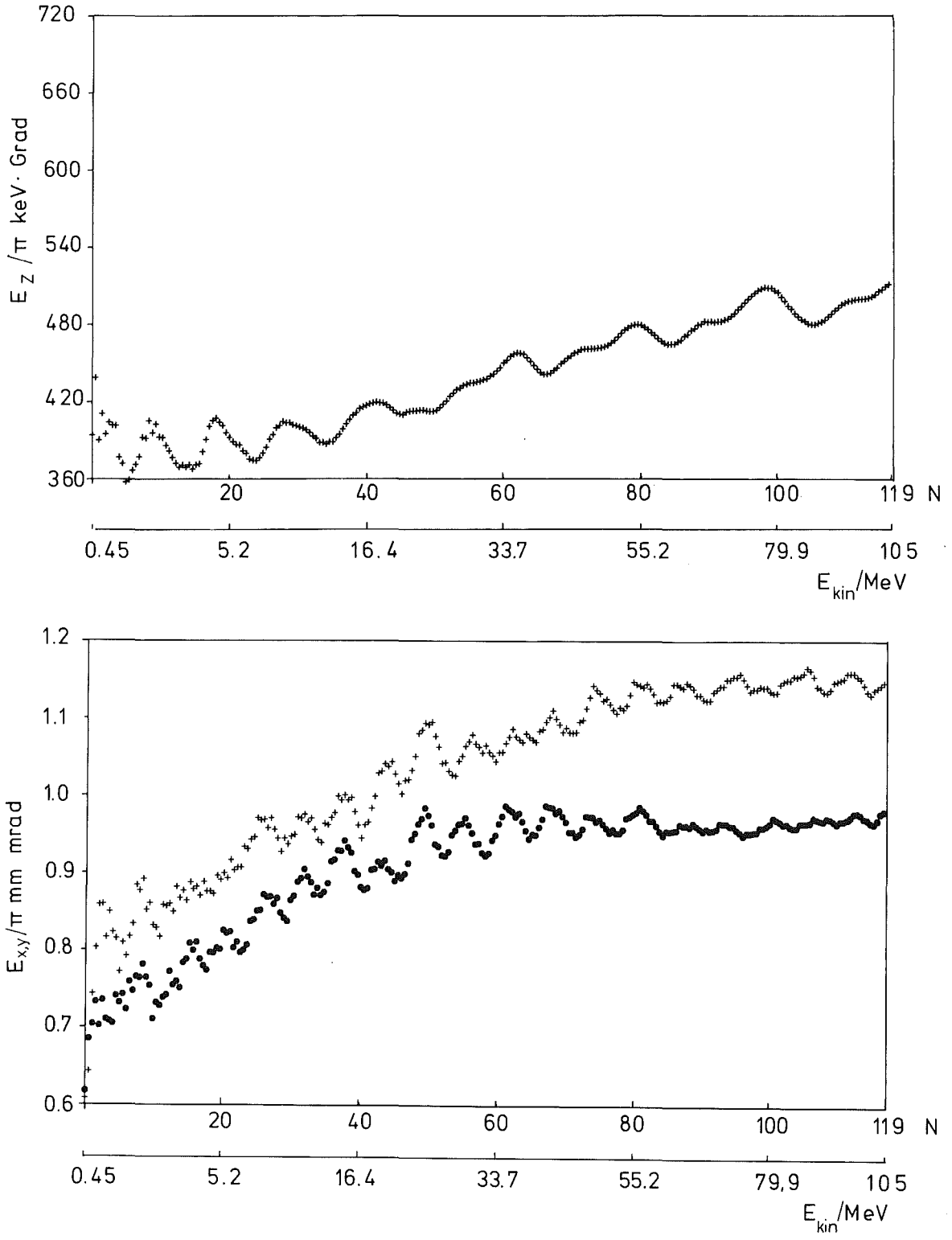

Fig. A 1.2 - 7: Normalized rms-emittance along the Alvarez accelerator (at the top the longitudinal E_z, at the bottom the transverse ones E_x, E_y; N = drift tube number, E_{kin} = proton energy)

Hence 10 % beam loss results from the insufficient bunching. The heat load caused by this loss inside the beam holes is at its maximum 110 Watt per drift tube (Fig. 1.2-8). The last macroparticle loss in the calculation happened at 13 MeV design energy with an 12 MeV actual energy. An accelerator activation by this kind of particle loss is small; however, the beam tubes have to be cooled.

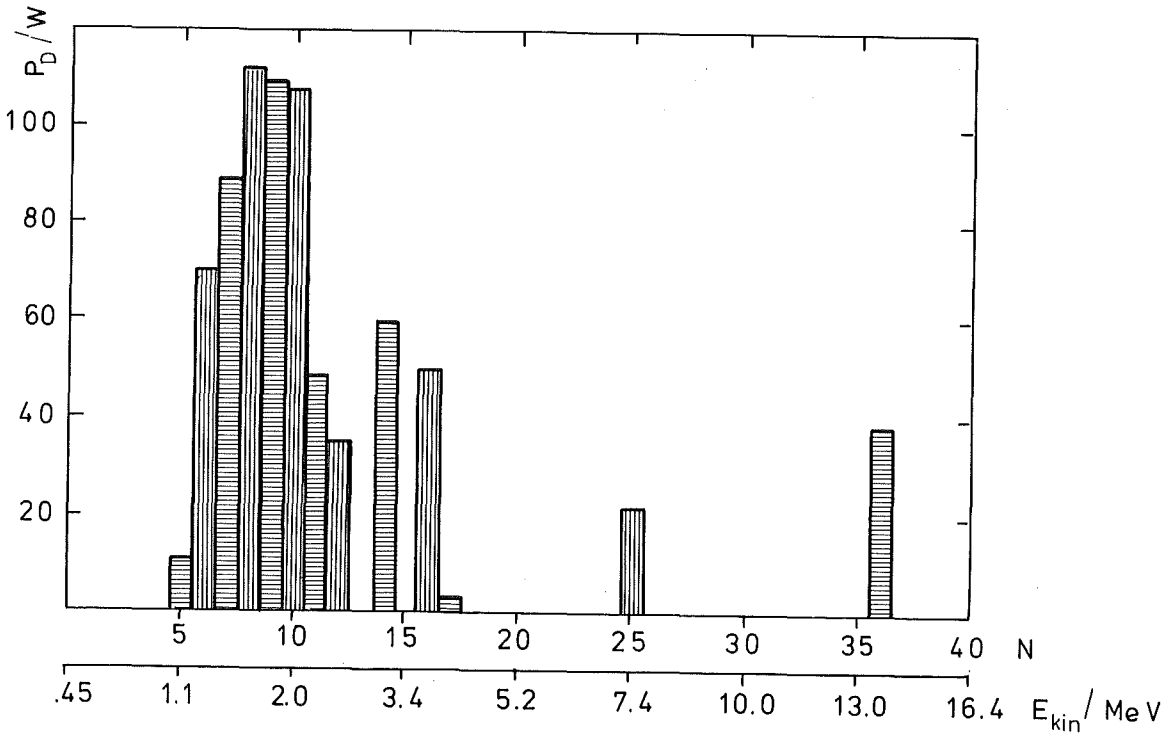

Fig. A 1.2 - 8: Beam power load P_D per drift tube at 5 % duty cycle resulting from particle losses due to insufficient bunching as a function of the drift tube number N and the proton energy E_{kin} (multiparticle simulation with 2000 macro particles; large statistical errors above 2.5 MeV)

Information about the bunch density distribution is given in Fig. A 1.2-9 both for the transverse and the longitudinal direction. The relative large transverse extension of the beam halo could be cut down effectively by apertures inside the drift tube beam hole in the energy range from 4 to 8 MeV:

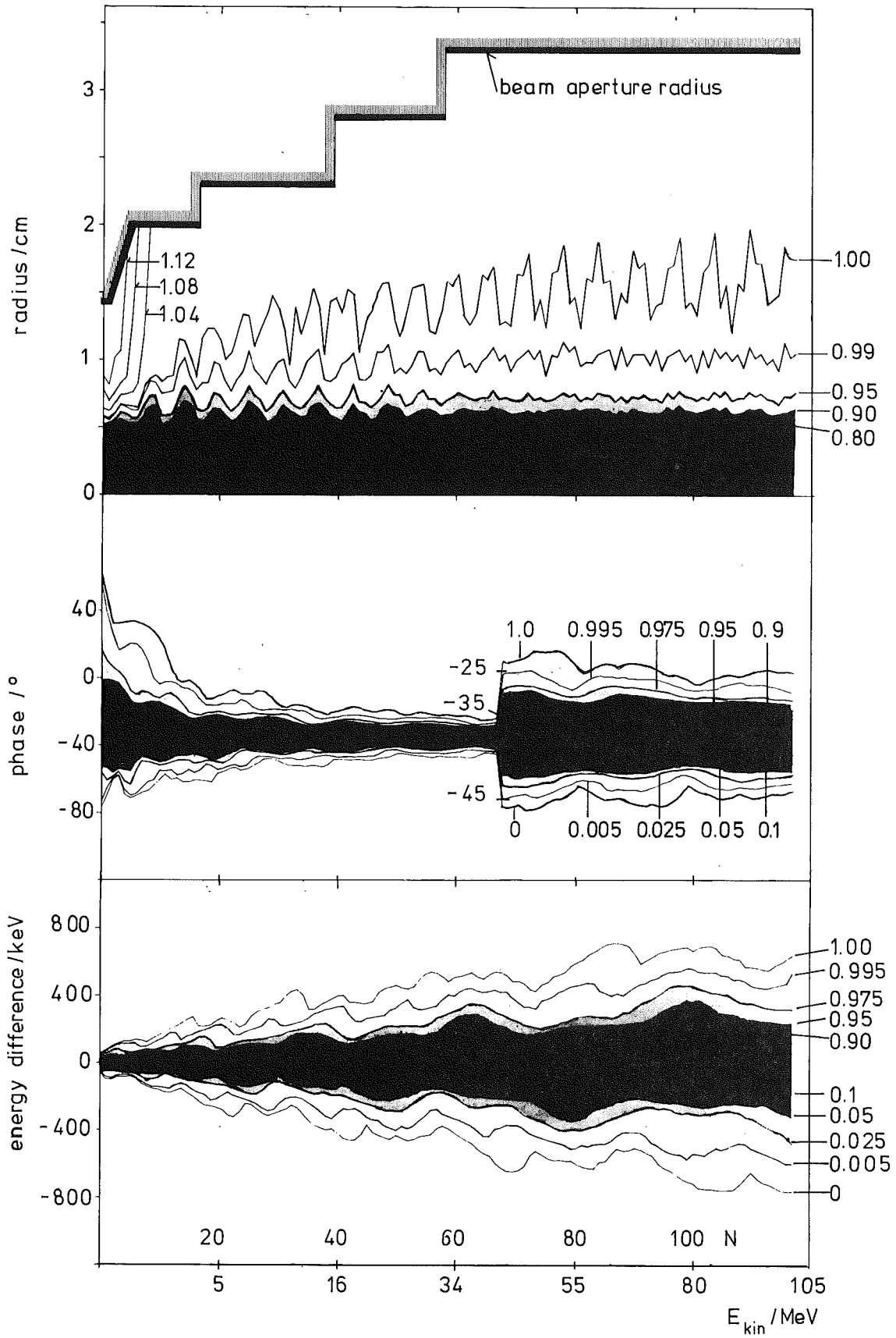

Fig. A 1.2 - 9: Transverse (top) and longitudinal (below) density distribution inside the bunch along the Alvarez accelerator. Parameter is that particle fraction having smaller radius, phase or energy than given by a considered curve. In the top diagram the bunching losses are included. N = drift tube number, E_{kin} = proton energy (multiparticle simulation, hence the curves labelled with 1.0 or 0.0 are subject to large statistical errors).

circular diaphragms with 1.2 cm hole radius would intercept only about 1 % beam current (about 300 W), but thereby reduce the "maximum" beam radius in the Alvarez accelerator from about 2 cm to about 1.5 cm. Also in the longitudinal phase space, that is in the phase and energy distribution functions, a halo is detectable: at 105 MeV the phase width for "100 %" of the beam is 18^{o}, whereas for 95 % it is only 11^{o}; the energy width for "100 %" of the beam is 1.4 MeV, whereas for 95 % it is down to 0.8 MeV.

1.2.6 Beam Matching at 105 and 350 MeV

The parameters of the longitudinal and the transverse particle motion change discontinuously at the transition from the Alvarez to the disk-and-washer accelerator at 105 MeV. Therefore, the axis ratios of the three emittances and their directions in the three two-dimensional phase spaces (xx', yy', φW) have to be matched to the new acceptances /25/, in order to avoid emittance growth due to mismatches which would cause increased particle loss in the disk-and-washer accelerator. To this end, a precise measurement of all beam parameters is necessary in the matching line. Hence there must be sufficient space for the required diagnostic equipment (Chap. A 1.3), and for a bending magnet to measure the energy spread followed by a beam guidance system to a beam dump.

The matching of the longitudinal parameters phase width and energy spread is done by two rebuncher cavities operating at 324 MHz. They are similar to the first disk-and-washer tank. The total length of the transition line is 27 m. The beam transport and the transverse matching procedure is done with 8 magnetic quadrupole doublets. For beam steering there are two pairs of steering magnets. Each pair has two dipole magnets which are acting separately on both transverse directions. In front of the second steering magnet there is one beam position monitor, the second one is located further downstream. All magnetic fields are below 1 T, such that Lorentz dissociation can be neglected for the H^--option /26/.

The position of the elements and the behaviour of the bunch envelopes are shown in Fig. A 1.2-10. The calculations were done with the linear transport program ENVELO including space charge effects. The design is not optimized as yet.

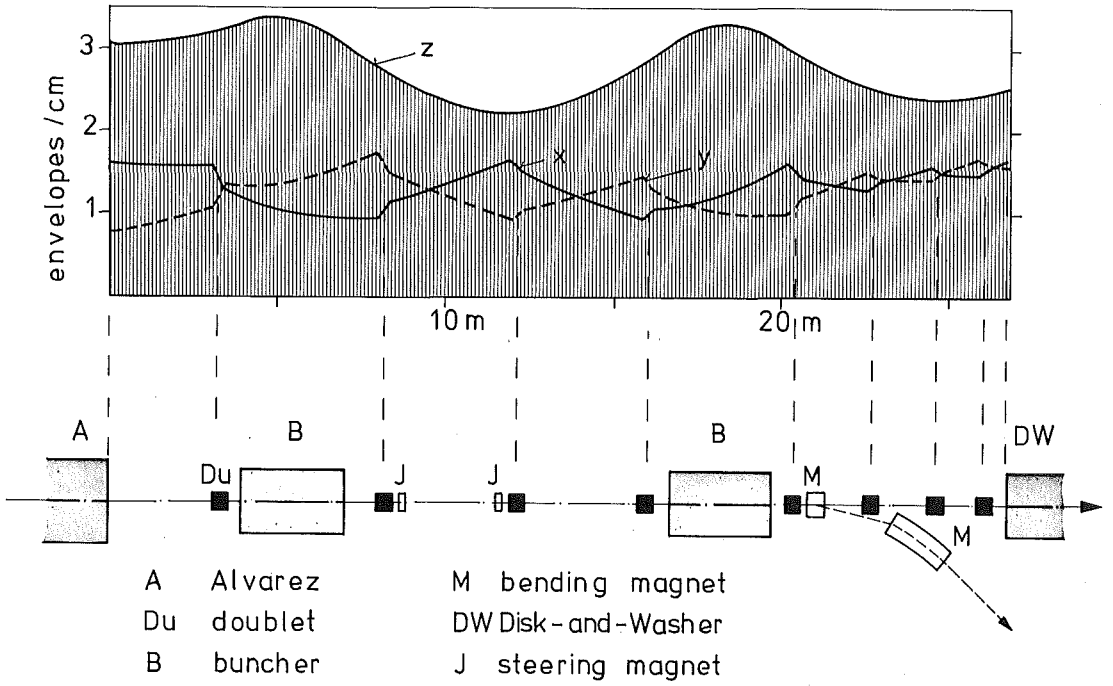

Fig. A 1.2 - 10: 105 MeV beam matching section: beam envelopes and beam line elements

At a proton energy of 350 MeV there is a fast ejection line for a small fraction of the beam to feed nuclear physics experiments (Chap. A 1.6), and the transverse focusing periodicity of the disk-and-washer accelerator is changed. For both reasons a rematching of the beam is required. The design of the matching line is similar to that at 105 MeV. Its total length is 30 m. Besides two 324 MHz disk-and-washer rebunchers it contains magnetic quadrupole doublets, steering magnets, diagnostic equipment, and also a fast beam kicker system. The bending magnet for the fast ejection line can also be used for an energy spread measurement.

Some nuclear physics experiments require a small energy spread beam. This can be achieved using the last three disk-and-washer tanks in front of the 350 MeV transition line to rotate the longitudinal phase space ellipse. By this means about a factor of five smaller energy spread can be obtained at the expense of a larger phase width. After the ejection line the next three disk-and-washer tanks rotate the longitudinal emittance back to match to the subsequent accelerator part.

1.2.7 Beam Dynamics in the Disk-and-Washer-Accelerator

After the 105 MeV beam matching section the beam is carried by the disk-and-washer accelerator to 1.1 GeV energy. Theoretically this is a much easier task than the beam matching and acceleration at the beginning of the Alvarez accelerator. The reason is that the proton momentum has increased by about a factor of 15 compared to the start of acceleration. Therefore, a given force causes a relatively smaller momentum change, the beam has become stiffer. Further, a given momentum change causes the same change in position only after a factor of 15 larger distance, as also the proton velocity has increased by nearly the same factor. Next, the bunch volume has increased due to emittance growth and longitudinal bunch lengthening (proportional to $(\beta\,\gamma)^{1/4}$); consequently, the space charge forces are reduced. Also, the beam self-focusing by means of its own magnetic field is more favourable (proportional to $(1-\beta)^2$). The rf field forces do not depend on the proton velocity for a fixed accelerating gradient. Altogether, the beam dynamics problems have decreased considerably.

These facts are taken advantage of by increasing the distance between the transverse focusing elements and changing over to intertank focusing by means of magnet doublets. The accelerating gradient can be optimized with regard to cost optimization, peak electric fields or other constraints, disregarding beam dynamics (Chap. A 1.5). The transverse acceptance is dominated by geometrical effects. Compared to the situation at the Alvarez injection the longitudinal to transverse coupling of the particle motion is now only a perturbation of higher order, because of the higher proton velocity, the higher frequency, and the smaller phase length of the bunch /10/.

Taking all arguments together the conclusion can be drawn that the beam dynamics in the disk-and-washer accelerator can be described well by fairly simple models with the exception of the particle loss problem. The detailed arguments and results leading to the beam dynamics layout of the disk-and-washer accelerator are compiled in the reports /11,26/. Table A 1.2-3 collects the main results. At 350 MeV there is a change in focusing periodicity, the rf tanks becoming twice as long.

The disk-and-washer accelerator design was checked by a multiparticle program /27/. The matching parameters for this calculation were not optimized as yet. Nevertheless, all macro particles were transported through the disk-and-washer accelerator without any loss. Fig. 1.2-11 shows the transverse beam envelope as a function of the proton energy. The beam diameter stays about a factor of 2 smaller than the beam hole up to 350 MeV energy. In the present design the beam was not properly matched to the change of the transverse focusing periodicity which caused large envelope oscillations thereafter. This can be avoided in an optimized design.

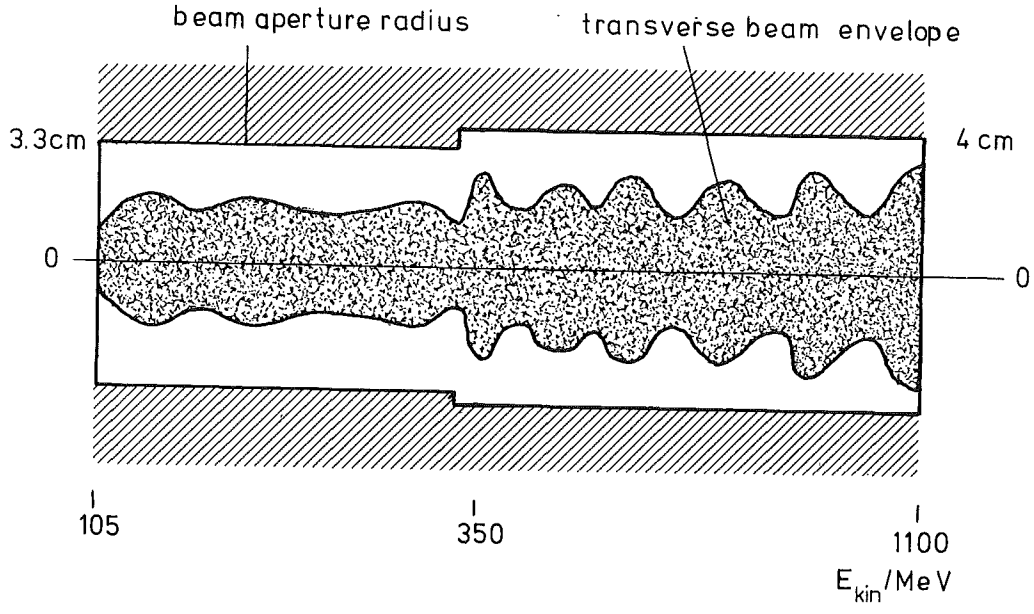

Fig. A 1.2-11: Transverse beam envelope along the disk-and-washer accelerator, E_{kin} = proton energy.

peak beam current/mA (averaged over 3 rf periods)	100		
frequency/MHz	324		
energy/MeV	105	350	1100
average axial electric field/MV m^{-1}	3,4	3,7	4,1
transit-time-factor	0,89	0,87	0,84
synchonous phase/°	-30	-25	-25
transverse tune (100 mA)/°	45	45	30
transverse tune (0 mA)/°	55	50	32
100 % phase width/°	44	30	20
rms - phase width/°	15	10	7
100 % energy width/MeV	1,7	2,5	3,7
rms - energy width/MeV	0,4	0,6	1
100 % beam diameter in the doublet/cm	3	3	3
rms - beam diameter in the doublet/cm	0,7	0,7	0,7
beam hole diameter/cm	7,0	8,0	8,0
100 % normalized transverse emittance/π mm mrad	6	10	15
rms - normalized transverse emittance/π mm mrad	1,2	2	3

Tab. A 1.2 - 3: Beam dynamics parameters of the disk-and-washer accelerator, analytical estimates

1.2.8 Tolerance Requirements for the Disk-and-Washer Accelerator

In the disk-and-washer accelerator even small deviations from the design parameters could result in particle losses because of the large length of this part. For this reason tne influence of realistic tolerances on the transverse beam motion was studied /28, 29/. The following errors were taken into account for quadrupoles, doublets, and rf tanks:

(i) parallel displacement of the longitudinal axis and rotation about the transverse axis

(ii) rotation about the longitudinal axis (for quadrupoles and doublets only, since rf tanks are rotationally symmetric)

(iii) field errors

(iv) displacement in the longitudinal direction

For the calculation of the beam displacement and of the beam size increase, the beam optic elements were treated as thick lenses. Space charge was neglected, as it has only a higher order effect. Two major results were obtained:

- Parallel displacements and rotation of type (i) only cause a beam displacement in linear approximation; the beam cross section and the emittance remain unchanged. The beam can be readjusted by means of steering magnets.
- The errors of types (ii) to (iv) do not change the beam center, but couple the two transverse emittances. Therefore the average beam radius increases.

For the tolerances assumed below the main perturbation is caused by parallel displacements and rotations (i) of the quadrupoles. The quadrupoles have to be preadjusted with higher precision inside a doublet than is necessary later for positioning the doublet relative to the ideal beam axis. To obtain quantitative results the required tolerances were estimated by statistical methods. The results quoted below therefore are average standard deviations over the total disk-and-washer length. The errors were assumed to be distributed homogeneously both for each single error interval and along the accelerator.

The maximum error intervals on which the estimates are based can be realized in practice (Chap. A 1.5). They are for errors of type (i):

- quadrupole deviation from the doublet axis: $\leq \pm 0.3$ mm
- doublet deviation from the ideal beam axis: $\leq \pm 0.5$ mm
- rf tank deviation from the ideal beam axis: $\leq \pm 1.0$ mm

An average quadratic beam deviation from the ideal axis of 18 mm results from these errors at the disk-and-washer end. For comparison, the beam radius is about 15 mm, the aperture radius 40 mm. In case a maximum beam displacement of only 5 mm is desired, this could be achieved by 7 steering magnet pairs.

The following maximum error intervals were used for errors of the types (ii), (iii), and (iv):

- quadrupole or doublet rotation about the ideal beam axis: $\leq \pm 0.2$ mrad
- magnetic field gradient deviation: $\leq \pm 0.1$ %
- electric field deviation: $\leq \pm 0.1$ %
- length tolerances: $\leq \pm 0.2$ %

From these error types results a beam radius increase of less than 0.7 mm at the disk-and-washer end.
Summarizing: errors of type (i) are of largest importance; however, they only cause a beam displacement which can be counteracted relatively easily by means of steering elements.

1.2.9 Beam Spill

The proton beam can be transported with a high reliability through the linear accelerator. Particle losses can result from the built-up of a halo around the main part of the beam, whose density decreases more slowly than theoretically expected with increasing distance from the bunch center /30/. The causes for the halo built-up are manyfold: principal deficiencies of the accelerator, non-optimal parameter choice because of approximate calculation methods, and the summation of many calculation deviations of accelerator parameters from their design values. The most important methods to minimize the beam spill are control and adjustment of the accelerator parameters during operation, beam limitations by aperture systems at well defined locations, and beam apertures chosen to be about twice the size of the beam /19/.

Beam spill due to principal deficiencies of the accelerator

All beam optics elements have abberations which have to be kept below predetermined limits by a proper design. This holds for example for the accelerating column of the injector, for the magnetic quadrupoles, for the bunchers, and especially also for the accelerating structures. Abberations lead to emittance growth through filamentation. The bunching system creates an inhomogeneous density distribution in the longitudinal phase space which can cause emittance growth via the space charge forces. The longitudinal focusing force in the accelerator is highly non-linear, especially for high space charge forces, resulting in further filamentations in the longitudinal phase space /13/. The longitudinal temperature in the bunch is for the SNQ parameter choice larger than the transverse one; space charge coupling can yield a temperature exchange between the phase spaces causing transverse emittance growth. The major parametric resonances of the particle motion can be avoided by a proper parameter choice; those of higher order cannot be excluded, however.

Each discountinuity of the longitudinal or of the transverse periodicity requires a beam rematching. Resulting mismatches lead to emittance growth. Examples for such discontinuities are the buncher system, the intertank sections in the Alvarez accelerator, and the matching lines at 105 and at 350 MeV.

The estimated transverse emittance growth caused by these effects will be about a factor of 2 each between the ion source and the Alvarez, along the Alvarez, and also along the disk-and-washer accelerator. Aperture systems in the low energy beam transport system, in the Alvarez accelerator, and also in the matching sections at 105 and 350 MeV limit the transverse emittance, hence cut away the halo. Despite these measures a new halo will built-up slowly after each aperture system by means of the imperfections of the subsequent accelerator part. Particle loss due to proton - proton scattering inside the bunch is negligible /23/.

Approximate calculation methods

An exact beam dynamics calculation would require self consistent solutions of the Vlasov equation under the real boundary conditions given by the accelerator design. This is impossible to achieve in this generality, solutions are only known for special cases under idealized assumptions. Multiparticle simulations are not self-consistant, especially the initial phase space distribution is idealized. Nevertheless, they allow a good description of the rms-emittances /1/, whereas the predictions for the halo are much more uncertain. The statistical accuracy for the halo can be improved over that of existing multiparticle codes by tracing halo particles in precalculated space charge fields. This method is under development.

Systematic errors can stem also from idealized models for the external fields: higher order moments are neglected in the quadrupole fields; the action of the rf fields is approximated by thin lenses, and taking velocity changes over the element into account only up to first order. The justification for the idealizations is obtained from more accurate test calculations.

It follows that the aim of the beam dynamics theory can only be to study the influence of various effects on the beam spill separately, and to develop methods to minimize the beam spill empirically during operation /19/.

Beam spill due to finite parameter tolerances

In operating the accelerator deviations of actual parameters from their design values are unavoidable. Some parameters of special importance for the beam spill are: vacuum conditions; peak beam current; injector voltage; buncher fields and phases; accelerating fields and phases; quadrupole currents; mechanical alignment of the Alvarez drift tubes, the Alvarez tanks, and the doublets between the disk-and-washer tanks. The influence of such errors can be estimated by statistical methods (1.2.8) from which the tolerance requirements can be deduced.

Methods to minimize beam spill during operation

To enable the minimization of beam spill during the accelerator operation, well developed diagnostic and feedback techniques are required for various accelerator parameters (Chap. A 1.3). An unambiguous judgement of error causes is only possible if the influence of given parameter changes on the beam quality is well known. The computer system helps in the quick analysis and localization of errors.

Operation experience

A prognoses about the beam spill and the resulting activation to be expected for the SNQ accelerator can be guided by the operating experience with the 800 MeV proton linear accelerator in Los Alamos (LAMPF) /16, 31/. At present this accelerator routinely achieves 0.6 mA average beam current. The accelerator tunnel is accessable soon after machine shut-down. Beam spill is no serious problem any more for this linear accelerator. Right now it could accelerate already 1.1 mA average current, the limitation being solely the meson target design.

According to this experience there exists a good chance that beam spill can be kept small also in the SNQ accelerator.

Contributors

K. Bongardt (University of Karlsruhe), K. Crandall (LANL), H.G. Hereward, K. Mittag (KfK), M. Pabst (University of Karlsruhe), D. Sanitz (KfK), D. Warner (CERN), M. Weiss (CERN).

References

/ 1/ F. Sacherer, CERN: "R.M.S. Envelope Equations with Space Charge", Nov. 1970, unpublished

/ 2/ E. Boltezar et al: "The New CERN 50 MeV Linac", Linear Accelerator Conference Montauk, USA (1979) 66, BNL 51 134

/ 3/ K. Mittag: "On Parameter Optimization for a Linear Accelerator" - A High Current Deuteron Linear Accelerator -, Kernforschungszentrum Karlsruhe, KfK 2555 (1978)

/ 4/ D.C. Hagerman: Private communication

/ 5/ Progress at LAMPF, January - June 1980, Los Alamos Report LA-8456PR (1980) 114

/ 6/ Catalogue of High Energy Accelerators, XI. International Conference on High Energy Accelerators, CERN, Genf (1980)

/ 7/ K. Mittag, G. Dammertz, G. Hochschild, R. Lehmann, B. Piosczyk, J.E. Vetter: "Choice of Frequency and Injection Energy for a Spallation Neutron Source", this study, part III A, vol. 1, unpublished

/ 8/ D.A. Swenson: "Low-Beta-Linac-Structures", Linear Accelerator Conference, Montauk, USA (1979) 129, BNL 51 134

/ 9/ T. Wangler, R. Lehmann: Private communications

/10/ K. Mittag: "Beam Dynamics in a Proton Linear Accelerator for a Neutron Spallation Source", Linear Accelerator Conference, Montauk, USA (1979) 253, BNL 51 134

/11/ K. Mittag: "On Parameter Optimization for a Linear Accelerator" - A High Current and High Energy Proton Linear Accelerator -, Kernforschungszentrum Karlsruhe, January 1979, unpublished report

/12/ I. Hofmann: "Emittance Growth of Ion Beams with Space Charge", Proc. of the Conference on Charged Particle Optics, Gießen, (1980), in press

/13/ H.G. Hereward: "Notes on Beam Dynamics in a Linear Accelerator for a Neutron Spallation Source III - Transverse Instabilities and Longitudinal Particle Loss -", Kernforschungszentrum Karlsruhe, this study, part III A, vol. 1, unpublished

/14/ J.W. Staples, R.A. Jameson: "Possible Lower Limit to Linac Emittance", IEEE Trans. NS-26, No. 3 (1979) 3698

/15/ H.G. Hereward: "The Implications of Parasitic H^--Acceleration in the Spallation Source Linear Accelerator", this study, Part III A, vol. 1, unpublished

/16/ D.C. Hagermann: "LAMPF Operation at 500 μA", Linear Accelerator Conference, Montauk, USA (1979) 78, BNL 51 134

/17/ M. Weiss: "Spallationsneutronenquellenprojekt - Kurze Zusammenfassung des Niederenergiestrahltransports", CERN/PS/LR-Note 80-13, CERN, Genf (1980)

/18/ E. Boltezar, M. Weiss: "Low Energy Beam Transport System for the German Spallation Neutron Source", CERN /PS/LR-Note 81-5, CERN, Genf (1981)

/19/ H.G. Hereward: "On Beam Losses in the Linear Accelerator of the Neutron Spallation Source", this study, part III A, vol. 1, unpublished

/20/ D.J. Warner: "Accelerating Structure of the CERN New 50 MeV Linac", Proc. of the 1976 Proton Linear Accelerator Conference, Chalk River, Ontario (Canada), AECL-5677 (1976) 49

/21/ D.J. Warner, M. Weiss: "Beam Optics in the CERN New 50 MeV Linac", Proc. of the 1976 Proton Linear Accelerator Conference, Chalk River, Ontario (Canada), AECL-5677 (1976) 245

/22/ K. Mittag: "Detailed Design Data of the Alvarez Linac for the Neutron Spallation Source SNQ", this study, Part III A, vol. 1, unpublished

/23/ H.G. Hereward: "Notes on Beam Dynamics in the Spallation Linear Accelerator (Intrabeam Scattering, Wavelength Scaling, Image Forces)", this study, Part III A, vol. 1, unpublished

/24/ R.A. Jameson, R.S. Mills: "On Emittance Growth in Linear Accelerators", Linear Accelerator Conference, Montauk (USA), (1979) 231, BNL 51 134

/25/ K. Bongardt, K. Mittag: "Matching Sections at 105 and 350 MeV for the Linear Accelerator of the Neutron Spallation Source SNQ", February 1981; this study, Part III A, vol. 1, unpublished

/26/ K. Mittag: "Parameters and Beam Dynamics of the Disk-and-Washer Linear Accelerator for a Neutron Spallation Source", this study, Part III A, vol. 1, in preparation

/27/ K. Crandall: Private communication

/28/ K. Bongardt, M. Pabst: "Note on Tolerances in Rf Linear Accelerators", Kernforschungszentrum Karlsruhe, February 1981, unpublished report

/29/ M. Pabst: "Note on Tolerances in the Disk-and-Washer Accelerator for the Neutron Spallation Source SNQ", this study, part III A, vol. 1, unpublished

/30/ H. Koziol, LANL: "Halo Measurements on the LAMPF 800 MeV Beam", private communication

/31/ P.R. Tunnicliffe: Los Alamos Scientific Laboratory, private communication

A 1.3 Beam Diagnosis

A 1.3 Beam Diagnosis

1.3.1 Introduction and Design Fundamentals

The loss-free transport of the proton beam from the ion source to the target is of particular importance for this high current linear accelerator. The problem can be solved only by means of an extensive beam diagnosis. It must be expected that comprehensive beam diagnosis will be necessary during the entire lifetime of the machine. It will initially play an important role in the first commissioning because the beam itself constitutes the most accurate probe, testing the performance of the individual components. Subsequently, as in all big accelerator systems, a process will start of many years of optimization during which the characteristic parameters of the beam must be measured and a comparison made with the beam dynamics calculations. Although for the subsequent routine operation of the system less diagnostics elements will be used for monitoring, quite a considerable number of them must be employed during the start-up phases and, in particular, for trouble shooting.

The diagnostics elements presented below have been selected on the basis of studies of devices in comparable accelerators.

According to experience gathered, the following criteria are important in selecting the techniques:

- no beam interrupting techniques
- no electronics close to the beam, use of radiation resistant materials
- low expenditure in terms of time for the measurements
- capability of convenient and quick replacement
- similar techniques to be applied over the entire range of energies
- suitability for processing by computer.

These conditions can be largely fulfilled with the familiar configurations. However, it is pointed out here, that the accuracy of techniques presently known will not be sufficient in most cases to assign the reasons for small beam current losses (beam halos) in an unequivocal manner. However, diagnosis is capable of examining the extent to which the hot spot (95% of the inten-

sity) of the particle beam has been adapted in an optimum way to the accelerator structure.

1.3.2 Intensity Measurements

All intensity measurements are non interceptive. The measuring system described is used to fulfill the following tasks:

- intensity display in the control room
- detection of losses $> 10^{-3} \times I_o$ (fast shut-down)
- display of the time dependence of macro-pulses
- observation of variations in intensity
- standardization of other techniques of measurement (e.g., in emittance measurements)
- controlling signals (e.g., for high frequency systems).

It is planned to perform non interceptive measurements of the intensity and the macropulse shapes by providing current transformers at about 20 locations along the accelerator. The measurement transducer is a toroidal ferrite core of high permeability (Fig. A 1.3-1) equiped with 100 windings /1,2/. An additional winding is used for calibration.

The beam pulse passing through induces a signal which is proportional to the beam current $I_o(t)$. With modern ferrite cores transmission of the macropulse rise and decay times does not cause problems (bandwidth 1 Hz-35 MHz). To obtain accurate measurements of intensity, the decay time constant $\tau = L/R_o$ must be made to last as long as possible during the pulse maximum. With a typical inductivity ($L \sim N^2$) of 0.5 H and a total resistance of 5 Ω this yields $\tau = 0.1$ s. To make very accurate measurements, an amplifier system has been developed at Los Alamos (100 MHz bandwidth) in which the effective input resistance was reduced by a factor of 50 so that the decay is 0.01 % at 500 μs pulse length. The accuracy of current intensity measurements is indicated to be 0.01 % for this system /3/.

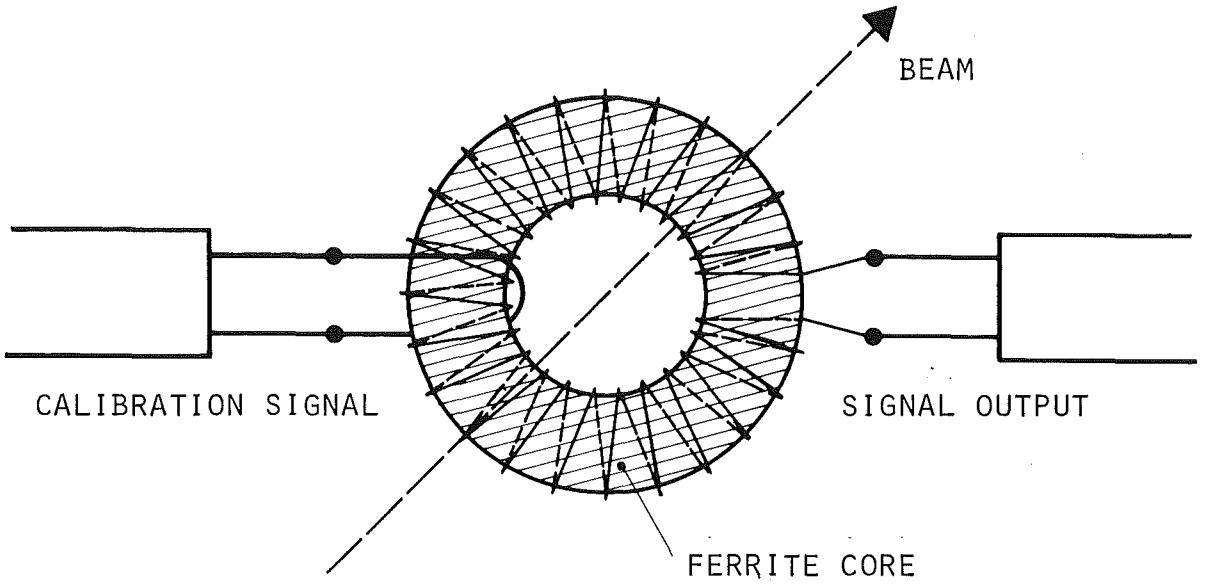

Fig. A 1.3-1: Principle of the toroidal current transformer for intensity measurement

1.3.3 Measurements in the Transverse Phase Space

For an accelerator to be operated with extremely small losses of beam current the measurements of the transverse (at right angles with respect to the direction of acceleration) beam properties become special importance. Information derived from these measurements is used to solve the following problems:

- verification of beam quality (emittance) in the low energy beam transport system according to the Alvarez and according to the Disk- and Washer-structure

- solving the beam matching problems

- focusing the beam on the nominal axis

- examination of the beam halo.

Transverse Emittance

In accelerator physics the coordinates x, x', y, y' are normally used to describe a particle beam in terms of space with the variables x', y' constituting the angles with respect to the beam axis (z-axis). On given assumptions the particles in the phase space can be represented in subspaces decoupled from each other. The emittance is defined as

$$\varepsilon = A/\pi \quad \text{with} \quad A = \iint dx\, dx'$$

i.e. ε is the area in which the coordinates of the beam particles lie (ch. A 1.2 uses the normalized emittance $\varepsilon_n = \beta\gamma\varepsilon$). It is implicitly assumed in this consideration that, within the area of emittance, all coordinates x, x' occur with the same abundance and that the boundary of emittance constitutes at the same time a sharp edge of the beam.

But actually the particle densities averaged over time are very different for different x, x' coordinates. The measurement of the shape and orientation (if the measured values are circumscribed by an ellipse) of the area of emittance is so important because it is directly incorporated into the beam dynamics calculations in this form (see ch. A 1.2).

Three methods exist of measuring transverse emittances:

I. The method of three spaces (tomography) /4/

II. The gradient method /5/

III. The scanning method /6/

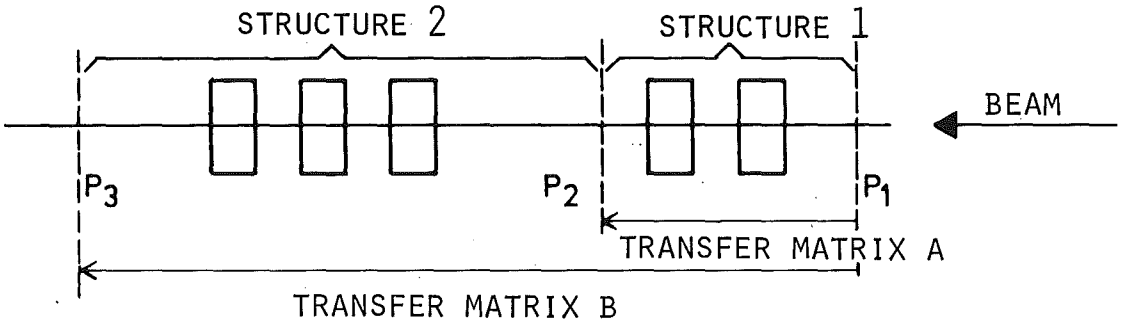

Fig. A 1.3-2: Principle of the method of three spacings for measurement of the transverse emittance

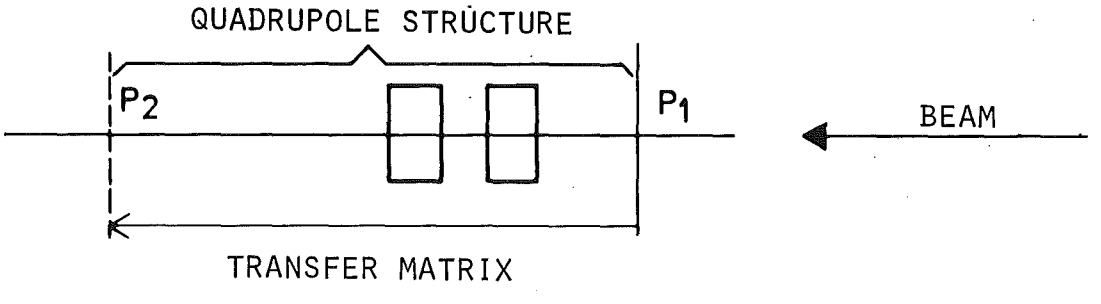

Fig. A 1.3-3: Principle of the gradient method for measurement of the transverse emittance.

I. The method of the three spaces (Fig. A 1.3-2) calls for a measurement of the beam profile at three points in a known achromatic transport system (see following section). Assuming that the area of emittance is elliptical and the transformations from P_2 and P_3 are known, the form and orientation can be derived mathematically from the measured beam cross section.

II. In the gradient method the beam profile is measured as a function of the excitation of a known (transfer matrix) quadrupole doublet (Fig. A 1.3-3). Also here a mathematical formalizm exists which, under the same assumptions as in I., allows the determination of the form and orientation of the area of emittance.

III. The scanning method consists of collimating by means of a slit in the x or y plane a small partial area from the main beam (Fig. A 1.3-4). The position of the partial area shall be given by small x_i. The related divergence is determined by measurement of the intensity distribution at a distance L.

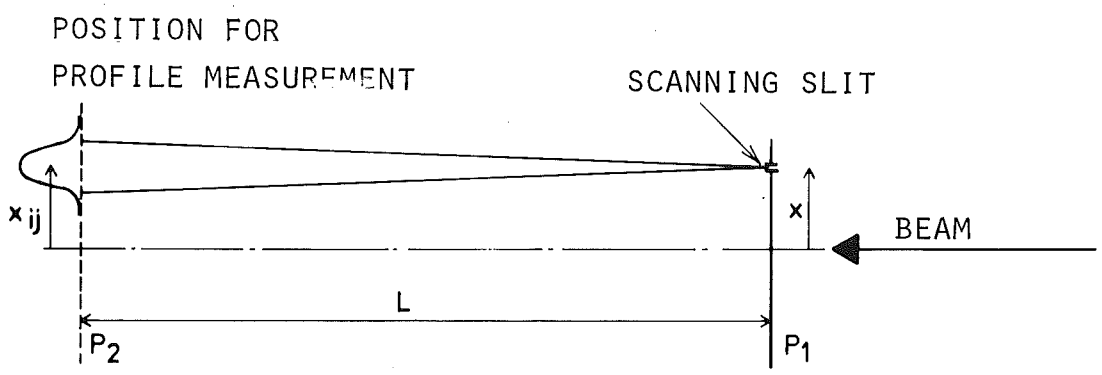

Fig. A 1.3-4: Principle of the scanning method for measurement of the transverse emittance

$$x'_{ij} = \frac{x_j - x_i}{L}$$

The shape and position of the areas of emittance can be calculated from the geometric data and the measured current distribution. Since no additional assumptions are made beyond those of method I and II, statements are also possible concerning

- the density distribution in the phase space
- the fraction of total intensity in the surrounding ellipse (normally 95 %).

But this method, except for the solved problem (e.g. at CERN) of controlling the high intensities at the defining slit, presents two physical complications which are connected with the high beam current:

- Space charge effects influence the beam between the slit and the collector, especially at low energies in the low energy transport system. This influence may be minimized by optimizing the distance L (in our case about 50 cm) /8/.

- Secondary electrons generated at the defining slit can be accelerated back into the incoming beam and have an impact there on space charge compensation. At CERN /9/, the influence of this effect was reduced by application of a bias voltage (in our case 1000 V).

Despite these complications the scanning method is currently the best method of measuring the transverse emittance and therefore two units of this type are proposed for the low energy beam transport system. The technical details from CERN can be completely taken over (slit width: 0.1 mm, material: tungsten, collector: 32 tungsten plates each of 0.1 mm thickness and insulated (Al_2O_3) with respect to each other).

A measurement unit working on the same technique will be provided at the outlet of the Alvarez system at 105 MeV. It will be used as an alternative to measurement by method I which can be made in addition. The unit was designed at Brookhaven /10/. The slits (1 mm wide) partly absorb the beam energy (3mm copper at 105 MeV imply a loss of energy of about 10 MeV). Due to angle and energy straggeling, the beam outside the slit eluminates homogeneously the plain of profile measurement (distance 7 m). On this background (1% of the maximum current signal at this point) the profile is measured by a wire scanner (see below).

At present, intensive work is being carried out in order to further improve and validate the algorithms for reconstruction techniques (method I). It can be expected, that sufficiently reliable information about the emittance can be extrated by this much more convenient method (in terms of performance, activation) which, at the maximum energy according to the disk- and washer-structure, has no alternatives. All measurements performed under method III are made with a reduced beam pulse length of 100 μs, at full peak current, and a frequency of about 1 Hz.

Beam Position and Profile Measurements

The most sensitive measuring system of the position and profile is the wire scanner shown schematically in Fig. A 1.3-5 which is moved through the beam plane via a stepping motor.

The wire scanner consists of a thin (1/10 mm) graphite wire through which the beam passes practically without loss (energy loss at 10 MeV about 0.96 MeV; at 100 MeV about 0.13 MeV and at 1000 MeV about 0.02 MeV). The secondary electron current is measured which amounts to only some % of the proton current (3-4 % at 40 MeV; 1-2 % at 200 MeV) /13/. Although on account of the missing moving devices the multi-wire assemblies (harps) seem to be more suitable at first sight, they are not proposed for application in the accelerator zone for the following reasons:

- The spacial resolution of harps is poorer by at least a factor 5.

- Since they interrupt the beam repeatedly, harps may cause a sensitive loss measuring system to react.

- Harps may influence the beam, especially at lower energies so that simultaneous measurement at several points is not possible.

- The secondary electron yield is influenced by surface effects i.e., different aging of the wires exerts an influence on profile measurement /14/.

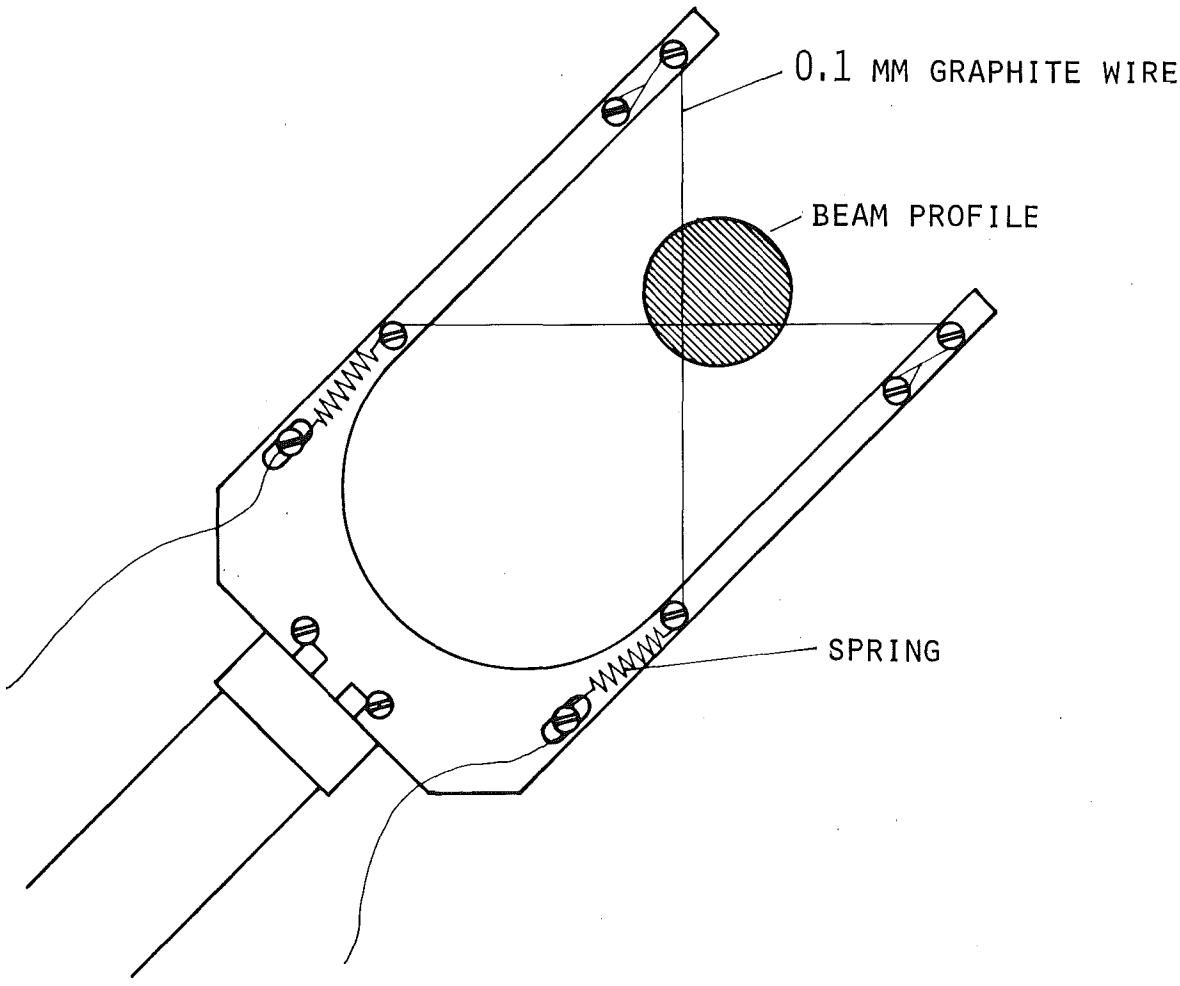

Fig. A 1.3-5: Principle of a beam profile measurement

Another very important property of these wire scanner consists of the fact that beam halo measurements can be made with them. Intensities of 1 μA (10^{-5} of our peak current) can be detected /15/.

Non-intercepting Probes for Position Measurement

To focus the center of mass of a charged particle beam to the nominal axis it is suitable to measure the position simultaneously at many points. For this purpose an inductive decoupling of the beam signal, as shown in Fig. A 1.3-6, is to be used. In the electronic system connected in series (according to the heterodyn principle) (Fig. A 1.3-7) the fundamental wave of the Fourier spectrum of the micro-structure pulses is further processed. A very similar configuration used at Los Alamos /16/ allows beam deviations of ± 0.1 mm from the nominal axis to be detected. Also the connection with a Δt-probe (copper ring for decoupling of the time signal) shown in Fig. A 1.3-6 was taken over from Los Alamos. This configuration offers the advantage for position measurements that their function can be verified by

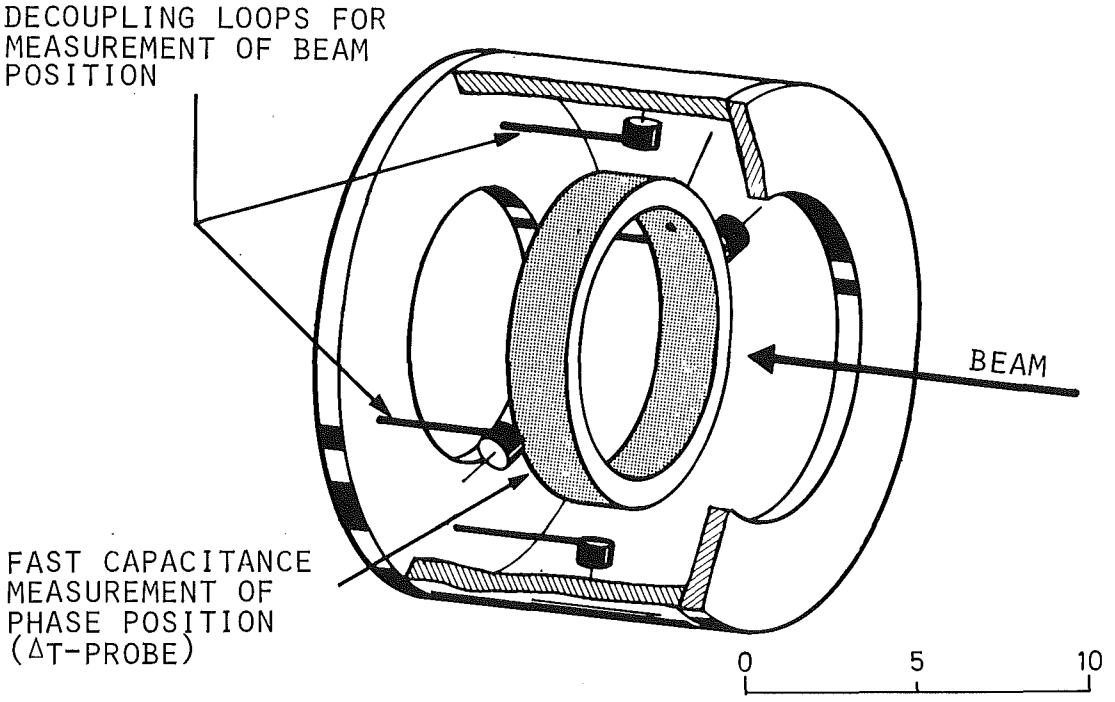

Fig. A 1.3-6: Δt-probe and non-interrupting position measurement

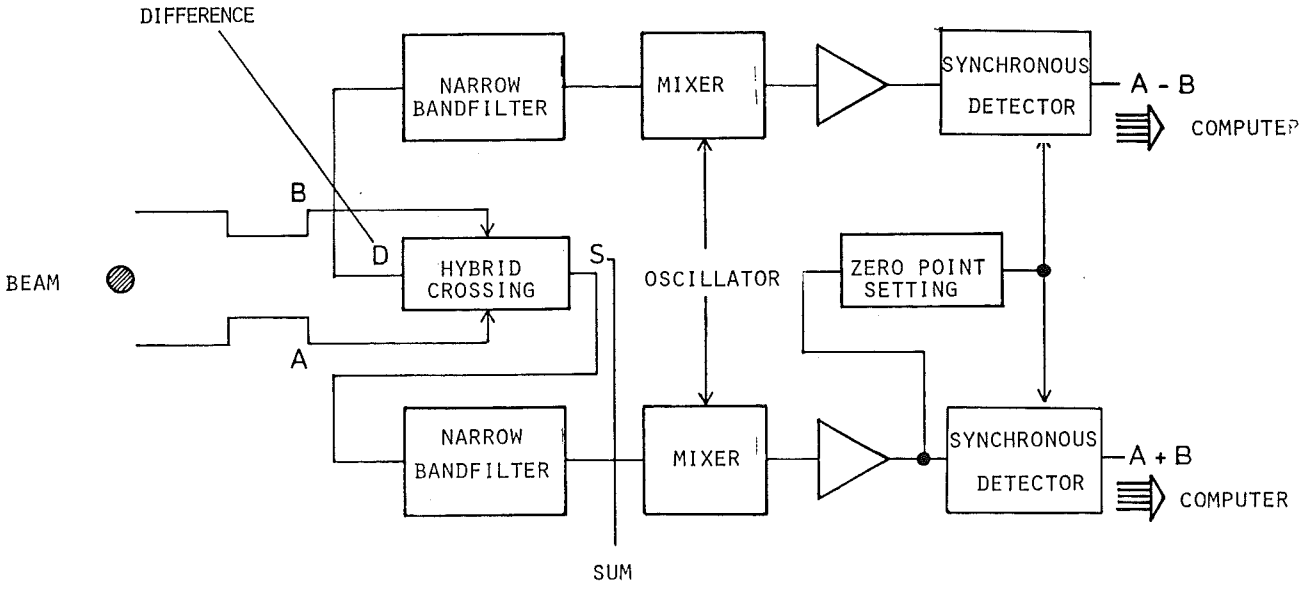

Fig. A 1.3-7: Detection electronics for measurement of the position (non-interrupting) according to the heterodyn principle

1.3.4 Measurements in the Longitudinal Phase Space

The accurate setting of the rf-accelerator structures, of the bunchers and rebunchers, calls for the most accurate possible knowledge of the beam intensity distribution in the longitudinal phase space. On account of the large expenditure, a complete measurement of the emittance in the (W, φ)-space was dispensed with, which is e.g. performed at the 50 MeV Linac at CERN /17/. With the help of the methods described the following tasks shall be solved:

- adjusting the bunchers in the low energy and beam matching ranges

- setting the rf-accelerator structures with respect to the amplitude and phase.

The requirements for measurement of the beam time structure result from the fact that the beam at the input of the Alvarez structure is initially compressed by the buncher system to about 70^{o} (1.8 ns). In the course of acceleration the phase width is reduced adiabatically. This means e.g., that the beam behind the Alvarez accelerator has already been compressed to about 0.4 ns. To measure the real phase width a detector should be used whose rise time reaches at least half the value of the variable to be measured. Assuming that the rise time τ_A/ns and the band width f_B/GHz are interconnected according to $\tau_A \times f_B \approx 0.35$ the requirement of about 2 GHz bandwidth is obtained for the detection behind the Alvarez unit. This constitutes the limit of fast real time oscilloscope presently on the market but it is no problem with sampling oscilloscopes.

Capacitive probes are proposed as measurement transducers /18/. But in the low energy range a coaxial Faraday cup should be used during the building up phase to have a cross check with the capacitive probe to be provided there.

Neither method is capable of furnishing quantitative statements concerning "tails" in the longitudinal phase space. For this purpose a method employed at Los Alamos, the so-called phase scanning, seems to be better suited. Therefore, it will also be described below.

Coaxial Faraday Cup for Measurement of Phase Profiles

The Faraday cup developed with GSI can be used after minor modifications have been applied /19/. The ions (450 keV) directly hit the front face of a coaxial cup inner conductor (50Ω wave resistance). To suppress the secondary electrons and to shield the leading electric field of non-relativistic charged particles, an inner conductor will be provided and a grid which can be connected with a low impedance high voltage source.

Capacitative Probe for Measurement of Phase Profile

The decoupled current can be calculated for a cylindrical probe of the length L and the radius r_o to be:

$$i(t) = \varepsilon_0 \frac{d}{dt} \int_{z=0}^{z=L} E_r (r=r_0)\, 2\pi r_0\, dz$$

The following facts must be taken into account when fixing the optimum probe geometry /20/.

If β and r_0 are given, the signal shape and amplitudes depend mainly on $L/\beta c\,\Delta t$ (probe length/geometric bunch length).

Shorter probes provide a better image of the bunch shape but a smaller signal amplitude must be expected in this case.

In a high current accelerator the time resolution may be improved by a short probe length (5 mm) at the expense of a relatively small signal amplitude.

There are different possibilities of determining the bunch width Δt from the signal development. For the bunch width of 1.8 ns at the input of the Alvarez system the bunch width Δt can be determined with good accuracy from the following relation:

$$\Delta t \approx \frac{2 u_{max}}{-(du/dt)_{u=0}}$$

where u_{max} is the maximum value of the measured signal amplitudes and $(du/dt)_{u=0}$ the slope at the point of signal zero crossing.

For pulse widths corresponding to that in the Alvarez accelerator it is recommended to make a Fourier analysis of the probe signal by means of a spectrum analysis and to determine Δt from the development of the amplitude spectrum in the frequency range /20/.

Phase Scanning for Measurement of Phase Profiles /21/

Linear accelerators posess a well defined (W,φ)-range in which they are capable of accelerating particles (acceptance). Such a range has been represented in Fig. A 1.3-8. If one varies the phase of an accelerator tank and measures at the same time the intensity at the nominal energy fixed A 1.3-8 will be found. Signal differentiation along the front ABC yields the phase width of the bunch. The nominal energy can be either determined by introduction of an absorber layer behind the structure, which corresponds to the nominal energy, or by magnetic analysis of the beam. In our case it is advisable to use the deflecting magnets to the beam catchers.

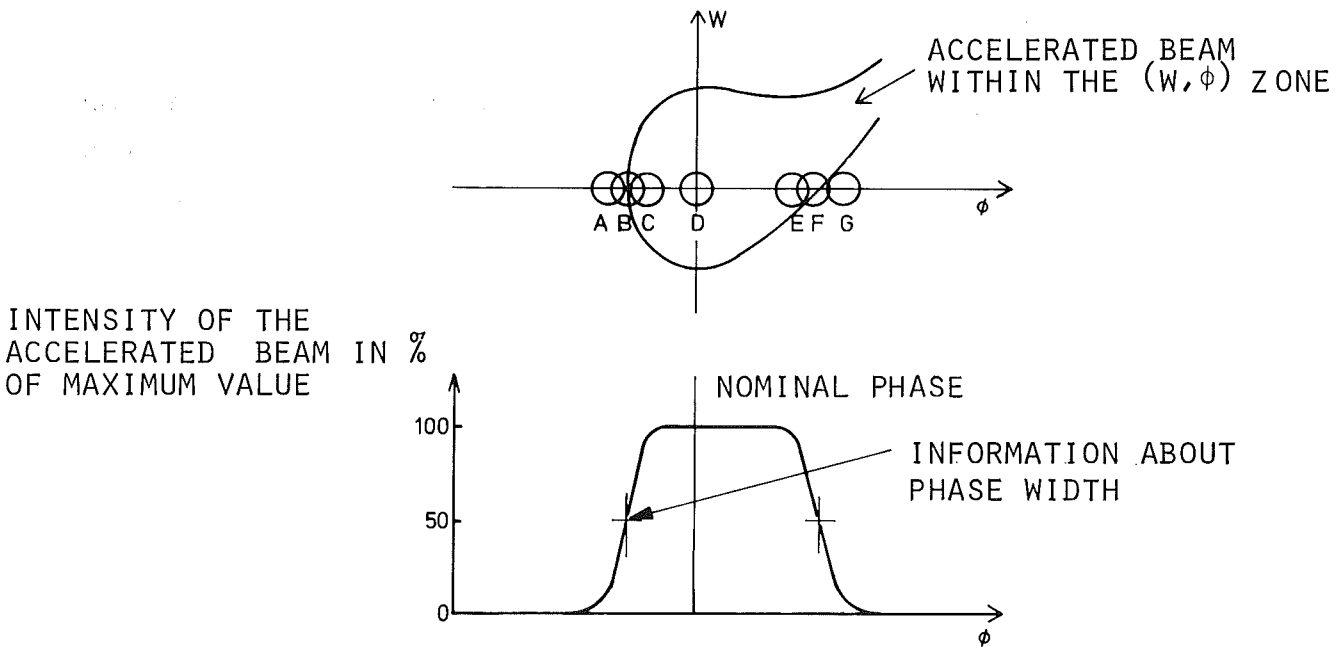

Fig. A 1.3-8: Principle of phase scanning for measurement of the phase width and the phase acceptance

Δt-Probes /22/

Δt-probes are plain ring capacitors (Fig. A 1.3-6) which filter out the fundamental wave from the microstructure of the bunches (signal amplitude 0.1 mW per 10 mA of peak current). Precise comparative measurements of phases relative to the phase axis (Fig. A 1.3-9) allow the measurement of the energy gain, the phase position of the bunches, and the absolute energy in the respective accelerator tank. The measurement procedure requires that all structures preceding the tank position N_o under consideration have already been adjusted and that all tasnks $N > N_o$ have been turned off. The interesting times t_B and t_C are determined from comparative measurements with the tank N_o turned on and turned off, respectively, in ortder to eliminate the effects of differences in the delay times:

$$t_B = t_{AB,\,off} - t_{AB,\,on}$$

$$t_C = t_{AC,\,off} - t_{AC,\,on}$$

Where t_{AB} and t_{AC} are the times of flight of the bunch from A to B to C.

It can be expected from experience gathered at Los Alamos that the time t_B and t_C can be measured with the accuracy of 13 ps (≙ 0.5° at 108 MHz) in a reproducible manner.

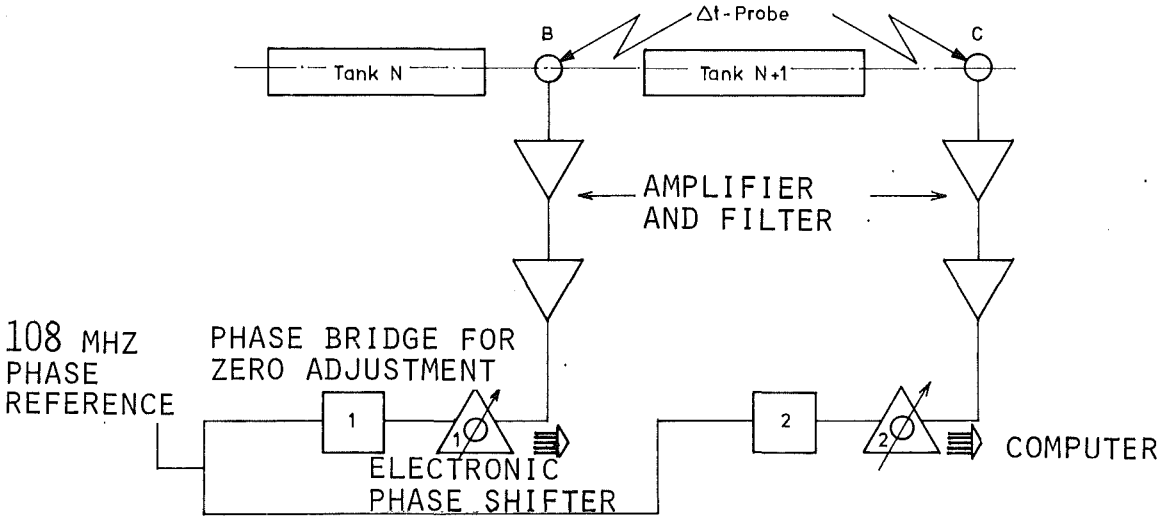

Fig. A 1.3-9: Principle of phase position measurement with the Δt-probes

1.3.5 Beam Loss Measurements

Loss monitors are installed at significant points along the accelerator. By detecting secondary radiation (fast neutrons and x-rays) these monitors are to solve the following tasks:

- Measurement of the loss profile along the accelerator

- fast ($\leq 3\,\mu s$ response time) detection in case the tolerable current losses are exceeded

- precise measurement of the dependence on time of the beam current losses in the macro structure (beam-loading-effects).

In principle, cheap ionization chambers or simple liquid scintillators can be used as measurement transducers. Unequivocal arguments in favor of one or the other system cannot be derived from experience gathered at Brookhaven (ionization chambers) /23/ and at Los Alamos (scintillators) /24/. The major arguments in favor of the ionization chambers are:

- long-term stability of the response sensitivity due to the plateau

- the high resistance with respect to radiation damage.

At Los Alamos, where very extensive beam loss diagnosis is performed, the arguments in favour of the scintillators are:

- fast response times ($\leq$100 ns)

- simple variability (change of voltage at the photo multipliers) of the sensitivity over several orders of magnitude.

The scintillator photo-multiplier system is more flexible in every case, which is certainly an advantage in the adjusting and training phase at the linear accelerator. Therefore, a simple system of this type is proposed (Fig. A 1.3-10).

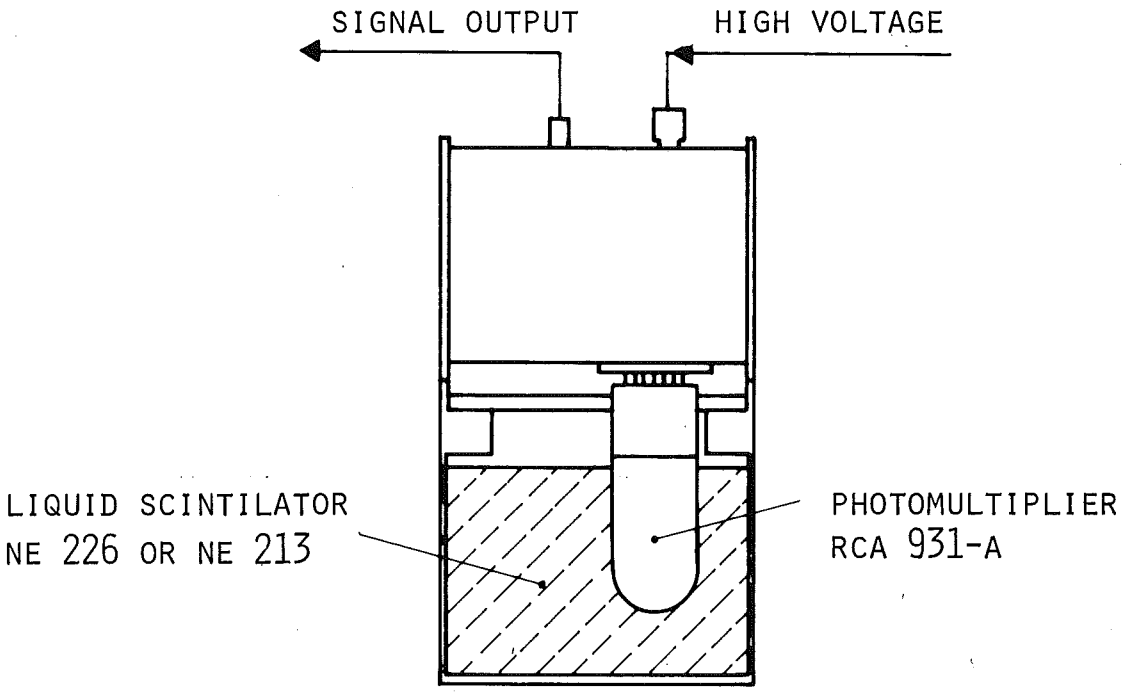

Fig. A 1.3-10: Simple scintillation measuring system for loss measurements.

1.3.6 Arrangement of the Beam Diagnosis Elements along the Accelerator

The diagnostic elements compiled in Table A 1.3-1 have been arranged along the accelerator as shown in Fig. A 1.3-11. An attempt was made to improve the reliability of results by providing for some measurements to be made at the same point using different techniques. Examples are:

- phase profile measurement at the input of the Alvarez accelerator through a coaxial Faraday cup and a fast capacitance probe

- emittance measurement at the output of the Alvarez accelerator through a conventional slit detector configuration and tomography

- position measurements in the DAW range through wire scanners and the non-interrupting inductive techniques.

In the Alvarez zone several diagnostic elements had to be combined in a vacuum chamber between the tanks (Fig. A 1.3-12). The consequence of this was that a number of measurements can be performed only as alternatives. For the DAW zone a somewhat simpler but compatible vacuum box is planned. All diagnostic boxes except for the boxes following the first two Alvarez-tanks can be replaced by remote handling.

The beam loss monitors are installed in the upper part of the shielding protecting the service tunnel.

1.3.7 Concluding Remarks

The beam diagnostics for the linear accelerator can be largely performed by instruments with which experience has been gathered in operating comparable facilities. It is not of major importance for the planned diagnostic elelemts whether the facility is operated with H^- or H^+ ions.

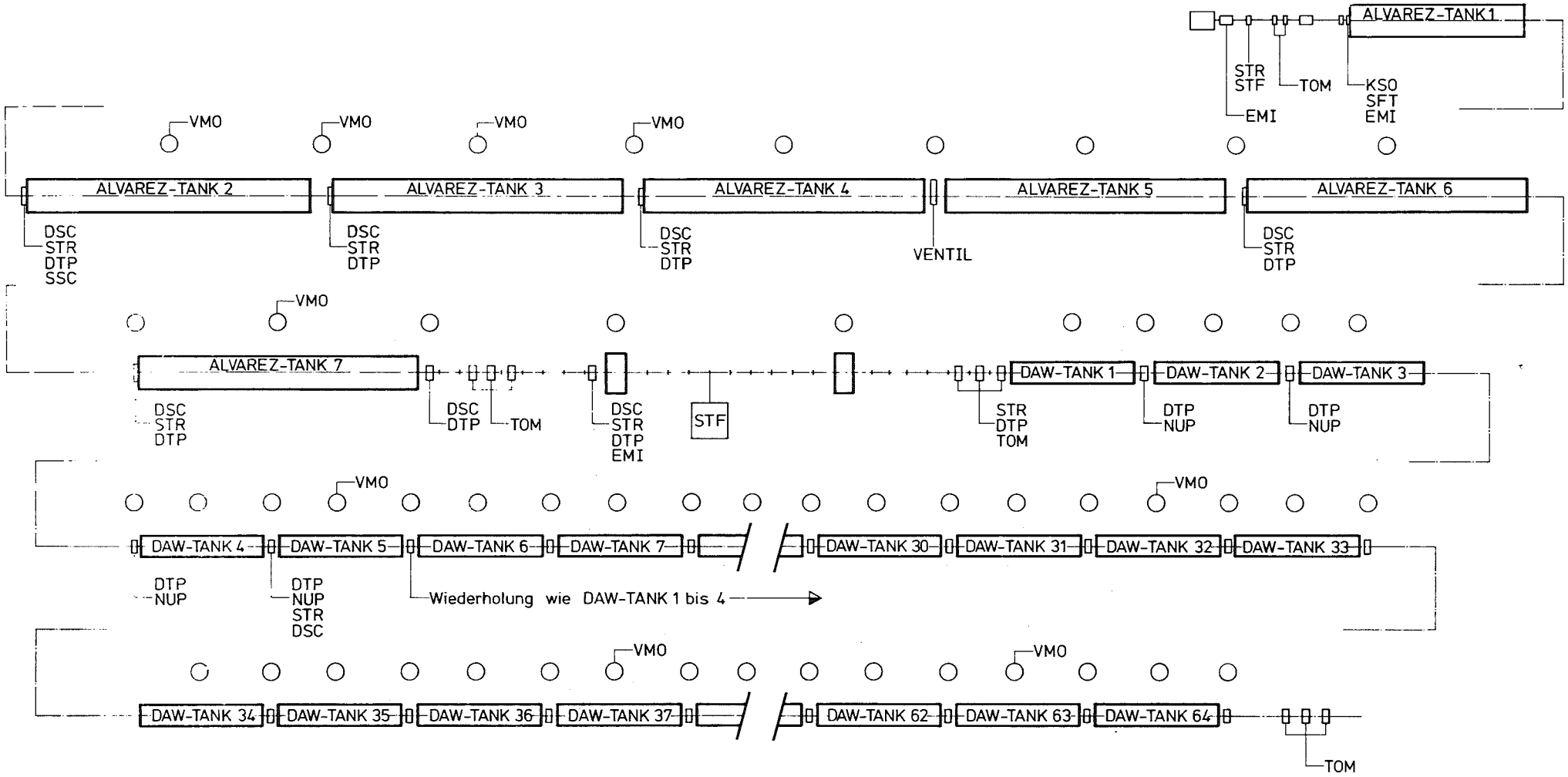

STR = BEAM TRANSFORMER
EMI = EMITTANCE MEASURING UNIT
STF = BEAM CATCHER
KSO = CAPACITIVE PROBE
SFT = FAST FARADAY CUP
VMO = LOSS MONITOR

SSC = SCRAPER
NUP = NON INTERCEPTING POSITION MONITOR
TOM = TOMOGRAPHY
DSC = WIRE SCANNER
DTP = Δt-PROBE

Fig. A 1.3-11: Arrangement of diagnostic elements in the accelerator

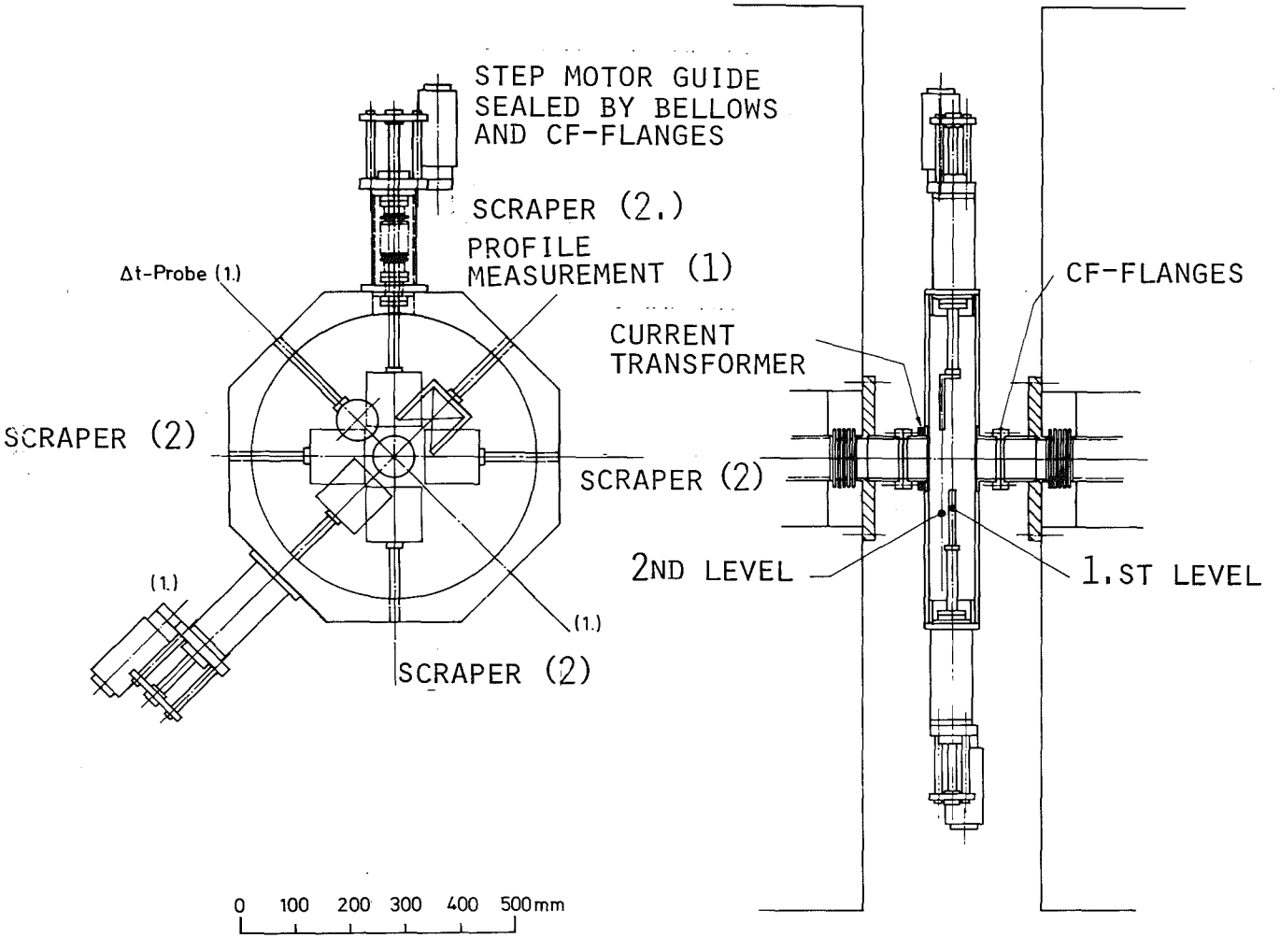

Fig. A 1.3-12: Diagnostic box for the Alvarez accelerator

Table A 1.3-1: List of Diagnostic Elements

Parameter	Method	Specifications	Location and Number
Beam current	Beam transformer	Bandwidth 10 MHz	2 low energy range 5 Alvarez acc. 7 D + W acc. 3 high energy beam transport area
Transversel emittance	Slit system with 32 detectors	Angular range ± 20 mrad Angular resolution 1 mrad Local resolution 0.1 mm Sensitivity 1 nA (detector)	2 low energy range
	Energy degrading slit with wire scanner	Angular range ± 15 mrad Angular resolution 0.1 mrad Local resolution 0.1 mm Sensitivity 100 nA (detector)	1 matching section (105 MeV)
	Three locations wire scanner (tomography)	Local resolution 0.1 mm	2 matching section (105 MeV) 1 high energy beam transport area
Position and profile	Wire scanner	Local resolution 0.1 mm Sensitivity 100 nA	5 Alvarez acc. 15 D + W acc. 6 high energy beam transport area
	Inductive position measurement	Local resolution for center of gravity 0.1 mm	16 D + W acc. 6 high energy beam transport area
Phase position and phase profile Energy gain	Coaxial Faraday cup	Time resolution 250 ps	1 low energy range
	Fast capacitance probe	Time resolution 250 ps	1 low energy range 2 matching section (105 MeV)
	Phase scanning t-probe	Time resolution 100 ps Time resolution 13 ps	6 Alvarez acc. 57 D + W acc.

But already it can be predicted that the aims of

- measurement with full scanning ratio

- increase in accuracy

- shortening of measuring time

call for the development of additional diagnostic elements parallel to routine operation.

Contributors

W. Kneis, H. Schweickert

References

/ 1/ R. Witkover: Proc. 1972 Linear Accelerator Conf., Los Alamos, p. 54

/ 3/ Andrew A. Browman, LANL, private communication

/ 4/ P. Brummer: "The Method of Measurement of the Emittance and the Betatron Phase Space Parameters in the Beam Transfer System of the ISR", CERN-ISR-OP/72-6

/ 5/ J. Parain: "Comparaison de deux méthodes pur mésurer l'émittance d'un faisceau", mars 1970, private communication

/ 6/ J.J. Livinggood: "Cyclic Particle Accelerators", D. van Nostrand Company, Inc., p. 314 f

/ 7/ J. Guyard, M. Weiss: Use of Beam Emittance Measurements in Matching Problems", 1976 Proton Linear Accelerator Conf., Chalk River, Ontario, Canada

/ 8/ J. Knott, M. Weiss, CERN: "Review of Results from the 500 keV Measuring Programme", private communication

/ 9/ L.R. Evans, D.J. Warner: "A Critical Study of Emittance Measurements of Intense Low Energy Proton Beams", Nucl. Inst. Meth. 104 (1972), 61-70

/10/ G.W. Wheeler, K. Batchelor, R. Chasman, P. Grand, J. Sheehan: "The Brookhaven 200 MeV Proton Linear Accelerator", Particle Accelerators 1979, Vol. 9, pp 1-156

/11/ John S. Fraser, LANL: "Beam Tomography or ART in Accelerator Physics", private communication

/12/ O.R. Sander, G.N. Minerbo, R.A. Jameson, D.D. Chamberlen: "Beam Tomography in Two and Four Dimensions", 1979 Linear Accelerator Conference, Montauk, BNL 51 134

/13/ N. Fewell, R. Witkover: "Beam Diagnostics at the BNL 200 MeV Linac", 1972 Proton Linear Accelerator Conf., Los Alamos

/14/ G.H. Mackenzie: "Beam Diagnostic Technique for Cyclotrons and Beam Lines", IEEE Transactions of Nuclear Science, Vol. NS-26, No. 2, April 1979

/15/ E.W. Hoffmann, LANL, private communication

/16/ P.J. Tallerico, LANL, private communication

/17/ P. Tetu: "New Linac Three Phase Planes Pulsed Emittance Measurements", 1979 Linear Accelerator Conference, Montauk, BNL 51 134

/18/ J.H. Cuperus: "Monitoring of Particle Beams at High Frequencies", Nuclear Instruments and Methods 145 (1977), 219-231

/19/ A. Nicklas, P. Strehl, H. Vilhjalmsson: "Strahldiagnose im Mikrostrukturbereich am UNILAC", GSI-PB-5-75

/20/ P. Strehl, J. Klabunde, V. Schaa, H. Vilhjalmsson, D. Wilms, GSI: "Phase Probe Measuring System in the Unilac", LATR-80-43

/21/ D.A. Swenson, LANL, private communication

/22/ D. Morris, LANL, private communication

/23/ J. Balsamo, N.M. Fewell, J.D. Klein, R.L. Witkover: "Long Radiation Detector System for Beam Loss Monitoring", IEEE Transactions on Nuclear Science, Vol. NS-24 (1977), 1807

/24/ A.R. Swanson, R.E. Hill: "LAMPF First-fault Identifier for Fast Transient Faults", IEEE Transactions on Nuclear Science, Vol. NS-26, No. 3, June 1979

A 1.4 Injector

A 1.4 Injector

1.4.1 Design Criteria

The part of the accelerator from the ion source up to the low energy beam transport system (LEBT) is here refered as injector. The "injection" of the rf-accelerator includes the LEBT, which was described in chapter A 1.2. The injector in particular consists of an ion source of the magnetic multipole type, an extraction system, the ion source beam transport system, the accelerating column, and the high voltage generator. The parameters of the injection system were chosen in order to fulfill the requirements of the rf-accelerator and to guarantee a reliable operation within the current state-of-the-art. The stability of the beam parameters during a beam pulse is of special importance for low beam losses in the accelerator. A normalized transverse emittance of 1 to 3 π mm mrad with a homogeneous intensity distribution is required.

When changing the ion, source the beam parameters have to be reproducible in a short time ($\sim$ a few hours). The macropulses are finally formed by a fast kicker in the LEBT (s. chapter A 1.7), but an additional pulsing of the ion source is foreseen to reduce the loading of the source and of the components in the beam line.

The parameters following from these requirements are summarized in Tab. A 1.4-1. They will be justified in the following sections.

1.4.2 The Principal Arrangement of the Injector and the Choice of Injection Energy

Limiting Effects

The experiences in the different laboratories (1,2,3) show that the number of high voltage breakdowns increases with increasing ion current and with increasing high voltage. High voltage breakdowns cause short interruptions of the accelerator operation. A breakdown may happen between the high voltage electrodes or along the surface of the ceramic insulator.

Ion Species	Protons
Injection Energy	450 keV
Energy Stability	$\pm$ 2.5 • 10^{-4}
Proton Current at the Entrance of the rf-Accelerator	$\sim$120 mA
Pulse Length	500 µsec
Repetition Rate	100 Hz
Type of Ion Source	Magnetic Multipole Source
Required Proton Beam Current out of the Source	150 mA
Total Ion Beam Current out of the Source	250 mA
Proton Content in the extracted Beam	$\geq$ 60 %
Extraction Voltage	$\leq$ 50 kV
Extracted Pulse Length	$\sim$1000 µsec

Table A 1.4-1: Parameters of the Injector and of the Ion Source

Breakdowns between electrodes are induced by electrons or ions hitting the surface of an electrode. Breakdowns along an insulator are related to a charging of the insulator surface by production of photo-electrons by bremsstrahlung from backstreaming electrons. The backstreaming electrons result from ionization of the residual gas and from secondary electrons caused by energetic particles striking the electrode surfaces. Designs of an electrostatic preaccelerator for high ion currents must include good vacuum conditions and a careful beam transport in the accelerating column to reduce the number of backstreaming electrons.

The Arrangement of the Ion Source and the Accelerating Column

Electrostatic acceleration may be achieved in one or two stages. In a one-stage arrangement the beam is extracted and accelerated up to the full energy in the same accelerating column. In a two-stage accelerator, the ion beam is extracted out of the source at low voltage ($\leq$ 50 kV), separated in a bending magnet, and then postaccelerated up to the desired energy in a high voltage column. For accelerating higher currents, a two-stage acceleration seems to be more advantageous for the following reasons /4,5/:

- The extracted ion current can be matched to the ion beam transport system by varying the extraction voltage ($I \sim U^{3/2}$). The total energy is kept constant by a corresponding voltage change of the postaccelerator section.

- The ion beam transport system, which follows the extraction system, may be used for matching the beam to the accelerating column. By removing the beam halo at the entrance of the accelerating column, beam spill in the column is reduced.
- Only the desired proton beam will be accelerated in the column. The parasitic ions, H_2^+ and H_3^+ as well as ions of impurities will be removed in an analysing magnet after extraction.

- A vacuum valve may separate the accelerating column from the ion source. This improves maintenance of the ion source.

A two-stage arrangement has the following disadvantages:

- At the low extraction energy ($\leq$ 50 keV) the beam can only be transported with a high degree of neutralization. Transporting a neutralized beam especially through magnetic transport elements may result in an emittance growth by beam-plasma oscillations /6,7/.

- A two-stage system is more complex. On the high voltage platform an extraction power supply, vacuum pumps and several beam transport elements are needed in addition.

Summarizing the arguments, one can say, that a two-stage arrangement allows safer operation mainly because of a reduction of the number of backflowing electrons in the accelerating column. The possibility of matching the beam to the different components also guarantees more reproducible beam properties. Furthermore, use of a low noise ion source, for instance the magnetic multipole source, should reduce the risk of beam-plasma oscillations in the neutralized beam.

Injection Energy

A high injection energy is desirable to reduce the beam dynamic problems at the beginning of the rf-accelerator (s. chapter A 1.2). As mentioned before, an upper limit for the high voltage is given by the increased number of breakdowns reducing the availibility of the accelerator. Taking into account the experience of other laboratories, the injection energy was chosen to be 450 keV for the discussed design. Table A 1.4-2 summarizes the parameters of some typical electrostatic accelerators. The electrostatic injectors used for the high energy accelerators, for example at CERN or at LANL, are operated at 750 keV /10/. The average current of these accelerators is up to a few orders of magnitude lower than the values discussed here. Consequently, experiences gained at these accelerators, are not directly transferable to our design. Three electrostatic accelerators were described /1,2,11/ which operate with energies above 350 keV and with continuous currents between 40 and 300 mA. The most reliable machine was operated about 10 years ago in the DCX 2 project at Oak Ridge. Ion currents up to 300 mA were accelerated to 600 keV /11/. Unfortunately, this accelerator is no longer in operation and detailed

Lab. or project	Achieved performances: Voltage drop/kV	Achieved performances: Accelerated ion beam/peak/average resp. dc-values/ mA	Type of accelerator	Remarks on operation
Pulsed machines with low average current				
CERN /8,10/	750	500/0.05	one stage	required values were achieved, reliable operation
LAMPF /9/	750	28/2	one stage	required values were achieved, reliable operation, on average 1 breakdown per few hours
Continuous high current machines				
ORNL /11/	600	100 - 300	one stage	at 100 mA stable operation for days, at 300 mA about 1 breakdown/hour. The facility is no longer operational
CRNL /1/	700	40	one stage	about 1 breakdown/hour, the breakdown rate increases with increasing current or voltage
LLL /2,3/	380	80 - 100	two stage	acceleration of D^+, about 2 breakdowns/hour facility routinely used
SIN	860	15	two stage	under construction
Pulsed machines with high average current				
NEN /13/	780	80/8	two stage	under construction
SNQ	450	140/10 option 10 % 140/20	two stage	study

Table A 1.4-2: Parameters of some electrostatic accelerators

info rmation is missing. Two accelerators, built later at Chalk River /1/ and at Livermore /2,4/ have not achieved the reliability of DCX 2. At Chalk River, after a development work of several years, a 40 mA dc ion beam was accelerated up to 700 keV although the design values were 120 mA and 750 keV. In comparison, the electrostatic accelerator of the RTNS II source at Livermore works more reliably. Today, a cw-beam of 80 mA is accelerated up to about 380 keV. High voltage breakdowns appear every 1/2 hour on the average. A further increase of the voltage or the currents results in an increased number of breakdowns /3/.

Taking into account the stringent requirements on reliability for the SNQ and considering especially the experiences at Chalk River and at Livermore, we think that for the discussed project an injection energy of 450 keV can be realized reliably. After an adequate development time, an increase of the injection energy up to 600 to 800 keV should be possible which might result in a better beam quality in the rf-accelerator. Valuable experience for operation at higher voltages will be obtained from the SIN and NEN projects /12, 13/.

1.4.3 Description of the Components

Ion Source

In order to get 100 mA protons at the entrance of the rf-accelerator, about 150 mA H^+ have to be extracted out of the source (Table A 1.4-1), assuming a buncher efficiency of 80 %. Additionally, 10 % beam losses result from charge exchange processes with the residual gas and about 10 % of the beam is scraped off as beam halo on collimators. For a proton fraction of 60 % in the extracted ion beam a total current of 250 mA is required from the ion source. Several ion sources are able to produce the required ion currents. For the SNQ-project a magnetic multipole source /14,15/ was chosen. Some investigations on a duoplasmatron ion source for use at high duty cycles have been done. The results are reported in /16/. The advantages of a magnetic multipole source compared to a duoplasmatron are the following:

- The arc discharge is quiet. The extracted ion current has a noise level of less than 1 % (1 MHz bandwidth).

- The operation at high duty factors up to a continuous operation does not produce any problems. In an operating source, ion current densities up to 500 mA/cm^2 have been continuously generated over a surface of about 25 cm^2 /17/.

- The ion current density is constant over the extraction aperture. Therefore, the beam can be extracted nearly free of aberrations with reproducible beam properties.

- The mechanical set up and the operation of a magnetic multipole source is relatively simple. The fig, A 1.4-1 shows one of the ion source tested.

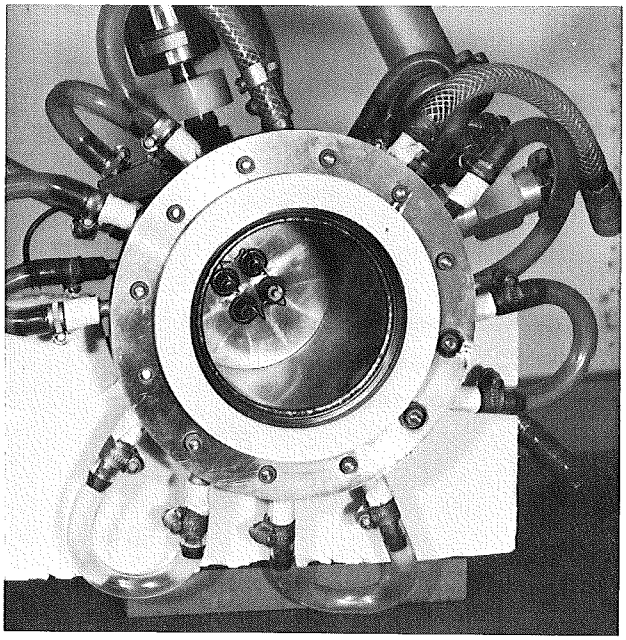

Fig. A 1.4-1: A cylindrical magnetic multipole source. The extraction electrode was removed.

Fig. A 1.4-2 shows a source with the extraction system schematically. In a cylindrical vessel the arc discharge is ignited between anode and cathode. To improve the ionization efficiency of the emitted electrons, the anode is surrounded by permanent magnets. The magnets produce a magnetic multipole field on the inner side of the anode. The cathode consists of heated tungsten filaments. Long term tests have shown /18/ that a lifetime of a tungsten filament of at least 2 weeks, presumably longer, is achievable.

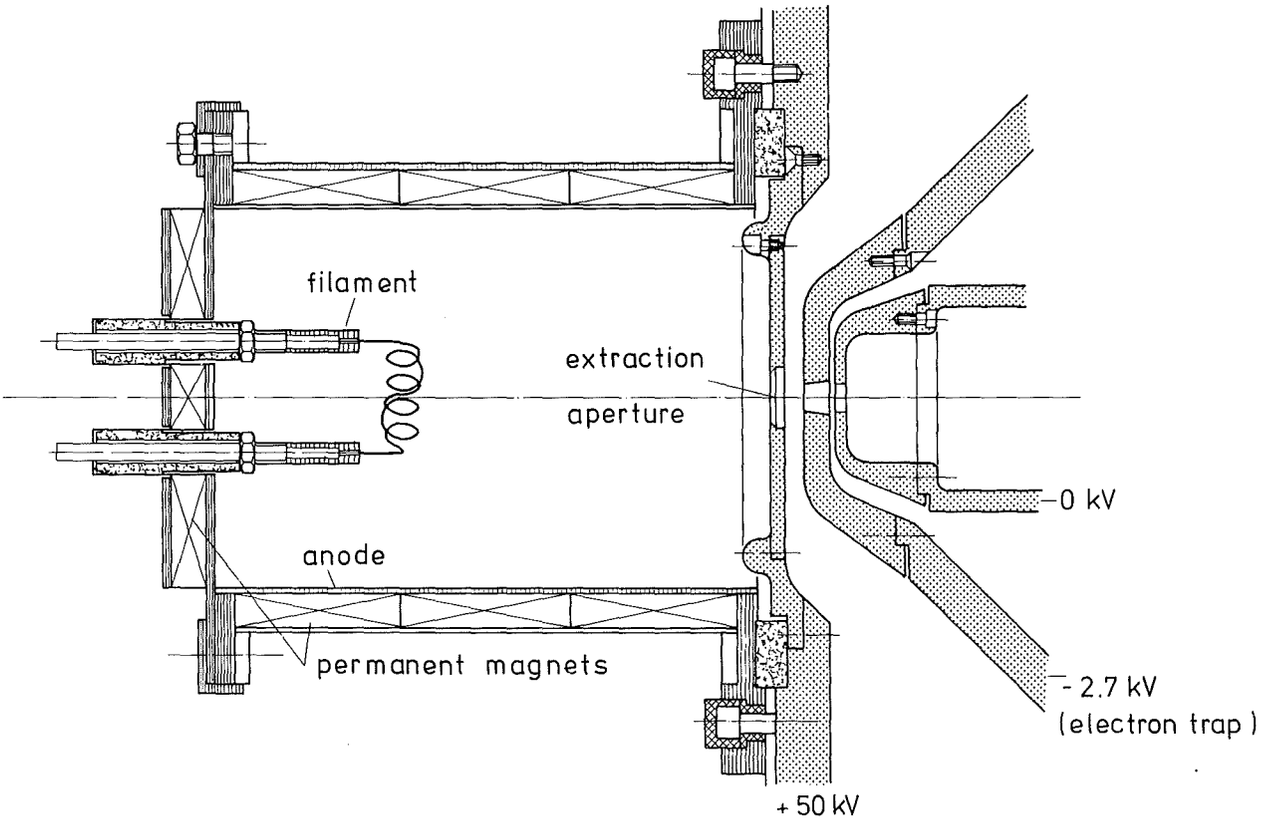

Fig. A 1.4-2: A schematic view of a magnetic multipole source with a 3-electrode extraction system.

Extraction

The 3 electrode accel-decel extraction system has been optimized with a computer code [x]). A 250 mA ion beam will be extracted out of a 13 mm aperture at an extraction voltage of about 50 kV. The maximum electric field between the electrodes is 87 kV/cm. Fig. A 1.4-3 shows the calculated trajectories.

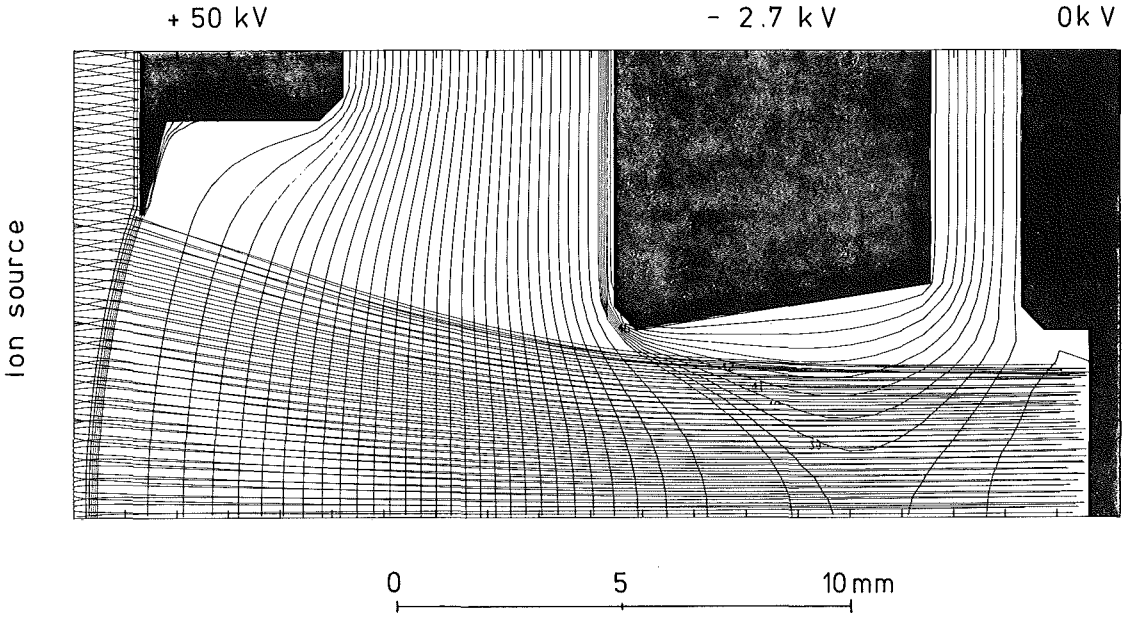

Fig. A 1.4-3: Beam forming in a 3 electrode extraction system. Extraction voltage = 50 kV, ion current density = 200 mA/cm^2, diameter of the aperture = 13 mm

The extracted beam has a divergence of less than 20 mrad. With an ion temperature of 0.7 eV /20/ a normalized rms-emittance of 0.05 π mm mrad was obtained. The emittance will, however, increase in the ion beam transport system and during the electrostatic postacceleration. From previous results a growth by a factor of 3 to 7 is expected. In case that the emittance at the entrance of the rf-accelerator should be too small, a multiaperture extraction system could be used. The emittance could then be varied by changing the diameter and the distances of the extraction apertures. Furthermore, in a multiaperture system the electric field could be lowered. Difficulties exist, however, to introduce multiple beamlets into the codes describing beam transport and beam dynamics. Preference was therefore given to a single aperture extraction.

[x]) ACEL-Code, CRNL-version, implemented by M.R. Shubaly, CRNL, and M. Rutz-Hochstrate, KfK

Pulsing of the Ion Source

The macropulse of the linear accelerator is produced by pulsing the discharge current of the ion source. To keep the beam parameters constant, the ion source pulses have to be longer than 500 μs by the rise time of the ion source. The final pulse will then be formed at the 450 keV by a fast beam deflector (s. chapter A 1.7). Chopping at 50 keV must be excluded because of the high space charge forces at that energy.

Ion Source Beam Transport System

In fig. A 1.4 a possible beam transport system between the ion source and the accelerating system is shown schematically. The extracted divergent beam is matched to the transport system by a solenoid. Leaving the solenoid, the beam is nearly parallel with a diameter of about 40 mm. The following beam transport system transfers the beam in a 1:1 scale to the entrance of the acceleration column. In addition to the solenoid, the system contains two quadrupoles, a 90^{o} - bending magnet and two further quadrupoles. A comparable system was optimized with the TRACE program [x]).

Quadrupoles destroy the rotational symmetry of the extracted beam. In the ideal case the rotational symmetry will be restored at the entrance of the accelerated column. The rotational symmetry can be preserved in a transport system, containing only solenoids and a bending magnet with a field index of 0.5. In a further optimization such a system will be tested.

The calculations have shown that with the proposed system (fig. A 1.4-4), at energies 50 keV, the ion beam can only be transported when the space charge forces are neutralized by at least 90 %. The neutralization of the beam results from the ionization of the residual gas /22/. The built-up time for that neutralization is determined by the ionization cross section as well as by the residual gas pressure. For a 50 keV proton beam the built-up time is about 30 sec at a pressure of 3×10^{-5} Torr. For a continuous ion beam a space charge neutralization of 95 to 99,9 % was observed /7,22/.

[x]) TRACE-calculations were carried out bei M. Weiss, CERN

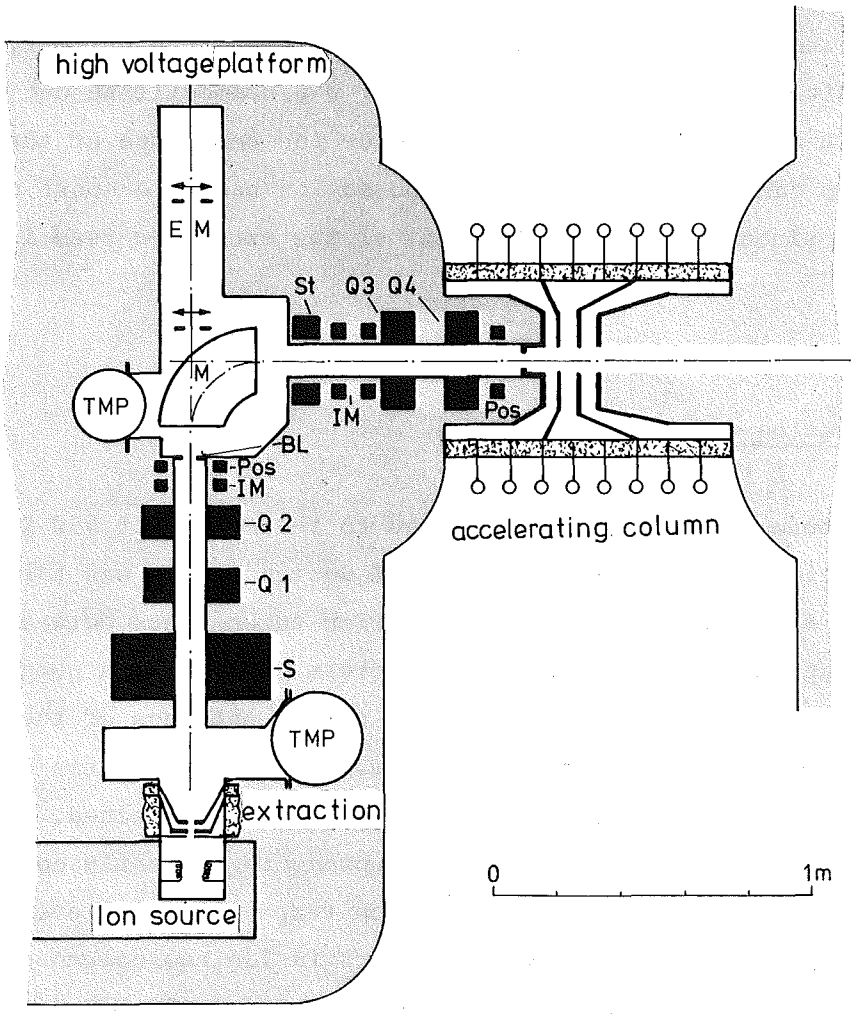

Fig. A 1.4-4: Ion source and the ion source beam transport system with the accelerating column. TMP = turbomolecular pump, S = solenoid, Q1-Q4 = quadrupoles, St = steering magnet, M = 90° bending magnet, IM = current transformer, Pos = beam position scanner, Bl = beam collimator, EM = emittance measuring device

Estimations from our measurements have shown a neutralization of at least 97 %. The total length between the ion source and the accelerating column is about 2.3 m. Ions are converted into energetic neutrals by charge exchange. On the way from the source to the column about 10 % of the ions are neutralized at a pressure of 3×10^{-5} Torr. Higher beam losses by charge exchange can be avoided by keeping the pressure low enough.

In addition to the focusing elements the beam line contains a steering magnet and some diagnostic elements for measuring the current, the profile and the position of the beam. The halo of the beam will be cut off by collimators. With an emittance measuring device the emittance of the total extracted beam can be measured. The proposed ion beam transport system is not achromatic, since the energy stability of the extracted beam is better than 2×10^{-3}.

The Accelerating Column

The proton beam will be postaccelerated to the energy of 450 keV in a high voltage accelerating column. The RTNS II design of LLL was followed closely /2/ for the following reasons: Acceleration takes place between electrodes with large apertures of 10 cm diameter. This gives a high pumping speed and minimizes beam spill on the electrodes. At the entrance of the column the beam is collimated to a diameter of 5 cm. With a vacuum pump on the ground side a vacuum in the column of about 10^{-6} Torr. is obtained. The total voltage is distributed over 3 accelerating gaps producing a nearly constant accelerating field of about 30 kV/cm. An electron trap (-15 kV) prevents electrons from flowing backwards. The beam transport inside the column was verified with a computer code /24/. The trajectories of a 150 mA, 50 keV proton beam, which is parallel at the entrance of the column, are shown in fig. A 1.4-5.

The beam transport inside the column is not free of aberrations. The effective emittance of the beam leaving the column is of the order of 0.5π mm mrad (100 %, normalized).

Techniques developed at CERN and for the RTNS II are suited for a detailed design of the SNQ column.

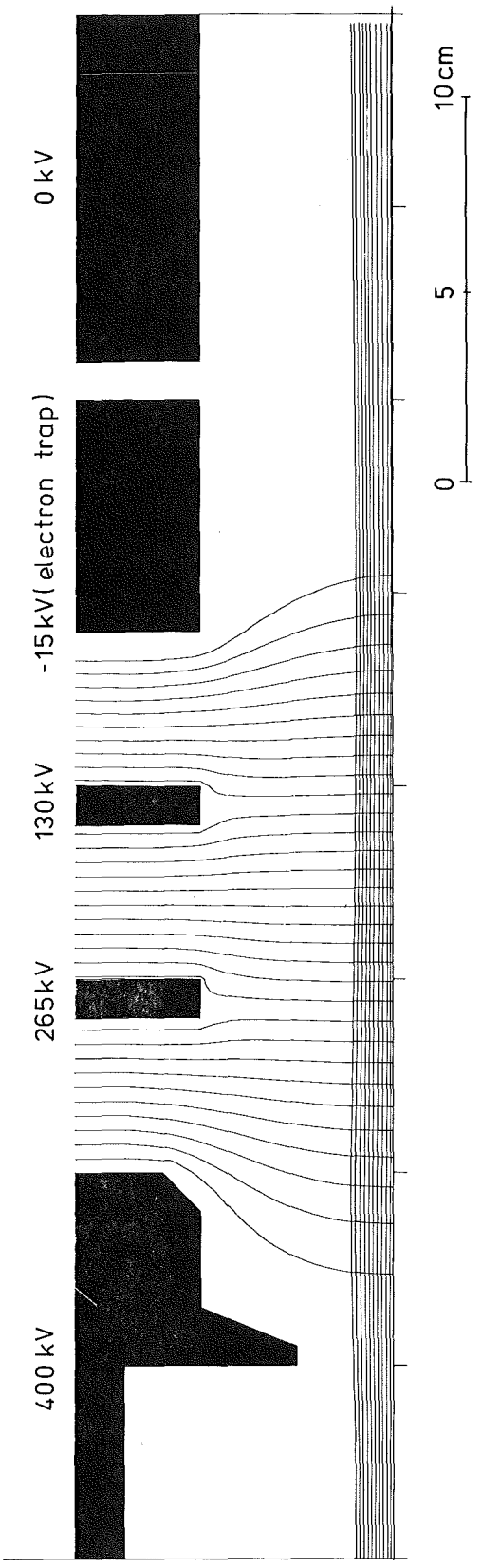

Fig. A 1.4-5: The trajectories of a 150 mA H^+-beam passing the 400 kV accelerating column

High Voltage Generator

The high voltage will be generated by a state-of-the-art Cockroft-Walton generator. Operated with a pulsed beam a stability of $\pm$ 2.5 x 10^{-4} can be achieved by use of a bouncer with a control time constant of about 60 μs /25/.

1.4.4 Consideration of the Options

No significant problems with the electrostatic acceleration are expected when increasing the duty cycle to 10 %. In order to generate a suitable 1000 μs beam pulse with the fast kicker, a pulse of about 1200 to 1500 μs has to be extracted out of the source and accelerated up to 450 keV. The corresponding average current in the accelerating column is 18 to 22 mA. The option of a higher average current was considered as an argument for a low injection energy. No additional problems are therefore expected in the electrostatic accelerator for the extended duty factor.

In converting the preaccelerator to H^--operation, the main problems are seen in the production of a suitable H^--beam /26,27/. In principle, magnetrons /28,29/ and magnetic multipole sources /30/ can be applied. H^--currents of the required order of magnitude have already been extracted from magnetron sources. But the properties of the extracted H^--beam (puls shape, noise, reproducibility) as well as the lifetime do not meet the requirements of the SNQ. An encouraging new development is the H^--source based on the magnetic multipole scheme /30/. First experimental results indicate that the SNQ-requirements of beam properties and lifetime may be easier to fulfill. In both cases development work of several years is needed to produce a suitable H^--ion source. Some modifications have to be made in the extraction system to match the H^--beam to the ion beam transport and to the accelerating column. The change of the polarity of the high voltage generator does not cause any problems. The vacuum requirements in the preaccelerator are similar as for acceleration of protons.

Contributors

P. Grundel, H. Oppermann, B. Piosczyk, G. Redemann (KfK);
M.R. Shubaly (CRNL)

References

/ 1/ J. Ungrin: "Voltage Breakdown Studies on a 750 kV High Current dc Accelerating Column", AECL-6584, Chalk River, Canada, December 1979

/ 2/ J.C. Davis et al.: IEEE Trans.Nucl.Sci., NS-26, No. 3, June 1979, p. 3058

/ 3/ D.W. Heikkinen: LLL Livermore, private communications, September 1980

/ 4/ J.E. Osher et al.: Proc. Prot. Acc. Conf., Chalk River, Canada, AECL-5677, 1976, p. 316

/ 5/ J.D. Hepburn et al.: "Future Development of High-Current dc Injectors for Accelerator-based Breeding Systems", AECL-6537, Chalk River, Canada, May 1978

/ 6/ M.V. Nezlin: Plasma Physics, Vol. 10, 1968, p. 337 - 358

/ 7/ J.E. Osher: Inst. Phys. Conf. Ser. No. 38, 1978, Chapter 5

/ 8/ M.A. Hone: "The Accelerating Column for the Preinjector of the New CERN Linac", CERN/PS-LR 79-38

/ 9/ R.R. Stevens Jr. et al.: Proc. Lin. Acc. Conf., Montauk, 1979, p. 465 BNL 51 134

/10/ C.D. Curtis: Proc. Prot. Lin. Acc. Conf., Chalk River, AECL-5677, 1976, p. 179 - 188

/11/ O.B. Morgan et al.: Rev. Sci. Instr., Vol. 38, 4, 1967, p. 467 - 480

/12/ M. Olivo et al.: IEEE Trans. Nucl. Sci., Vol. 26, No. 3, June 1979, p. 3930

/13/ R.F. Bantley: Proc. Lin. Acc. Conf., Montauk, 1979, p. 462

/14/ K.W. Ehlers et al.: Rev. Sci. Instr. 50 (11), 1979, p. 1353

/15/ A.P.H. Goede et al.: IEEE Trans. Nucl. Sci., Vol. 26, No. 3, June 1979, p. 3980

/16/ W. Eyrich: "Entwicklung einer Duoplasmatron-Ionenquelle für hohe Dauerströme", this study, part III A, vol. 1, unpublished

/17/ B. Piosczyk: " Eine zylindrische magnetische Multipolquelle", this study, part III A, vol. 1, unpublished

/18/ B. Piosczyk et al.: "Untersuchung der Lebensdauer von Wolfram-Kathoden in einer kontinuierlich betriebenen magnetischen Multipolquelle", this study, part III A, vol. 1, unpublished

/20/ A.J.T. Holmes et al.: Proc. Lin. Acc. Conf., Montauk, 1979, p. 424, BNL 51 134

/22/ A.J.T. Holmes: Phys. Rev. A, 19, 1, January 1979, p. 389 - 407

/23/ L.R. Evans et al.: IEEE Trans. Nucl. Sci., Vol. NS-18, No. 3, March 1971, p. 2068

/24/ D. Dirmikis: " A Computer Program for Numerical Analysis of Electron Flow Systems", Thesis, Univ. Sheffield, March 1975

/25/ M. Baumann, Basel, private communications, August 1980

/26/ S. Göring: "Literaturstudie über die Erzeugung eines H^--Ionenstrahls für den Betrieb eines Linearbeschleunigers", this study, part III A, vol. 1, unpublished

/27/ B. Piosczyk: "Stand der Entwicklung bei H^--Quellen, Bericht über eine USA-Reise", this study, part III A, vol. 1, unpublished

/28/ C. Schmidt et al.: IEEE Trans. Nucl. Sci., NS-26, No. 3, June 1979, p. 4120

/29/ J.G. Alessi et al.: "Regular and Asymetric Negative Ion Magnetron Sources with grooved Cathodes", BNL 27942, Brookhaven National Laboratory, 1980

/30/ K.W. Ehlers et al.: Rev. Sci. Instr., 51 (6), June 1980, p. 721 - 727

/31/ M. Shubaly: "High Current dc-Extraction Column Design", this study, part III A, vol. 1, unpublished

A 1.5 Accelerating Structures

1.5.1 Design Aspects

An Alvarez structure was chosen to generate the accelerating fields in the low energy part of the machine. At higher energies, a Disk-and-Washer structure (DAW) is used.

High shuntimpedances, simple fabrication, and, at least for the DAW, low dispersion were the major reasons for this choice. As particle losses can not be completely excluded, simple handling of components was a demand, enabling remote handling, if needed (ch. A 1.1).

Addition of an optional compressor ring requires, that H^--ions can be accelerated. A vacuum of about 10^{-8} mbar is needed to avoid neutralization in this case. These vacuum requirements have to be considered in the initial design.

1.5.2 Alvarez-Structure

The Alvarez accelerating structure is a "quasi-periodic" structure, excited in an E_{010}-field configuration. The "periodicity" arises from the drift tubes, which shield the particles from the rf field when the particles would be decelerated.

In order to get a high shunt impedance, the structure is excited in the 0-mode. Thus the dispersion is very high, i.e. low group velocity. This leads to a very strong dependance of the field distribution on fabrication tolerances, on transients and beam loading /1/.

1.5.3 Compensation of the Alvarez-Structure

In order to reduce this dependance, the operating mode has to become a centre-band mode. Another passband has to be produced which must be joined continuously to the operating passband. The second passband is generated either by using more than one stem per drift-tube (a stem-mode can then be excited), or by posts, which extend from the outer cylinder to the drift-tubes without touching the drift-tubes.

For "confluence" of the passbands the compensation-mode has to have the same frequency as the operating-mode for all different cell geometries.

Using a multistem structure, confluence can be achieved by varying the diameters of the stems. In a post-coupled structure distance between posts and drift-tubes is changed.

Though the compensation by stems seems to be more effective (the group velocity can be as high as .35 of velocity of light /2/), for the spallation neutron source the post coupled structure is favoured ($v_g/c = .1$). This enables simple installation of the drift tubes, because these are supported by girders and can easily be removed from the tank (ch. B 2.1).

As a further advantage, field flatness can be controlled in a post coupled structure. This is done by changing the coupling between adjacent cells by rotating excentric tabs at the end of the posts.

In order to minimize the coupling between posts and stems and to get a larger mode spacing around the operating mode, the posts should be positioned at 90^o with respect to the stems, each post alternating by 180^o from one drift to the next /2/.

1.5.4 Parameters of the Alvarez-Structure

Parameters of the 7 Alvarez tanks are listed in table A 1.5-1. The geometry and the rf-parameters were calculated with the computer-code "CLAS" of CERN /3/. The lengths of the tanks are determined by the requirement of good mechanical stability, of high shunt impedance and minimum interruption of the periodicity.

At the length of about 12 m chosen, rf excitation by two combined amplifiers is required, each producing an output power of 1.5 MW (ch. A 1.7).

The Alvarez-accelerator is operated at a frequency of 108 MHz. The reasons for the choice of this frequency are beam dynamics, available rf-power sources, and injection problems (ch. A 1.2).

Apart from the requirements of beam dynamics, by which the beam hole diameter and the synchronous phase are fixed, the geometry of the tanks was chosen to obtain a constant outer diameter for one tank and to optimize the shunt impedance (a conical layout of the drift tubes, which increases the shunt impedance by about 10 % /4/, is not yet included). The optimization of the shunt impedance requires a small diameter of the drift tubes. The outer diameter of the drift tubes chosen is given by the dimensions of the quadrupoles, which are installed in the drift tubes.

The accelerating field is defined by the maximum tolerable surface fields on the drift tube. In order to avoid a break down by electrical discharge, the electrical field amplitudes on the surface were limited by the Kilpatrik-criterion. This defines, according to present experience , a very conservative upper limit for electrical surface fields.

Following this rule, the field amplitude on the drift tubes of the Alvarez structure was limited to 12 MV/m, independent of the geometry.

Tab. A 1.5 - 1: Parameters of the Alvarez-Structure

Tank-No.	1	2	3	4	5	6	7
Injection energy /MeV	0.45	15.7	31.8	47.3	62.4	77.4	91.7
Tank length /m	11.20	11.48	11.67	11.80	12.16	12.14	11.79
Tank diameter /m	1.76	1.68	1.60	1.60	1.60	1.60	1.60
Drift tube diameter/ cm	33.8	30.0	30.0	30.0	30.0	30.0	30.0
Beam hole diameter/ cm	2.8..4.6	5.6	6.6	6.6	6.6	6.6	6.6
Gap / cell length	0.22..0.35	0.23..0.30	0.26..0.31	0.31..0.34	0.34..0.37	0.37..0.39	0.39..0.41
Transit-time factor	0.69..0.79	0.85	0.83	0.80	0.76	0.73	0.7
Number of cells	39	19	15	13	12	11	10
Average accelerating field / MV m^{-1}	2...2.2	2	2	2	2	2	2
Peak field / MV m^{-1}	12.2	12.2	11	10.5	10.5	10.5	10.,5
Dissipated power [r]/MW	1.50	1.30	1.38	1.43	1.52	1.55	1.55
Gain of beam power/MW	1.53	1.60	1.56	1.51	1.49	1.43	1.34
Length of quadrupoles/ cm	4.9..13.6	27	38	38	38	38	38
Quad. gradients/T m^{-1}	41..14.2	6.7	4.4	4.4	4.4	4.4	4.4
eff. shunt impedance/ MΩ m^{-1}	25.9	32.0	27.9	25.0	22.5	20.2	18.2

[r] Losses are calculated with a 20 % decrease of the theoretical Q.

1.5.5 Alignment Requirements

Beam loss may activate structures and beam tunnel to a degree, that access is limited or remote handling has to be provided. Under the design assumptions of this study (see Fig. A 1.1-1), activation beyond the limit for hands-on-maintenance is anticipated even for the Alvarez accelerator.

The accuracy of the alignment of the quadrupole magnets and the surrounding drift-tubes is of particular influence on the beam losses. It is, however, difficult to predict the magnitude of the beam losses due to misalignments. Qualitatively, a transverse displacement of a quadrupole magnet leads to a beam displacement, whereas a magnet tilt about a transverse axis or a rotation about the magnetic axis lead to an amplitude growth /6/.

Rotation of a quadrupole (by up to 25 mrad) can be easier tolerated as a radial displacement /7/. The values documented from experience /8,9,10/ differ, but are within a few tenths of a mm.

For the SNQ-linac, a displacement of neighbouring magnets by $\pm$ .2 mm is tolerated. Along a tank, deviations shall not exceed $\pm$ .5 mm. A higher precision for the alignment seems to be not realistic /8/, but presumably also not necessary.

Drift tubes are aligned individually by adjustment screws, situated on the girder and acting on the stems. The girder itself will be adjusted optically using a laser beam (ch. B 2.1).

Remaining misalignments are corrected by steering magnets. The number of the steering magnets and the distances between them have to be calculated in an optimization procedure.

1.5.6 Quadrupoles

The Alvarez-accelerator contains 112 drift tubes, each housing one quadrupole magnet. Another 14 magnets are placed in the half drift tubes of the endplates. To facilitate fabrication, the dimensions of the quadrupoles should not differ too much. The quadrupoles of the first drift tubes can, however, not be made identical, because of the varying diameters of the beam hole. The other quadrupoles are combined to three groups with different apertures.

About 10 magnets will be powered by one power supply. This makes it possible to vary the quadrupole gradient of all the magnets over a wide range, but also to vary the gradient of every quadrupole individually by about 10-20 %.

Because of the radiation, the windings of the magnets have to be insulated by radiation-resistent material. Mineral-insulated copper windings, as for example Al- or Mg-oxides, are a convenient choice /11,12/.

Use of permanent magnets /13,14/ from rare earth is not considered in this study because 1) a variation of the field strength is possible only via a mechanical device which looks complicated for a drift tube magnet and 2) operation experience under radiation is lacking.

1.5.7 Vacuum

For acceleration of protons a vacuum of about 10^{-6} mbar is sufficient. The scattering of protons is negligible at this pressure.

A much better vacuum is required for the acceleration of H^--ions. The electron is bound very loosely and may be lost by scattering at the molecules of the residual gas. The cross section for this neutralisation process is inversely proportional to the energy. For an energy of 800 MeV, e.g. the cross section is about 1.3×10^{-18} cm^2/molecule /15,16/.

The requirement that the losses due to neutralisation should be smaller than 1 W/m, which corresponds to the remote handling limit, leads to a vacuum of about 2 x 10^{-8} mb for the whole structure. Though the acceleration of H^--ions is foreseen only as a later stage, the demand for the vacuum has to be kept in mind for the accelerator design in order to avoid major modifications. Measurements in different laboratories /17, 18/ have proven that this vacuum can be obtained in the Alvarez-structure as well as in the DAW-structure, as described below.

The method for producing the copper surface was not yet decided. Two possibilities were discussed: either to use copper plated material /20,21/ or to electroplate /19/ a copper surface on other material. Because of the small penetration depth of the rf-field (about 7 m) a very small roughness is required. Experiments at small cavities have shown that both methods - copper plated material or an electroplated surface - are similar concerning the required outgasing rates (a few 10^{-11} mbar l/s cm^2) /8, 19/.

1.5.8 Biperiodic Structures

The shunt impedance of the Alvarez-structure decreases with increasing energy (Fig. A 1.5-1). Therefore, a different accelerating structure should be used at higher energies. This structure should have a high shunt impedance and a low dispersion, i.e. a high group velocity.

The first demand could best be achieved by excitation of the π-mode (each cell accelerates). But for this mode the group velocity vanishes. The second requirement is fulfilled for the $\pi/2$-mode, but each second cell does not accelerate. These "field-free" cells reduce the shunt impedance by a factor of 2 compared to the π-mode. The advantages of both modes can be combined if either the "field-free" cells will remain on the axis, but will be shortened (on-axis-coupled), or if they will be removed from the axis (side-coupled, ring-coupled structure).

The on-axis-coupled structure is developed at the Chalk River National Laboratory. In particular the problem is studied how to achieve a high group velocity without reducing the shunt impedance to an untolerable value /22,23/.

The side coupled structure /24,25/ is used for the 800 MeV-proton accelerator at Los Alamos. In principle it could also be used for this accelerator.

The Disk-and-Washer-structure was invented and first developed in the USSR /18, 26/. In this structure, the coupling cells are removed from the axis and enclose the accelerating cells (Fig. A 1.5-1).

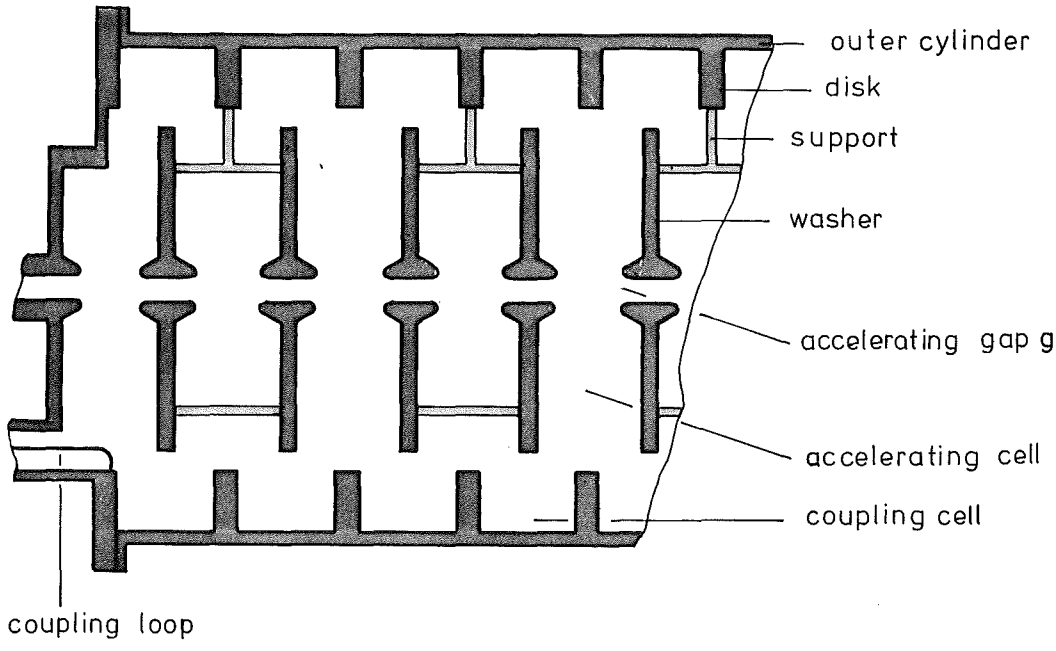

Fig. A 1.5-1: DAW-structure

As seen in fig. A 1.5-1, coupling between accelerating and coupling cells can be made very strong, and, compared to other structures, it can be increased by a factor 5-10. The coupling cell has a different geometry. This leads to the "bi-periodicity", for which the period length consists of two different cells. For the operating mode, the $\pi/2$-mode, a stop band in the dispersion diagram may occur (Fig. A 1.5-4). For this mode, two field distributions are possible. The frequency of the accelerating mode is determined by field configuration and frequency of the accelerating cells, the frequency

of the coupling mode is defined by the geometry of the coupling cell (Fig. A 1.5-2). In an ideal configuration, only the accelerating mode is excited. In a real accelerator, fields in the coupling cells are established by beam loading (ch. A 1.5-15) and by consequence of fabrication tolerances.

The existence of a stop band leads to a low dispersion. This can be avoided by choosing the eigenfrequencies of the coupling cells and the accelerating cells identical. The frequency gap vanishes and a finite group velocity is obtained.

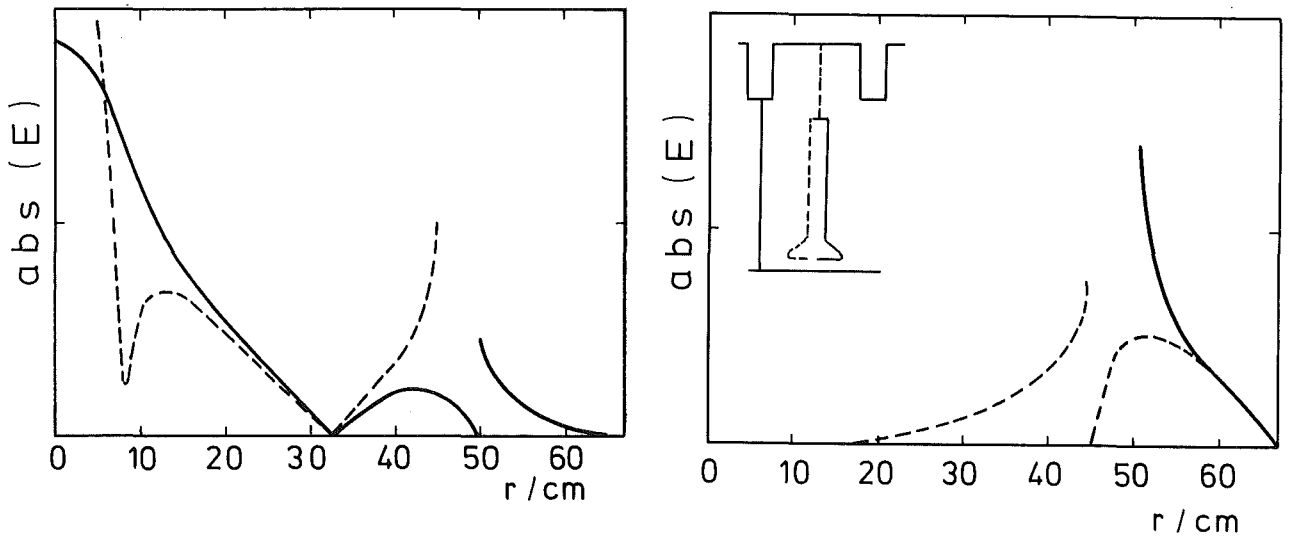

Fig. A 1.5-2: Absolute value of the electric field amplitude for the accelerating mode (left) and for the coupling mode (right) as function of distance r from the beam axis.

1.5.9 Choice of Structure for the High Energy Part

From 105 MeV up to the final energy of 1100 MeV the Disk-and-Washer structure was chosen. Compared to the side-coupled structure, operated at LANL, the following advatages are of importance:

1) For $\beta > 0.6$, the shunt impedance is higher /27/. This means: the dissipated power is about 16 % less and the required input rf-power is about 10 % less.

2) The coupling constant between neighbouring cells is very high. Thus the field amplitude is insensitive against manufacturing tolerances.

3) Apart from the supports of the washers, the structure has a rotational symmetry. So manufacturing should be cheaper.

4) The vacuum-conductance is higher (this is important for acceleration of H^--ions).

These advantages have to be compared to the disadvantage, that the DAW-structure is not yet fully developed and that there is no experience of operation with an intense beam.

The experiments performed until now do not indicate difficulties. In 1975 experiments with high power were done at the Radiotechnical Institute (Moscow) with a 20-cell-model, operated at 900 MHz /18/. After a short period (15 hours) of processing, an accelerating field of 3.6 MV/m was achieved and could be maintained without difficulties. The vacuum pressure was about 3×10^{-8} mbar.

Beam effects must be studied in future. First calculations show that a cavity-beam coupling, which decreases the beam quality to an intolerable extend, should not occur (ch. A 1.5.17).

An experiment with electrons simulating an ion beam /28/ is very time consuming, the extrapolation of the results to a real proton beam is difficult. Therefore, it is proposed to study the influence of the beam theoretically.

1.5.10 Transition Frequency; Transition Energy

The diameter of the DAW-structure, if operated at 108 MHz, would become very large ($\sim$4 m). Therefore, the DAW-structure has to be operated at a higher frequency. In addition, the shunt impedance increases with the square root of the frequency.

As discussed under beam dynamics (ch. A 1.2) a frequency step by a factor 3 is preferred

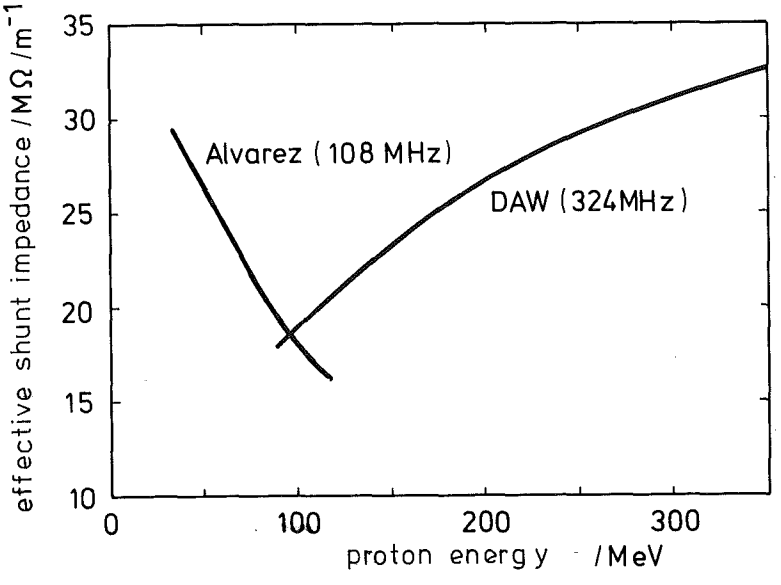

Fig. A 1.5-3: Shunt impedance for the Alvarez-structure (f = 108 MHz) and for the DAW-structure (f = 324 MHz) as function of the energy

From fig. A 1.5-3 it can be seen that the transition energy should be at about 100 MeV to get highest shunt impedance. Due to the modular design of the Alvarez-structure the transition energy was chosen to be 105 MeV.

1.5.11 Geometry of the Disk-and-Washer Structure

The geometry of the DAW-structure was calculated with the "Superfish" code /29/. The supports for the washers were not taken into account. Their influence has to be determined experimentally.

Shunt impedances were optimized in the design procedure. The main parameter of influence is the ratio of gap to cell length g/L /23/. In addition, the shunt impedance increases with the outer diameter of the tank. As a consequence of larger size, a decrease of the π-mode frequency follows (Fig. A 1.5-4), and mode-mixing with the operating mode may occur.

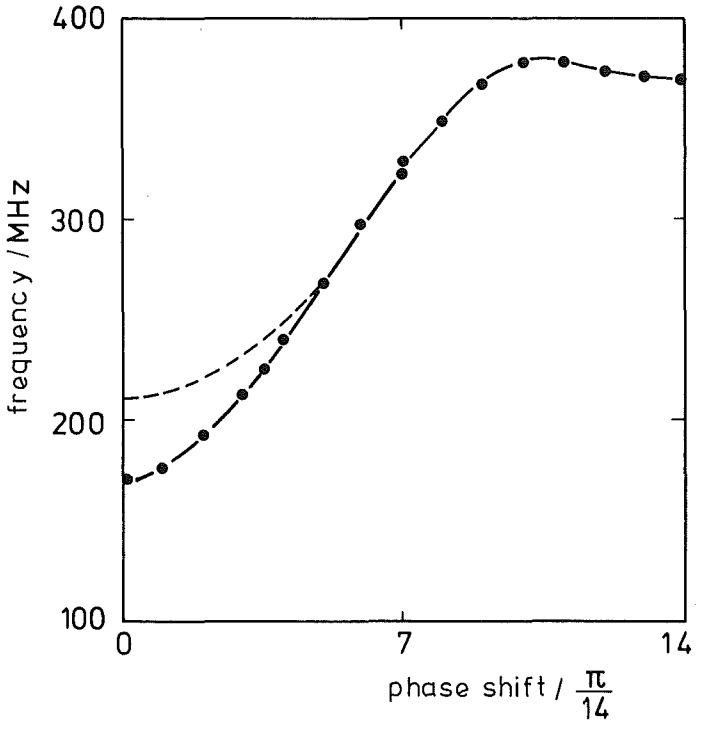

Fig. A 1.5-4: Dispersion curve of a DAW-structure (points). The dashed line shows a fitted dispersion curve that is used in the equivalent circuit for the determination of the manufacturing tolerances (ch. A 1.5.15).

In the design of the accelerator for the spallation source the diameter of the washers was chosen smaller than that of the disks, in order to fabricate the outer cylinder including the disks as one part (in sections of one full tank or half a tank) and to insert the washers into this prefabricated unit (ch. B 2.1).

An outer diameter of 134.8 cm was chosen. With this diameter, the loss of shunt impedance up to 600 MeV is less than 2 % and up to 1100 MeV it is less than 5 %, compared to higher diameters. For this selection the decrease of the π-mode frequency is also tolerable.

The other dimensions are determined by the requirement that the frequency gap be closed at the operating frequency of 324 MHz.

Table A 1.5-2 shows the parameters of the DAW-structure for different energies /30,31/.

1.5.12 Supports of the Washers

In the Los Alamos National Laboratory, experiments were performed to determine suitable supports for the washers /27/.

The mechanical most stable and simplest supports are radial stems connecting the washers to the outer cylinder. These stems influence the field distribution considerably, because electrical fields are short circuited. As a further result, the experiments have shown, that supports, assymetical with respect to the disks or the washers, lead to different coupling constants and to a perturbation of the field distribution. The most favourable support is the "T"-support, where two washers are combined by one or more stems. Each stem is radially fixed to a disk, the supports forming a T (Fig. A 1.5-1). Fig. A 1.5-2 shows that the stems can be placed between the washers at a location where the axial component of the electrical field vanishes. Also the radial part of the T can be placed in a region of zero electric field.

Tab. A 1.5 - 2: Geometry of the DAW-structure

Energy / MeV	109	177	325	376	533	900
Velocity v/c	0.445	0.54	0.67	0.7	0.77	0.86
Beam hole diameter / cm	7.0	7.0	7.0	8.0	8.0	8.0
Gap / cell length	0.300	0.353	0.425	0.461	0.499	0.535
Tank diameter / cm	134.8	134.8	134.8	134.8	134.8	134.8
Disk diameter / cm	96.22	99.04	103.38	104.3	106.9	110.6
Washer diameter / cm	90.12	87.72	85.0	84.4	82.6	79.66
Disk thickness / cm	3.95	6.12	9.94	10.75	13.2	16.42
Washer thickness / cm	3.0	3.0	3.0	3.0	3.0	3.0
Cell length / cm	20.58	24.98	31.0	32.4	35.62	39.8
eff. shunt impedance / $M\Omega m^{-1}$	22.9	29.0	35.9	35.2	38.25	41.8
Transit-time-factor	0.89	0.89	0.88	0.86	0.85	0.84
Unloaded Q-value / 10^3	44	54	69	72	82	95
Ep/E_o	5.38	5.07	4.76	4.20	4.38	4.29

An influence on the electric field distribution - except in the nearest vicinity of the stems - does not appear, the frequency of the structure will only be changed slightly by perturbation from the magnetic field. This effect can be calculated and corrected by a variation of the disk- or the washer radii.

1.5.13 Tank Parameters, Field Gradients

Tanks shall be made as long as possible for two reasons:

1) to avoid additional losses by end plates

2) because a high coupling constant maintains fixed phase and amplitude relations for acceleration.

Bridge couplers between the tanks are used in the PIGMI accelerator at LANL /33/. These bridge couplers introduce strong coupling and, at the same time, house focusing, tuning elements and rf-couplings.

For the SNQ design, care was taken that all elements in the vicinity of the beam can be handled easily. This could not be garanteed if the elements were part of the tank. Bridge couplers were therefore excluded and relatively short, separate tanks were preferred.

The length of the SNQ tanks is determined by the allowable distance of the focusing elements and by the power delivered by the klystrons. The field gradient is again determined by the - conservative - Kilpatrick-criterion which limits the surface fields to about 18 MV/m.

With a klystron power of 3 MW (ch. B 2.2), the average length of the first 25 tanks (up to 350 MeV) is 3.4 m (Table A 1.5-3).

For higher energies ($E \gtrsim 350$ MeV), the distances between focusing elements may be higher. In this range, 32 tanks with an average length of 7.5 m are installed. A metallic wall divides them into two independent resonators (ch. A 1.7).

1.5.14 rf-Coupling, Tuning

As shown in Fig. A 1.5-2, the field of the accelerating mode decays exponentially towards the outer tank. Radial coupling and tuning at the tank wall is therefore excluded. These functions can be combined in a coaxial stub line terminating the tank /27/. As the length of this line must be at least a quarter of a wave length, this would lead to a prolongation of the tanks without additional acceleration.

In the proposed accelerator, coupling and tuning elements are therefore mounted axially to the end plates (see Fig. A 1.5-1).

1.5.15 Fabrication Tolerances

The limitation of the length of one resonator to $\sim$3.4 m results in a low number of cells. At injection energy, the number of cells per rf-unit is 15, decreasing to 9 at the final energy. Fig. A 1.5-4 shows a dispersion diagram of a DAW-structure tank containing 15 accelerating cells.

The low number of cells together with the high group velocity reduces the requirements of manufacturing precision and simplifies fabrication.

In table A 1.5-4, parameters which are most important for fabrication, are listed. The influence on the frequency is also shown. The tolerances for the outer diameter (cylinder, disks, washers) are chosen $\pm$ 1 mm, tolerances for the thicknesses of disks and washers should not exceed $\pm$ .3 mm.

With these values, the frequency gap for one tank is less than 1.6 MHz, the frequency deviation is less than .45 MHz.

To compensate this frequency deviation for 15 cells by a tuner in one end cell, this single cell must be detuned by about 7 MHz. For a compensated structure (no frequency gap) the field amplitude in the accelerating cells remains unchanged.In the coupling cells a field amplitude less than one fourth of that in the accelerating cells would follow /25, 34/.

Tab. A 1.5 - 3: Parameters of the DAW-tanks

Energy / MeV	105	200	330	380	670	950
Peak fields on surface / MV m^{-1}	18.4	18.3	18.3	18.1	16.8	18.4
Accelerating field on axis E_0T/ MV m^{-1}	3.03	3.3	3.4	3.4	3.3	3.6
Synchronous phase	-30^o	-30^o	-30^o	-25^o	-25^o	-25^o
Length of the tank /m	3.07	3.53	3.6	7.6	8.28	7.16
Number of cells	15	13	11	22	22	18
Drift space between tanks / m	1.3	1.3	1.3	1.3	1.3	1.3
Beam hole radius / cm	3.3	3.3	3.3	4.0	4.0	4.0
Dissipated power +)/ MW for one tank	2.05	1.96	1.85	3.64	3.44	3.46
Change of beam power / MW for one tank	0.81	1	1.07	2.3	2.4	2.3
Losses +)/ kW per cell on - cylinder	0.01	0.03	0.11	0.15	0.36	0.63
- disk	1.26	3.0	5.06	5.91	9.5	15
- washer	133	143	156	154	137	160
Quadrupole gradient / Tm^{-1}	23	23	23	18	18	16
Quadrupole length /m	0.15	0.15	0.15	0.2	0.2	0.25
Doublet length /m	0.4	0.4	0.4	0.5	0.5	0.6

+) Losses are calculated with a 25 % decrease of theoretical Q.

For an uncompensated structure, the accelerating fields are influenced by manufacturing errors as well /25/. For N cells, a frequency gap f_g, and a detuning Δf of one end cell, the change of amplitude is given by

$$\frac{\Delta E}{E} \leq 2\pi^2 \frac{L^2}{v_g} \Delta f \cdot f_g \cdot N$$

with the group velocity

$$v_g = L \cdot \frac{df}{d\phi}$$

the period length L, and the phase shift ϕ for one period.

With the above mentioned detuning of one end cell and the group velocity determined from fig. A 1.5-4, the change in amplitude for the accelerating cells is less than 3 %.

For a practical case, the influence of fabrication tolerances is expected to average over the tank. For compensation, two tuners in each end cell, can be used. Tolerances of $\pm$ 1 mm for the diameters and $\pm$ 0.3 mm for the thicknesses are therefore acceptable.

1.5.16 Coupling Constants

Besides of a perturbation of the eigenfrequencies, coupling constants between cells are affected by manufacturing tolerances as well. The relative changes of coupling constant between accelerating and coupling cells are of equal magnitude but opposite sign. A 2 % change of coupling constant yields a 2 % change of field amplitude. The deviations can be either systematic or statistical.

A systematic variation of the coupling constants is caused by the washer supports. This effect can be calculated and taken into account in the design.

Tab. A 1.5 - 4: Effect of Frequency Determining Dimensions and Tolerance Requirements on Frequency

Parameter	Deviation / mm	Effect on Frequency / kHz mm^{-1}			Frequency Deviation / kHz		
		Acceler. mode	Coupling mode	Difference	Acceler. mode	Coupling mode	Difference
Outer diameter	± 1	0.33	-586	586	0.3	586	586
Disk diameter	± 1	5.0	456	461	5	456	461
Washer diameter	± 1	215	9	224	215	9	224
Disk thickness	± 0.3	105	12	117	32	4	36
Washer thickness	± 0.3	-638	316	954	191	95	286
	Max. frequency deviation for one cell / kHz				443	1150	
	Average frequency deviation for one cell / kHz				289	748	
	Max. frequence gap / kHz						1593
	Average frequence gap / kHz						830
	Max. frequency deviation for one tank / kHz				443		
	Average frequency deviation for 15 cells / kHz				75		

Statistical perturbations are caused by manufacturing errors. Their influence has to be determined experimentally. For the tolerances listed in table A 1.5-4, changes of coupling constants by no more of 2 % are anticipated. For axial symmetry, an amplitude error of at most 2 % follows. The most essential influence on coupling constants results from axial displacements of the disks with respect to the washers. Adjustment after fabrication will greatly reduce this effect.

1.5.17 Beam-induced Effects

The following effects of a high intensity beam have to be considered:

1) A change of the accelerating field in amplitude and phase (beam loading). This effect is less important for this design as the beam power is only about 50 % of the dissipated power and the DAW-structure allows for a fast energy flow.

2) Excitation of a dipole-mode for one rf-unit (regenerative break up) /35, 36/. The excited mode leads to a deflection of the particles. Beam loss happens at beam currents above a critical current I, which depends on the shunt impedance Z and the wave length λ_D of the dipole mode by

$$I = \frac{\pi^2 \rho c^2 \lambda_D}{4 l^2 Z}$$

The critical current is inversely proportional to the square of the resonator length l and is lowest for low proton momenta p, i.e. at the entrance of the DAW-accelerator.

For a resonator length of about 3.4 m and a peak current of 100 mA, the shunt impedance of the dipole mode has to be at least 750 MΩ/m λ_D/m to excite an instability.

At wavelengths beyonds cutoff ($>$ 0.33 m corresponding to table A 1.5-2) the shunt impedance has a minimum value of 250 MΩ/m to create instable conditions. This value exceeds all measured values by far.

For higher modes, or wavelengths shorter than twice the distance of the disks, the energy transfered by the beam can be dumped by coupling elements, selective for higher order modes.

3) Excitation of a dipole mode for more than one resonator (cummulative beam break-up). This effect reduces the above mentioned critical current for electron accelerators, but not for proton accelerators where the frequencies of the dipole mode differ from tank to tank due to a changing geometry. Critical currents are thus increased essentially (up to 2-3 orders of magnitude /37/). Cummulative beam break-up is therefore not considered important for the SNQ-design.

Contributors:

E. Boltezar (CERN), G. Dammertz (KfK), N. Münch (KfK).

References

/ 1/ A. Carne, in "Linear Accelerators" by P.N. Lapostolle, A.L. Septier, North Holland Publ. Co., Amsterdam, 1970, p. 587

/ 2/ G. Dome, s. ref. 1, p. 637

/ 3/ K. Mittag: "Design Data of the Alvarez Linear Accelerator for the Neutron Spallation Source SNQ", this study, part III A, vol. 1, unpublished

/ 4/ G.P. Boicourt, D.A. Swenson, IEEE Trans. Nucl. Sci NS-26, No. 3, 1979, p. 3012

/ 5/ W.D. Kilpatrick, Rev. Sci. Instr. 28, p. 824

/ 6/ R.L. Gluckstern, s. ref. 1, p. 797

/ 7/ K.R. Crandall, unpublished report, Los Alamos, 1967

/ 8/ E. Boltezar, CERN, private communication

/ 9/ s.a. W.B. Hermannsfeldt et al., IEEE Trans. Nucl. Sci NS-14, No. 3, 1967, p. 903

/10/ V.E. Hart, E.W. Colston, Proc. 1972 Lin. Acc. Conf., Los Alamos, 1972, p. 358

/11/ A. Harvey, Proc. 1970 Proton Lin. Acc. Conf., Batavia, 1970, p. 707

/12/ A. Harvey, S.A. Walker, IEEE Trans. Nucl. Sci. NS-16, No. 3, 1969, p. 611

/13/ R.L. Gluckstern, Proc. 1979 Lin. Acc. Conf., Montauk, 1979, p. 245, BNL 51 134

/14/ R.F. Holsinger, K. Halbach, Proc. 4th Int. Workshop on Rare Earth Cobalt Perm. Magnets and their Applications, Hokone Nat. Park, Japan, 1979, p. 37

/15/ R.C. Webber, C. Hojvat, Trans. Nucl. Sci. NS-26, No. 3, 1979, p. 4012

/16/ J.R. Richardson, Proc. 7th Conf. on Cyclotrons and their Applications, 1975, p. 41

/17/ D.A. Swenson, Proc. 1970 Proton Lin. Acc. Conf., Batavia, 1970, p. 175

/18/ V.G. Andreev et al., Proc. 1976 Proton Lin. Acc. Conf., Chalk River, 1976, p. 269

/19/ D. Böhne, IEEE Trans. Nucl. Sci. NS-16, No. 3, 1969, p. 390

/20/ C.S. Taylor, s. ref. 1, p. 879

/21/ E. Boltezar, Proc. 1979 Lin. Acc. Conf., Montauk, 1979, p. 392, BNL 51 134

/22/ J. Mc Keown, AECL-6406, 1979

/23/ S.O. Schriber, Conf. on Future Possibilities for Electron Accelerators, Charlottesville, 1979, L 1

/24/ B.C. Knapp et al., IEEE Trans. Nucl. Sci. NS-12, No. 3, 1965, p. 159

/25/ E.A. Knapp et al., Rev. Sci Instr. 39, 1968, p. 979

/26/ V.G. Andreev, Zh. Tekh. Fiz. 41, No. 4, 1971

/27/ J.M. Potter et al., IEEE Trans. Nucl. Sci. NS-26, No. 3, 1979, p. 3763

/28/ G.E. Mc Michael et al., Proc. 1979 Lin. Acc. Conf., Montauk, 1979, p. 180, BNL 51 134

/29/ K. Halbach et al., Proc. 1976 Proton Lin. Acc. Conf., Chalk River, 1976, p. 122

/30/ S.O. Schriber, G. Dammertz: "Parameters of Disk-and-Washer Structures for the Neutron Spallation Source SNQ", this study, part III A, vol. 1, unpublished

/31/ S.O. Schriber, Proc. 1979 Lin. Acc. Conf., Montauk, 1979, p. 164, BNL 51 134

/32/ S.O. Schriber, Proc. 1979 Lin. Acc. Conf., Montauk, 1979, p. 176, BNL 51 134

/33/ D.A. Swenson, LANL, private communication

/34/ G. Dammertz: "Abhängigkeit der Feldverteilung einer Disk-and-Washer Struktur von Herstellungstoleranzen", Kernforschungszentrum Karlsruhe, unpublished report

/35/ R.H. Helm, G.A. Loew, s. ref. 1, p. 173

/36/ R.L. Gluckstern, H.S. Butler, IEEE Trans. Nucl. Sci. NS-12, No. 3, 1965, p. 607

/37/ R.L. Gluckstern et al., Proc. 1966 Lin. Acc. Conf., Los Alamos, 1966, p. 281

A 1.6 Pulse Forming, Beam Splitting and Beam Transport

A 1.6 Pulse Forming, Beam Splitting and Beam Transport

1.6.1 Requirements for the Time Structure

Slow neutron experiments are the dominant use of the SNQ. A repetition frequency of 100 Hz and a pulse length of 500 µs were defined as useful parameters for this kind of research /1/. Nuclear physics experiments require time structures covering a wide range from continuous beam current to intense pulses with ns duration and up to MHz repetition frequencies. A survey is given in table A 1.6-1.

Not all requirements can be fulfilled simultaneously. To operate the accelerator economically, pulsed operation is necessary and a duty cycle of 5 % was therefore selected. Pulse duration and repetition frequency can, however, be chosen for the given duty cycle. Power supplies and line filters were designed for a maximum repetition frequency of 100 Hz, lower frequencies are possible. In a special mode of operation, as a testing procedure for adjustment of acclerator parameters, single pulses can be produced.

From the duty cycle given and the maximum repetition frequency, a pulse length of 500 µs follows. After upgrading the power supplies, prolonged pulses of 1 ms can be delivered. Superimposed on the macropulses is always the rf microstructure of 108 MHz. For most of the experiments, this substructure is, however, of no importance.

1.6.2 Method of Pulsing and Splitting of the Proton Beam

The peak current during a macropulse is fixed to 100 mA. This is an important alleviation of operation. All machine parameters which depend on space charge, can be adjusted for this particular current. The time structure required is realized by fast switching of the beam at low energy. Fast switching also helps to split the beam at high energies with virtually no beam loss.

experiment	pulse length	repetition frequency	aver. intensity	peak intensity	proton energy
neutron scattering (therm.)	$\leq 500\,\mu s$	50...200 Hz	mA	I $\geq$ 100 mA	$\geq$ 500 MeV
neutron scattering 100 meV	$\leq \mu s$	50...200 Hz	-	high	$\geq$ 1 GeV +)
neutrino physics	200 ns	$\leq$ 100 kHz	-	high	$\geq$ 500 MeV
n-n scattering (therm.)	$\leq 500\,\mu s$	100 Hz	mA	high	1 GeV
fast p, n time of flight experiments	$\lesssim$ ns	$\leq$ MHz	-	high	$\geq$ 200 MeV
p, n nuclear physics coincidence experiments	cont.	cont.	-	-	$\geq$ 200 MeV
solid state research π-channeling μsr	cont. $\leq$ 2 ns $\leq$ 200 ns	cont. $\leq$ 10 MHz $\leq$ 50 kHz	mA	high	$\geq$ 500 MeV

Table A 1.6-1: Survey of users requirements of time structure and intensity

+) Energy chosen in view of a compressor ring

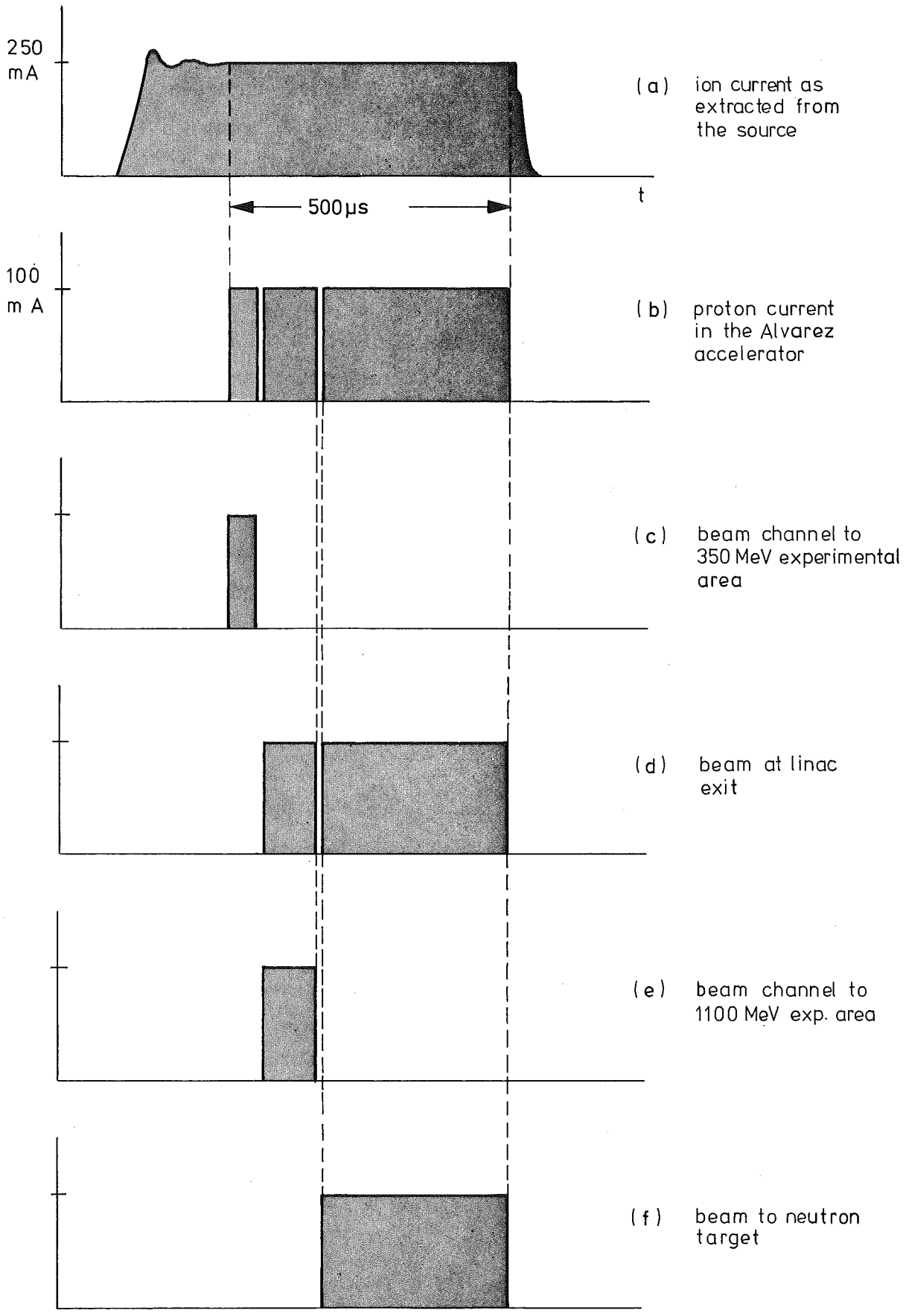

Fig. A 1.6-1: Pulse formation and beam splitting

Short duration blanks are cut into the beam. Within these interruptions, a beam deflector can be actuated at the particular area where beam shall be split off. Pulse shaping and beam splitting is schematically shown in fig. A 1.6-1 which is explained as follows:

a) Prolonged macropulses, 700 to 1000 μs long, are extracted from the ion source. Beam current at this point consists of different ion species with a total current of $\sim$250 mA. Pulsing of the ion source is done by switching of the arc power. After selecting the atomic ions out of the beam and after preacceleration, a proton beam of $\sim$120 mA passes the low energy beam transport line. Before rf-bunching, a fast deflector (see ch. 1.6.3) cuts the pulses into a rectangular shape, and, at the same time, provides for the blanks within the pulse.

b) Macropulses are shown as accelerated in the Alvarez accelerator. After some loss from imperfect bunching and collimation, the beam current amounts to 100 mA.

c) and d) The front part of the pulse is separated by a deflecting magnet and guided into the 350 MeV experimental area for nuclear physics and medical experiments.

e) and f) Another fraction of the main beam is split off in the 1100 MeV beam transport area for nuclear physics experiments.

When, as an upgrading option, the compressor ring will be added to the accelerator, beam can be split by a further defletor in a similar way. In this case, H^--ions are accelerated instead of protons. Moderate bending fields are required as not to strip off the loosely bound electron. Operation of the compressor ring requires a special substructure within the macropulse. Pulses of 660 ns duration will be spaced by 100 ns intervals. This sequence is repeated with the revolution frequency of the ring, which is operated in an isochronous mode. The blanks are thus superimposed and preserved during the accumulation procedure. A fast magnet can thus provide beam extraction with low losses /2/.

1.6.3 Components for Beam Splitting and Pulse Forming

Deflection of the beam from the main line is achieved by combined action of two components, kicker and septum. The kicker is a low field, fast excited magnet which deflects the beam with an angle of $\sim$ 10 mrad. The deflected beam traverses the high field region of the septum magnet, positioned a few meters downstream (Fig. A 1.6-2). The septum magnifies this deflection by at least a factor of 10. This gives enough separation that, in the channel of the deflected beam, normal bending and focusing elements can be used. The combination of kicker and septum is used for splitting the beam at 350 MeV and at the final energy.

During the switching time t_s of the kicker, the beam current is interrupted for about 10 μs to avoid loading of the septum magnet by beam spill. These blanks in the beam are obtained by the fast deflector in the low energy beam transport line, as described below.

The switching time is a compromise of different arguments: power requirements for the kicker critically depend on t_s. On the other hand, prolonged blanks cause more pronounced transient effects in the rf cavities. As during switching the rf fields in the accelerator are maintained, but the beam is suppressed, the overall efficiency decreases. Duration and frequency of the switching intervals should therefore be kept to a minimum.

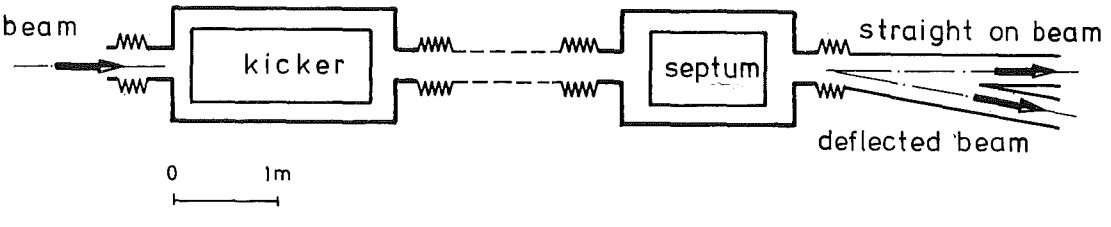

Fig. A 1.6-2: Schematical arrangement of kicker and septum

Fast Chopper /3/

Electric deflection can be applied to chop the beam in the low energy (450 keV) beam transport area. The energy range, where an electric deflector can be used, is, however, limited. At lower energies, e.g. behind the ion source, space charge forces are too strong and the beam would be blown off within the drift space.

Analoguous to magnetic deflection, a minimum product of voltage U and deflector length L can be calculated, which deflects the beam by twice its divergence:

$$UL = \frac{4 W_0}{\pi e} \beta \varepsilon_n$$

W_0 = rest energy, ε_n = normalized emittance
β = v/c particle velocity

An effective length L of 450 mm was chosen for the proposed system (see fig. A 1.6-3). The deflector consists of two rows of electrode plates with adjustable aperture. Single plates are connected to a delay line (meander strip line), which is subdivided into cells. Delay time between cells is adjusted to the beam velocity of 0.9 cm/ns. With this traveling wave deflecting system, rise and fall times in the order of a few ns can be obtained. For the kicker magnet of the compressor ring, a time resolution of 10 ns is required, to cut the "ejection hole" into the beam. To split the linac beam, rise- and decay-times of 100 ns are adequate.

The deflected part of the beam is absorbed by slits, which are cooled by a two phase flow of water and water vapour.

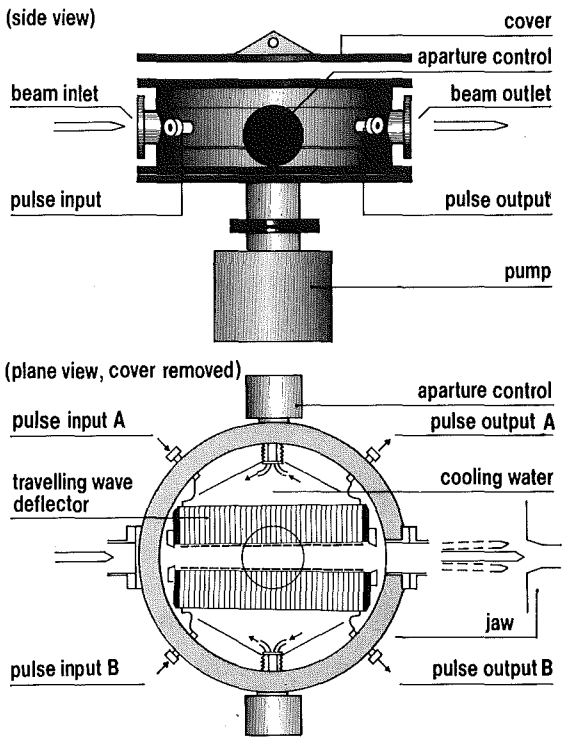

Fig. A 1.6.-3: Fast chopper in the low energy beam transport area

Kicker Magnet

The minimum deflection angle of the kicker shall be twice the beam divergence. From a more detailed discussion /4/ follows, that the normalized emittance ε_n is an important quantity: the product of ampere turns I and kicker length L is proportional to ε_n. A beam displacement of typically 0.5 cm within the kicker has to be taken into account when choosing the aperture. More clearances have to be provided for misalignments and emittance growth of the beam. In a practical situation, where stray fluxes are present, additional excitation current is needed. Without these additions, an IL of 280 Am is required for a normalized emittance of 3π cm mrad. Including all effects, an aperture of 50 mm and an IL of 1,1 kAm follow at an energy of 350 MeV. Assuming a further emittance blow-up by a factor of 2, from 350 MeV to 1100 MeV, IL = 2.2 kAm is obtained for the kicker in the high energy beam transport area.

Flux variation within 10 μs yields an induced voltage of 140 V (350 MeV kicker) or 280 V (1100 MeV), respectively, for a quadratic aperture. The minimum switching power is thereby determined.

The kicker magnet is operated in a vacuum tank. Its length was assumed to be 2 m at 350 MeV. The aperture is surrounded by high permeability ferrite ($\mu_r > 100$) with low conductivity ($< 10^{-3}$ Sm^{-1}). Construction as a comb-like structure without ferrites can be alternatively used, but requires twice the excitation current because of stray fields /5/. Details have to be studied in prototype experiments.

The problem of producing a clearly pulsed excitation current merits particular attention and early prototyping work. About 1 MW of active power is required during the deflecting pulse, which corresponds to 50 kW of average power at a duty cycle of 5 %. Solid state elements can be used to switch these power levels.

Pulse production by an LC-network with a high characteristic impedance and consequent high voltage operation was alternatively considered. In this case, the kicker magnet is divided into cells, each consisting of several turns /6/. Ignitrons have to be used as high voltage switches because of long pulse duration. At the high repetition rate of 100 Hz, alternating operation of several groups of switches is feasible. To save power, the resistive load of the

kicker magnet can be replaced by an LC-type delay line. Pulse power is stored and fed back inbetween pulses. Losses are compensated by the rectifier /6,7/. A loading voltage of 30 kV, a characteristic impedance of 200Ω for the delay line, and a cut-off frequency around 0.5 MHz are the essential parameters of the feedback load.

The kicker at 350 MeV will be built with a high current single loop whereas at 1100 MeV, cascaded LC-units will be applied. Shorter switching times at lower current levels are achieved with the latter system although it is somewhat more expensive.

Septum

A magnetic induction of 0.3 T was chosen for septum design to bend protons or H^--ions, respectively. The number of ampere turns required for an aperture of 50 mm is 12 kA. At an energy of 350 MeV, a deflection of 85 mrad per m septum length can thus be obtained. A length of 1 m is sufficient. For 1100 MeV, twice the deflection is required. 4 units of 1 m length are positioned on a bending radius of 20 m without spacing.

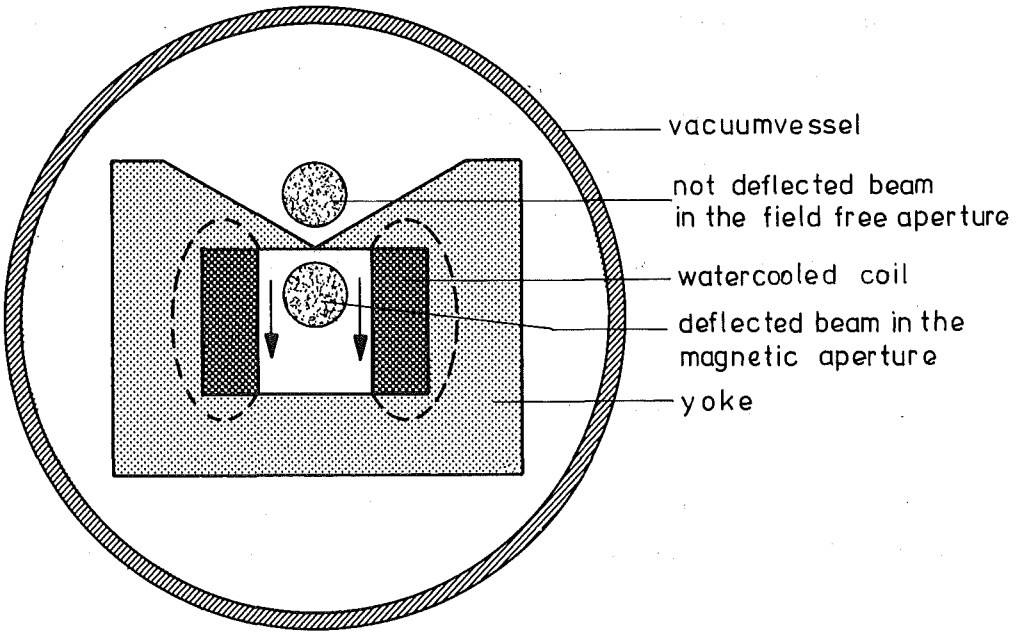

Fig. A 1.6.-4: Lambertson-Septum

Fig. A 1.6-4 shows a sketch of the Lambertson-type septum, as proposed for the SNQ. This component is used in major accelerator installations. Operation reliability and radiation hardness are major advantages of this construction /8/. Direction of the deflecting force and beam separation at the entrance of the septum are orthogonal. Distance from the medium plane of the kicker to the septum entrance is 3 m at 350 MeV, and 5 m at 1100 MeV, respectively.

Kicker and septum are constructed to be remotely handled. Connections for vacuum and cooling pipes as well as current and signal leads are designed for easiest handling with remotely handled tools. Experience from e.g. the CERN-SPS target beam and beam dump magnets can be introduced into the design. Kicker and septum are protected against impact of the particle beam by collimators.

1.6.4 General Aspects of Beam Transport

Beam transport in the low energy region (LEBT) and in the matching sections between acelerator parts was discussed in ch. A 1.2. Magnetic quadrupole lenses are used for transverse focusing in the whole accelerator and beam transport system. In the LEBT, quadrupoles are grouped as triplets to maintain an almost circular cross section of the beam. Space charge forces can thus be reduced. In the Alvarez accelerator, singulets with alternating polarity are installed into the drift tubes. From 105 MeV on, intertank focusing greatly facilitates adjustment and maintenance of components. The focusing lattice of the high energy part of the DAW-accelerator extends to the high energy beam transport (HEBT). Identical focusing elements can be used in most of the beam channels.

Apertures of the quadrupoles are defined by beam dynamics (ch. A 1.2). In order to take into account some emittance increase, the bore holes increase along the accelerator. Large apertures within the machine are believed essential to prevent the accelerator from impact of lost particles. As a disadvantage, the magnet power increases drastically with larger apertures.

Fields of focusing elements, or, at least groups of elements, are variable to a certain degree to allow for adjustment. Radiation proof windings are provided above 50 MeV. Provisions for remote handling are made in the DAW part and in all high energy beam channels.

To reduce cost of construction and operation, as many identical elements as possible are used.

Adjustment tolerances of beam optical elements to $\pm$ 0.1 mm are required and can be obtained. Stability of the field gradients is specified to be 10^{-3} in the dipoles. Beam switching magnets have to be built free of remanence.

Permanent magnets were further developed recently /9/. Low field errors and variable gradients could be demonstrated in experimental quadrupole modules. Questions of radiation resistance and cost could, however, not yet be sufficiently answered within discussions of this study.

Current breaks and faults of the cooling system are the major origins of faults in operation. Time constants in both cases are long enough that the beam can be stopped in a safe way. Beam shut-off in between macropulses (10 ms) is sufficient for protection of beam transport components.

Beam diagnostics correspond to those described in ch. A 1.3 for the DAW-accelerator. Secondary radiation of x-rays and neutrons was found the most sensitive method of beam loss detection. Loss neutrons can be measured outside the machine by sensitive counters, placed at fixed points or movable along the tunnel. Time structure of the loss can also be monitored. Errors of magnet fields and deviations of field amplitudes and phases of accelerating cavities can be detected and localized. The time dependent registration of the beam loss during a macropulse is of particular value for interpretation of the origin of beam spill, as shown in experiments at the CERN new linac /11/.

Vacuum requirements in the HEBT are the same as in the linac. 10^{-6} mbar is sufficient for acceleration of protons. In case of H^--ions, pressures two orders of magnitude lower have to be maintained. Within the neutron target block higher pressures than 10^{-6} are tolerable.

1.6.5 High Energy Beam Transport and Beam Distribution (HEBT)

The HEBT system is shown in fig. A 1.6-5. From the exit of the accelerator the beam is guided via a straight section of 50 m length (1) to the first kicker-septum-unit. At this point (3), a defined fraction of the beam pulse can be split off into the area for nuclear physics experiments. Further downstream, a magnet (8) switches the beam straight on to the beam dump (7) or bends it to the neutron target (5/15). The HEBT-components are described below in more detail.

Straight Section

Beam diagnostic elements can be installed in the 50 m long drift length following the linac exit. They offer means to measure beam position, transverse and longitudinal emittances. Within this drift space, beam can be split off for the optional compressor ring as shown in fig. A 1.6-6 and described below.

The same quadrupoles as in the high energy part of the DAW-accelerator are used for the straight section. The parameters are as follows:

effective length	l_{eff}	= 25 cm
aperture radius	a	= 4.5 cm
max. field	B_{max}	= 0.7 T
gradient	g	= 15.6 Tm^{-1}

The focusing period from the DAW of 10 m is maintained to obtain smooth transition into the HEBT.

Beam Switch to the Nuclear Physics Area

The main components are a kicker (2) and a septum magnet which allow for fast deflection of a fraction of the macropulse into the nuclear physics area. The technical details of the system are described in part III of this study /6/. The beam channel into the experimental area is 70 m long and is equiped with the same quadrupoles as used in the main line.

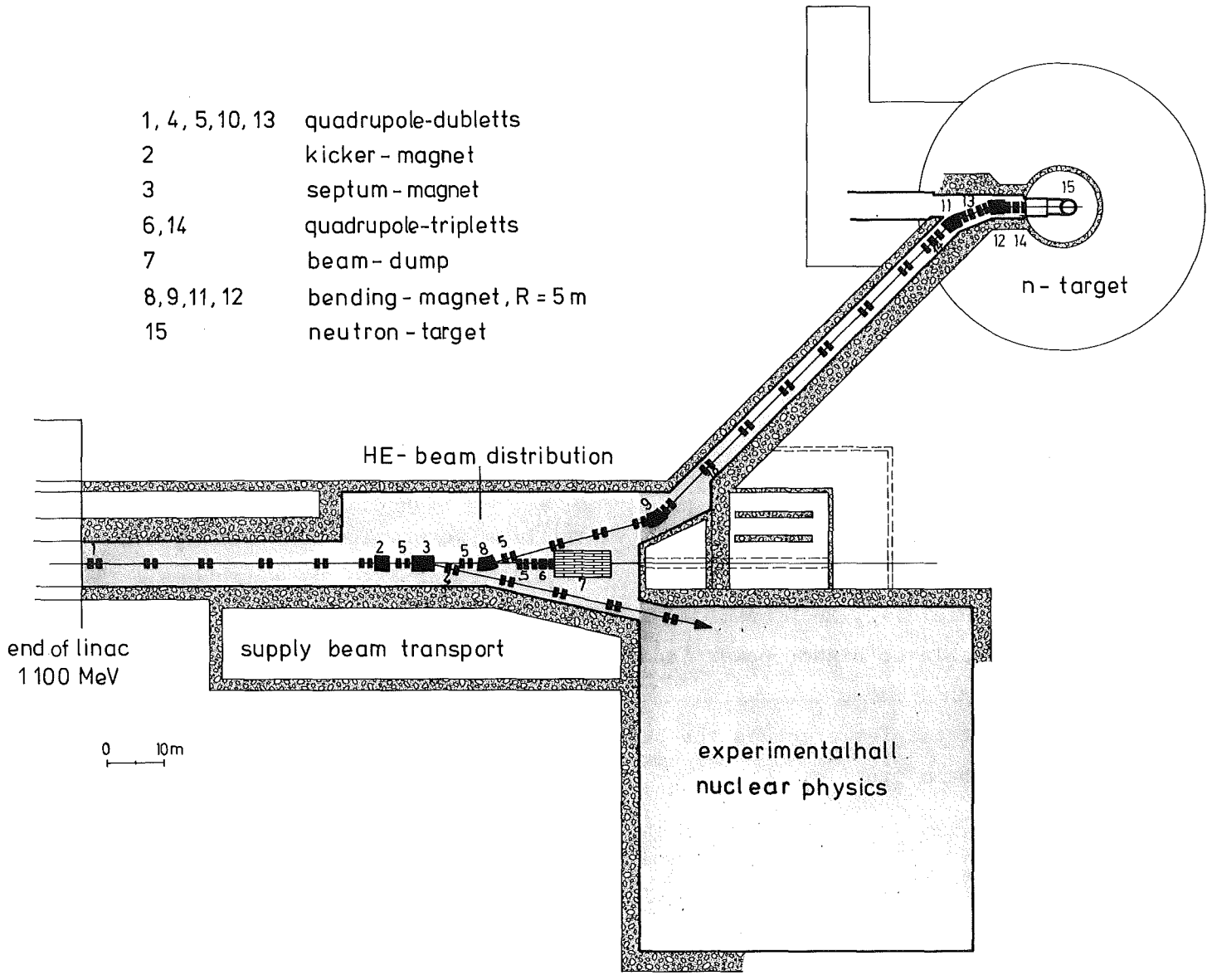

Fig. A 1.6-5: High Energy Beam Transport

Beam Switch to Neutron Target and Beam Dump

This switching magnet operates in a stationary mode. It allows to bend the beam by 15° into the channel of the neutron target (normal operation) or, for test purpose, to the beam dump. Field strength is B = 1.2 T, magnet length is 1.31 m and the bending radius amounts to R = 5 m. The gap width was assumed to be 8 cm, the precise value depends on a more detailed beam transport calculation. Again, the same quadrupoles are used as in the upstream channel.

Beam Dump

The beam dump is provided for absorption of the linac beam during test operation. It is designed to dump single macropulses of full length. The maximum anticipated repetition frequency is 1 Hz.

The energy contained in a macropulse is 55 KJ, which, at 1 Hz repetition, gives a target power of 55 kW. The beam dump is a coaxial arrangement. The water cooled insert dumps about 50 % of the beam power. The high energy secondary radiation carries the other half of target power into the surrounding radiation shielding. Such beam dumps were built with modified parameters but with comparable or higher power capabilities at CERN, LANL, SIN and TRIUMF.

A quadrupole triplet precedes the beam dump to obtain stigmatic focusing with a circular beam profile.

Bending Magnet and Beam Transport Line to the Neutron Target

Magnet (9) bends the beam by 30°. The orbit length is 2.62 m, construction data correspond to magnet (8). Larger beam envelopes are expected in the target channel (10). As pointed out in A 1.2, the beam leaves the accelerator with an energy spread of 1.8 MeV. The bending magnets (8) and (9) convert this dispersion into an increase of the transverse emittance. An angular spread of $\pm$ 0.5 mrad is produced by magnet (9) only. For this study, no change of quadrupole aperture was assumed, which may be revised after a detailed beam transport calculation.

When the compressor ring will be added, larger apertures are needed anyhow in the target channel. The emittance of the compressed beam will be 5 times higher than the linac emittance /2/. The replaced elements can, however, be used in that case for the injection channel to the ring.

Injection Channel to the Neutron Target

Particular requirements have to be considered in the neutron target area with respect to beam properties and beam loss. Beam spill shall be kept as low as possible to reduce shielding thickness and to win space for the experiments situated around the target block. Beam transport components are constructed in a way that they can easily be removed to facilitate handling of the rotating target insert. Neutrons and protons scattered back from the target and emerging out of the beam tube have to be captured in a way that the bending magnet is prevented from additional activation.

The 45^{o} bending magnet is designed as an achromatic system. This takes into account the emittance increase from former bending and the energy dispersion in the beam. The bend is subdivided into two parts, separated by focusing elements:

Bending magnet (11):

magnetic field strength	$B = 1.2$ T
bending radius	$R = 5$ m
bending angle	$= 22.5^{o}$
aperture, height	$g = 10$ cm
orbit length	$l_m = 1.96$ m
shape	H-type, slanted poles

2 quadrupole dublets (13):

aperture radius	$a = 7.5$ cm
eff. length (singulet)	$l_{eff} = 39$ cm
field gradient	$g = 7.5$ T/m
max. pole field	$B_{max} = 0.56$ T

Bending magnet (12) corresponds to (11) except that the yoke is C-shaped to house a 15 cm straight channel passed by particles scattered back from the neutron target. These particles are absorbed in some distance from the magnet in a controled way.

The magnet arrangement is followed by a quadrupole triplet (14). The beam optics are thereby not only achromatic but also stigmatic, i.e. rotational symmetric, as required on the neutron target. Beam profile at the target is gaussian with 4 cm FWHM. Tails beyond 4 cm radius are cut. The beam is slightly convergent. If required, the current density of the beam can be varied by means of the triplet. The singulets combined to this triplet are identical with the ones situated in between the bending magnets (13).

1.6.6 Addition of a Compressor Ring and Changes for H^--Operation

Changes for H^--Operation

Magnetic field strengths of beam transport components have to be limited to avoid Lorentz-stripping. For the HEBT, 0.3 T are a safe value. Field limitation is strict because the probability of neutralization rises exponentially with the field strength.

Limitation of the field was taken into account in the bending magnets over the whole aperture. For the quadrupoles, pole tip fields were assumed 0.7 T for the reference concept to shorten the intertank drift spaces. As a consequence, only half of the bore can be used for stable beam transport in case of H^--ions. Calculations of beam dynamics in the DAW-accelerator have shown, that the envelopes stay within this range, somewhat larger apertures were chosen to cope with mismatches or misalignments. It is assumed, that with the experience gained in operation with protons, beam transport can be improved so that the beam safely stays within half the aperture radius.

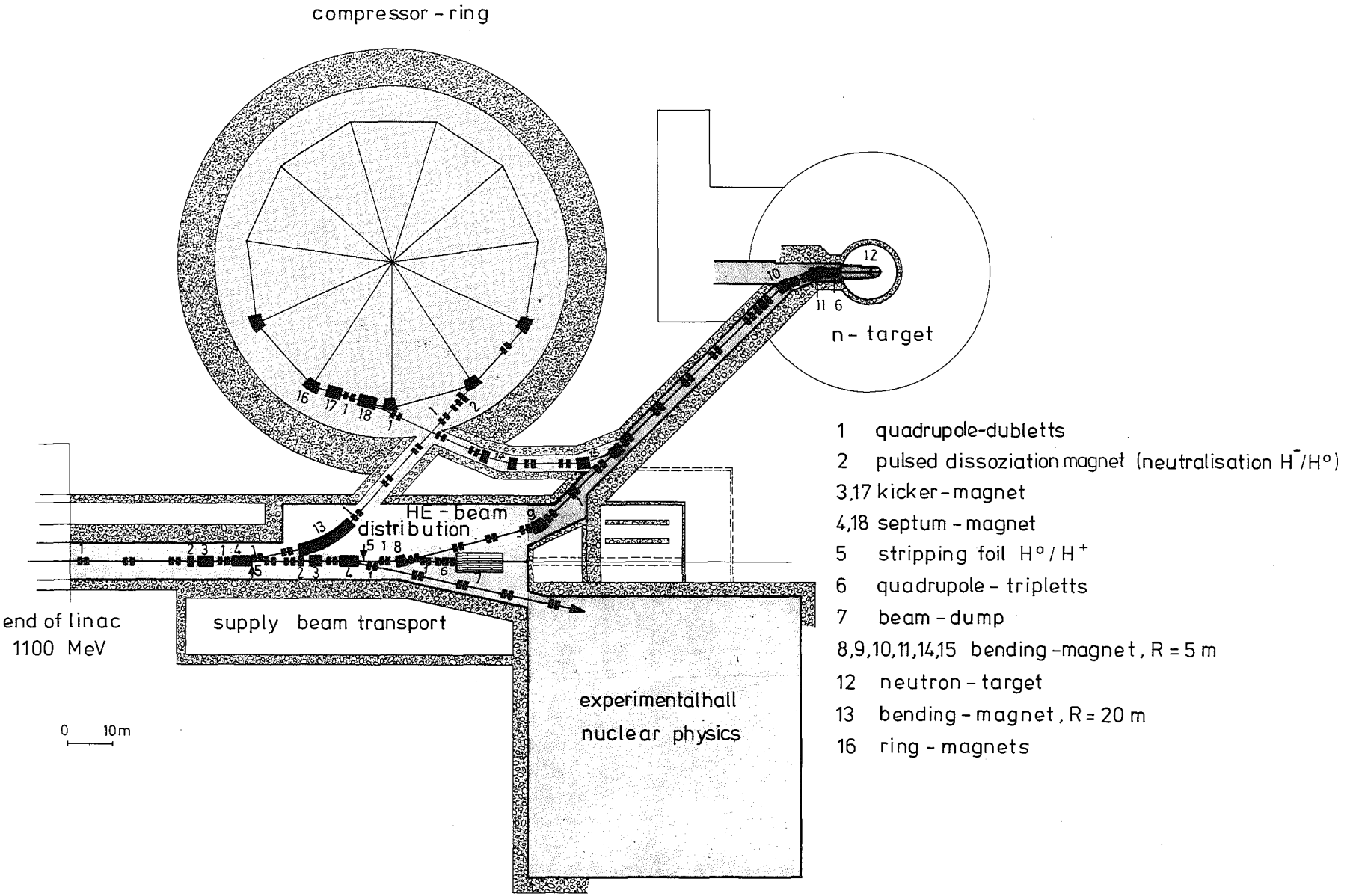

Fig. A 1.6-6: High Energy Beam Transport, including the Compressor Ring

Fast Beam Splitting by Charge Exchange

Dissociation of H^--ions into H^0 and electrons by strong magnetic fields can be applied advantageously for beam splitting. Charge exchange is partitioned into two steps $H^- \rightarrow H^0$ and $H^0 \rightarrow p$. Neutralization is done by Lorentz-stripping in a small high field magnet, which can be switched fast. In a field of 1.5 T, the medium decay length of the H^--ions amounts to only 0.4 mm. The difficult and expensive kicker magnet can thus be replaced in an elegant way. Charged and neutral beams can then be separated by a normal bending magnet instead of a septum. No blanks are needed in the beam pulse, as there is no sweep which might cause beam spill; the two charge states are cleanly separated. The second step of charge exchange into protons is achieved by foil stripping in the well known manner /12/.

Contributors

W. Kühn, G. Schaffer, KfK

References

/ 1/ This study, part I, ch. 2, JÜL-Spez-113/KfK 3175, to be published

/ 2/ This study, part II, ch. D2, unpublished

/ 3/ G. Schaffer: "Hf-Einrichtungen zur Dunkeltastung des Linacstrahls einer Spallationsneutronenquelle", this study, part III A, vol. 1, unpublished

/ 4/ G. Schaffer: "Strahlpulsung und Strahlverteilung", this study, part III A, vol. 1, unpublished

/ 5/ G. Stange: "A New Type of Pulsed Air Core Multipoles of extremely simple Construction", IEEE Trans. Nucl. Sci. NS-28, 3, June 1981.

/ 6/ W. Kühn: "Entwurf einer schnellen Strahlweiche für den hochenergetischen Protonenstrahl des SNQ-Linac", this study, part III A, vol. 1, unpublished

/ 7/ G. Schaffer: "Laufzeit-Kicker mit Impulsreflexion", this study, part III A, vol. 1, unpublished

/ 8/ E. Weisse, CERN: private communication
L. Evans et al: "The Steel Septum Magnet for Beam Splitting at the CERN SPS", CERN-SPS/ 77-13

/ 9/ Proc. of the 1979 Lin.Acc.Conf., Montauk, BNL 51 134, p. 373

/10/ G. Schaffer: "Auslegung und thermische Belastung von Strahlfängern in der Niederenergiestrahlführung der SNQ", this study, part III A, vol. 1, unpublished

/11/ W. Kühn: "Strahlverlust-Neutronen am 50 MeV Linac im CERN", this study, part III A, vol. 1, unpublished

/12/ W. Kühn: "Strahlweiche für den Linearbeschleuniger der Spallationsneutronenquelle zur schnellen Aufspaltung eines hochenergetischen H^--Strahls in verschiedene Strahlkanäle", this study, part III A, vol. 1, unpublished

A 1.7 Radio Frequency Generation and Control

A 1.7 Radio Frequency Generation and Control

1.7.1 Design Considerations

The function of the radio frequency system is to build up the accelerating fields in each of the 96 resonators of the linear accelerator and to maintain accurate phase and amplitude values during the beam pulses. The stability of the accelerating voltage is an essential condition for the acceleration with small beam losses. The rf power required for acceleration of the beam has to be generated with an optimized efficiency.

The Alvarez accelerator consists of 7 tanks, each with a pulse power demand of 3 MW (+ 10% reserve) at a frequency of 108 MHz. The same power per unit is required for each of a total of 89 disk-and-washer resonators, operated at 324 MHz. The rf system is already specified for the optional beam pulse length of 1 ms at 100 Hz repetition rate, whereas the power supply allows later upgrading and is specified for a pulse length of 500 μs.

The amplitude and phase tolerances of the rf fields are determined by the requirement to minimize beam loss (see also ch. A 1.2). The tolerance of existing accelerators /1-3/ of typically $\pm$ 1 % in amplitude and $\pm$ 2° in phase is considered insufficient to eliminate an influence on beam loss. Calculations of beam behaviour with multiparticle codes cannot predict losses with the precision required so that assumptions on the required field stability had to be made. An amplitude error of $\pm$ 0.1 % and phase deviations of $\pm$ 0.2° were specified for the SNQ design.

The choice of the operating frequencies (108 and 324 MHz) - as discussed in chapter A 1.2 - was strongly influenced by the aspects of economy and reliability of rf power generation. At 108 MHz, an approved amplifier design (GSI/ Herfurth) is already available. Klystrons operated for the PETRA storage ring at DESY represent the state of the art and were used in this study as a basis for the development of a 324 MHz rf power amplifier.

1.7.2 Radio Frequency Supply at 108 MHz

Tank lengths of the Alvarez accelerator were determined by handling considerations. The Alvarez tanks are 12 m long. 3 MW of rf power are required for each tank. To have a uniform energy flow during the beam pulse, two feeds were provided for each tank, situated at 1/4 and 3/4 of the tank length. By splitting the power, the requirements for the feedthroughs are reduced. Rf windows at high power are still considered as a critical components, still requiring development /4/.

Individual inputs to a common resonator have to be synchronized. This can be accomplished either by symmetrical branching of the feed line or by adequate control of separate amplifiers. Because of problems expected with separate amplifiers in particular during transients, branching of the feeding line was chosen (see ch. A 1.7.4).

1.7.3 The 108 MHz Final Amplifier

Different concepts are feasible for the final stage of a 108 MHz amplifier chain, using different species of tubes:

(1) Several tetrode amplifiers with output power accumulated by a hybrid cascade.

(2) A high power tetrode amplifier.

(3) A single triode amplifier.

Applications of these concepts are compared in table A 1.7-1. The triode amplifier in operation e.g. at LAMPF has sufficient pulse power for the SNQ application, but its major disadvantages are the nonlinear amplitude control behavior, low efficiency and the questionable long-term availability of these special tubes. Tetrodes, presently operated at CERN and at GSI, are designed for broadcast transmitters and are in long-term series production.

Application	CERN-SPS	CERN-SPS	GSI	LAMPF	SNQ
Frequency /MHz	200	200	108	201.25	108
Power /MW	0.5	0.5	1.6	3.0	3.5
d.f. max / %	100	100	25	_ 14	12.5
Tube species	Tetrode	Tetrode	Tetrode	Triode	Tetrode
Number	4 + 1	16 + 1	1	1	2
Concept (see text)	(1)	(1)	(2)	(3)	(2)

Table A 1.7-1: High power tube amplifiers

The advantage of concept (1) using several tetrode amplifiers and cascaded hybrids is a relatively small degradation of output power in case of a tube failure, interruption of operation is therefore avoided. The expense for maintainance and alignment of this system is evident. An amplifier system with a minimum number of tubes should therefore be preferred.

This principle is followed in the concept of the rf supply for the GSI Alvarez accelerator. Since initial problems with the high power tetrode amplifiers are solved by a new design (see B 2.3). These amplifiers, suitable for SNQ, are now available for series production (fig. A 1.7-1). The new GSI final amplifier reliably delivers >1.6 MW of output power at 25 % duty factor.

At the smaller duty factor of the SNQ rf system (6 to 12 %) even a slight increase of output power can be achieved (2 MW). Two such amplifiers are combined by a hybrid to feed one Alvarez tank.

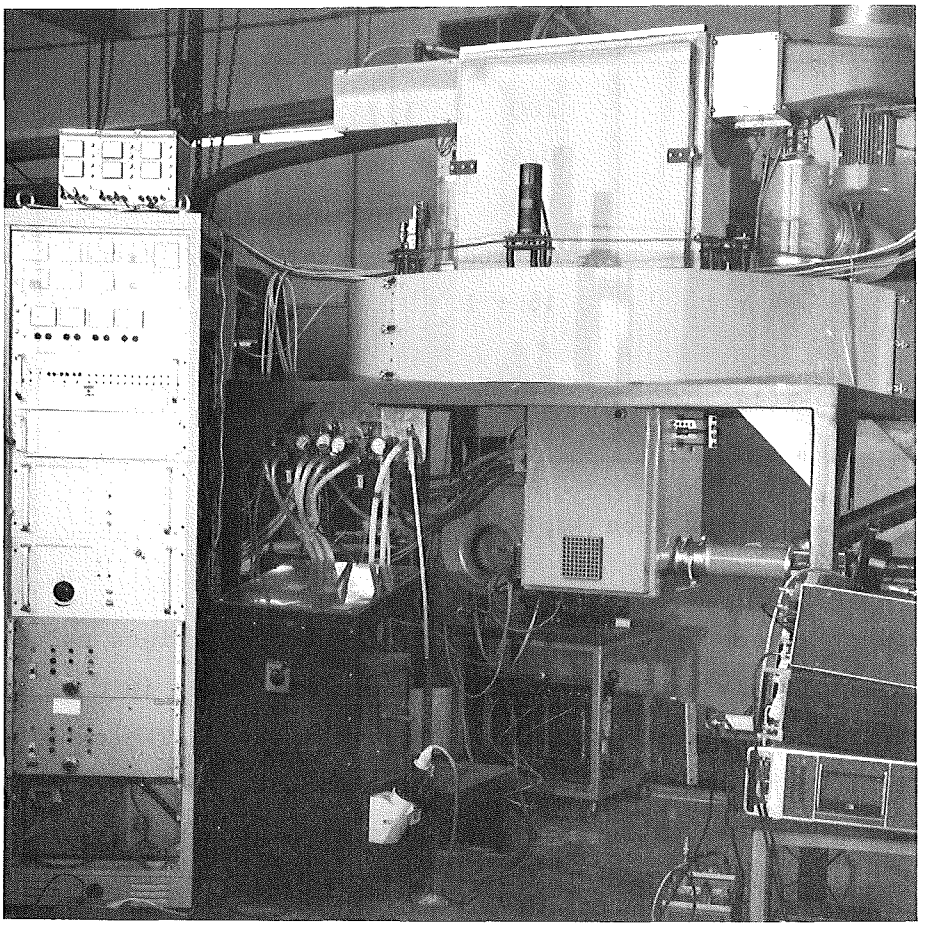

Fig. A 1.7-7: Tetrode final amplifier for 2 MW pulse power at 108 MHz

1.7.4 Hybrid Combination of 108 MHz Final Amplifiers

Because of the extended geometry of high power tetrodes, the assembly of two tubes in a common rf circuit is difficult. In order to avoid problems of synchronization, the output power of the individual amplifiers was combined into a single transmission line by a 90^{o} hybrid, as shown in fig. A 1.7-2. Neglecting circuit losses, the addition of the forward power coming out of both amplifiers appears at the hybrid output toward the resonator, if the amplitudes are equal and the phase relation is 90^{o}. The wave reflected by the

resonator is divided into both input branches of the hybrid. Assuming equal output impedances of the amplifiers, these waves are once more reflected and finally absorbed by the load resistor.

Seen from the resonator, the combined amplifiers appear as a single generator, matched to the impedance of the transmission line. The load mismatch seen by the generators is considerably reduced.
A description of the hybrid functions can be found in the literature, e.g. /32/.

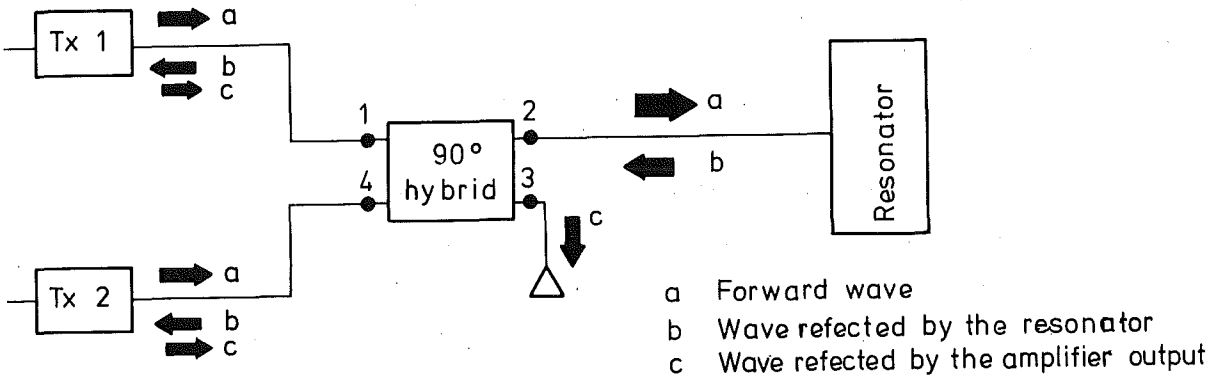

Fig. A 1.7-2: Hybrid combination of 108 MHz final amplifiers

At the input of the final amplifiers, hybrid junctions are feasible, but adequate control of amplitude and phase is difficult at the high levels of drive power involved. In order to allow for electronic symmetrization at low power levels, separate amplifier chains are provided.

1.7.5 Radio Frequency Supply at 324 MHz

A total of 267 MW of pulse power is necessary to feed the 89 sections of the DAW-structure. Additional requirements for the rf amplifiers are a suitable control behaviour, high reliability and high efficiency. These attributes cannot be obtained with tube amplifiers. Gyrocons and Trirotrons promise both high output power and high efficiency, but are still under basic development and can therefore not be considered for the SNQ-design. The most suitable alternative are klystron amplifiers. Extrapolating moderately tne present state of the art, a saturated peak power of 3.7 MW per klystron can be obtained. In order to achieve a high efficiency in the partial-power region, fast and continous control of the electron beam of the klystron is necessary. Both the peak power proposed and the control method require some technological development, which is justified with respect to the number of klystrons required.

Based on the experience of development and construction of the PETRA-klystrons /5/, a long-pulse klystron has been developed by Valvo for this study. This klystron is a first approach towards the SNQ specifications, still limited in its performance by existing production equipment and test facilities. Detailed test results are compiled in /6/. Fig. A 1.7-3 shows the study klystron during the tests. Some essential results are compared to data of other high power klystrons in table A 1.7-2.

By the klystron tests performed, the design parameters could be corroborated. The intrinsic power capability of the klystron could not be verified so far because of limitations of the test equipment. In particular, the cathode voltage supply and the rf power absorber were inadequate for operation at higher power levels.

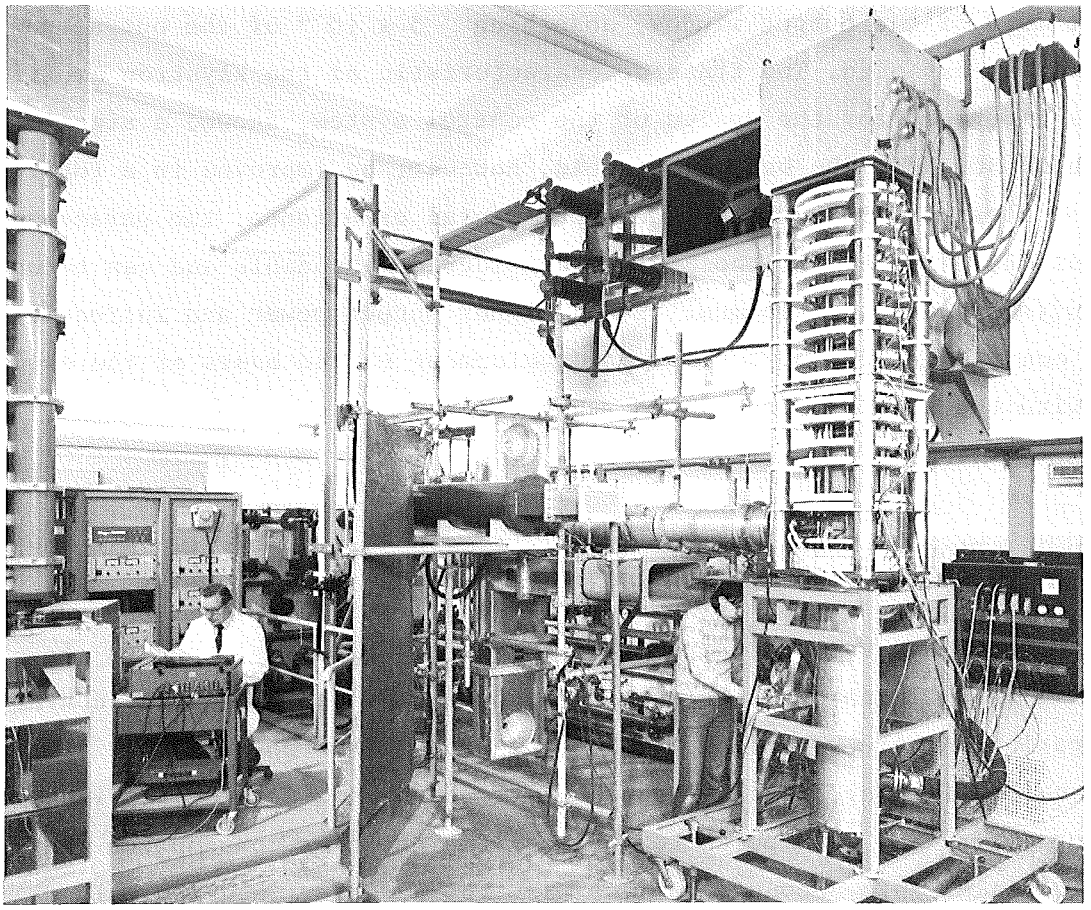

Fig. A 1.7-3: The study klystron assembled for tests

Table A 1.7-2: High power klystrons at low frequencies

Application	DESY/PETRA	SLAC/PEP	LANL/LAMPF	EISCAT	SNQ[2]
Frequency /MHz	500	353	805	225	324
Output Power/MW	0.6	0.5	1.25	5[1)]	0.6
Duty factor /%	100	100	12	≤ 5	30
Efficiency /%	60-65	65	45/55	50	70
Modulation	Anode	-	Anode	Anode	Anode

1) 2 klystrons

2) study klystron V 107 SK

The heat load of the output window, absorbing 5×10^{-4} of the output power, was as low as expected. The transfer characteristic of the klystron amplifier, which is important for the design of the control system, showed a signal bandwith of 300 kHz. The bandwith should, however, be improved in a future prototype klystron. Summarizing the experimental experience, the parameters of the klystrons designed for the SNQ are considered reasonable and can be obtained without major development risks. Higher output power and introduction of grid control are the next steps of development on the basis of the experience gained with the test klystron during this study.

1.7.6 Modulation Methods

Klystron efficiency values reported (60 to 65 % with series products /5,7-9/ and up to 75 % with laboratory samples /10/ describe the internal power conversion at saturation. A more significant information on the rf power supply is the operational efficiency, which relates the rf power fed into the accelerating resonator during the beam pulse to the total mains power consumption. This definition takes into account also the klystron periphery and the pulsed operation.

The traces of the rf pulse signals are shown in fig. A 1.7-4. During the filling process, where the accelerating fields are built up, the klystron is operated in saturation, which shortens this period. During the particle beam pulse, the field amplitude has to be controlled and the klystron must therefore be operated under partial-load conditions.

For optimization of the operational efficiency, the method of amplitude modulation is important.

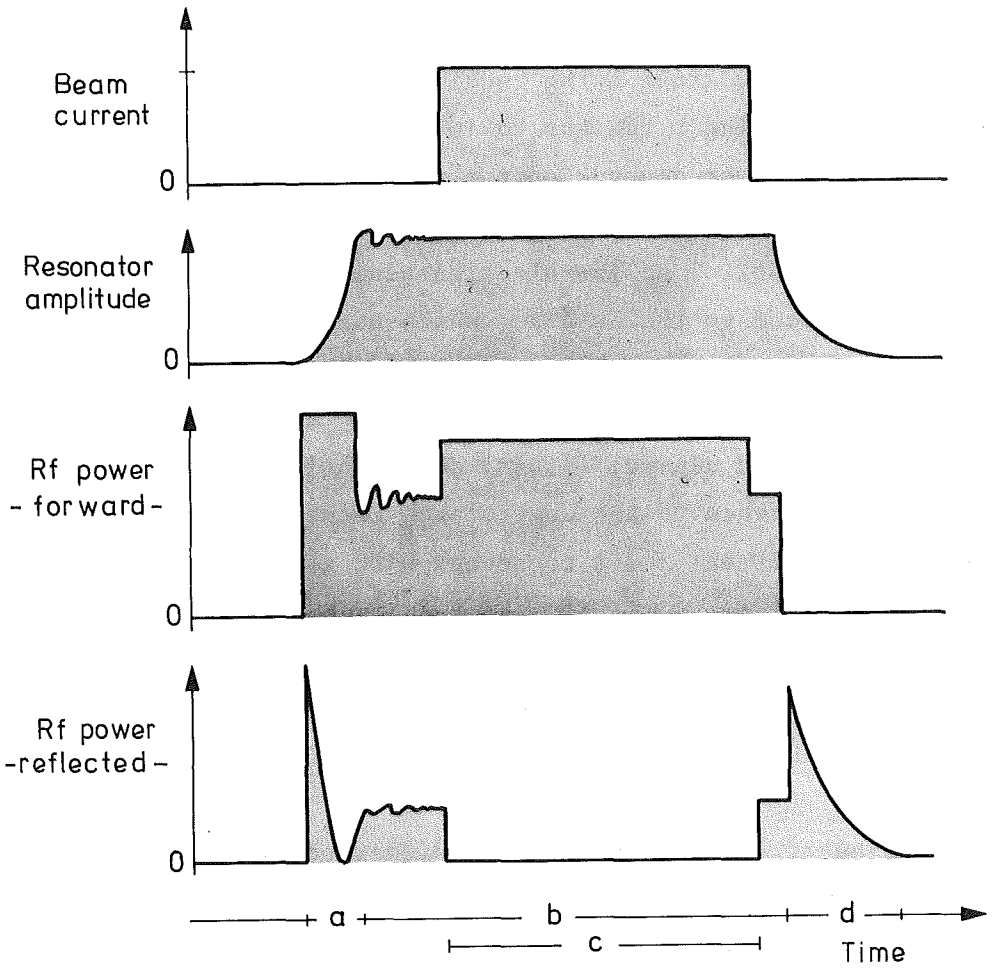

Fig. A 1.7-4: Traces of the rf pulse signals

a - filling process

b - nominal field operation

c - particle beam pulse

d - field decay

Alternative methods of modulation are:

1. Rf input modulation: The dc power input is completely independent from the rf drive level, thus the efficiency decreases considerably below saturation. The speed of the amplitude control is limited only by the rf part of the klystron which acts as a band pass filter. This method of modulation can be applied any type of klystron.

2. Anode modulation: Klystrons commercially available mostly are equiped with a modulation anode which allows for a control of the electron beam current. Because of the high voltage swing required, only slow modulation (up to 1 kHz) or low switching times (up to 10 μs) could be achieved. Since in this case the dc input power depends on the rf output power, the efficiency remains relatively high at reduced output power.
3. Grid modulation: Control of the electron beam current by a control grid close to the cathode, which has a strong influence and consequently a low voltage swing, has not been applied at high power klystrons so far. With a voltage swing of 5 kV and a grid capacity of 100 pF, a fast analogue (5 MHz) and digital (1 μs) control of the beam current can be obtained, in accordance to the control requirements specified. Technological problems and development risks connected with grid modulation are discussed in chapter B 2.2.

4. Cathode voltage modulation: This method involving a hv series modulator was excluded because of high cost and low efficiency.

The control of the rf pulse course can be either obtained with a combination of anode and rf low-level modulation (i.e. anode pulsing and continous control of rf-drive) or with grid modulation. Both methods differ significantly with respect to efficiency (see fig. A 1.7-5). Grid modulation yields an operational efficiency of 52 %, whereas by the combined anode and rf low-level modulation only 45 % are achieved /11/. In addition, anode modulators are expensive and, according to experience at LANL, have to be considered as components of critical life time /1, 12/.

For these reasons, grid modulation was chosen for the SNQ-design. As stated by industry, grid-modulated klystrons and suitable modulators can be developed in time (see ch. B 2.2).

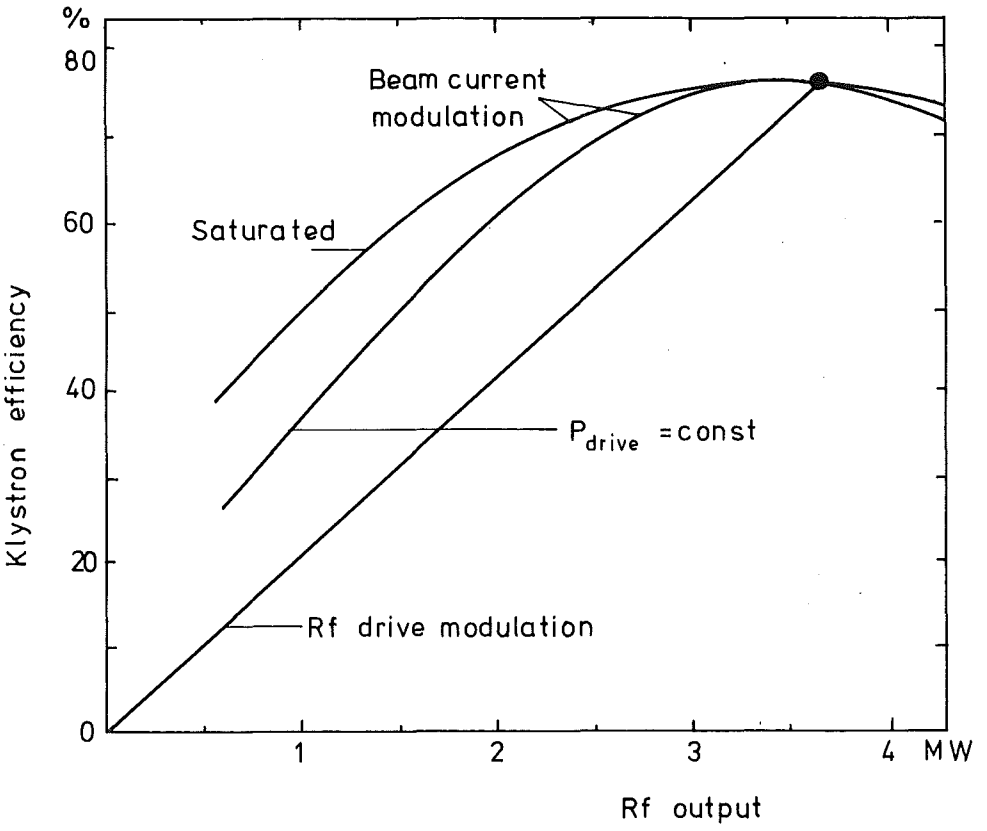

Fig. A 1.7-5: Klystron efficiency for different modulation methods

1.7.7 Load Behaviour

For the klystron, the accelerating structure represents a resonant load counteracting instantaneously any change of amplitude or phase by a heavy mismatch, even if a matched condition exists in stationary operation. Further, the influence of the particle beam must be considered, which represents an complex load. For operation the resonator is tuned to resonance and coupling is watched for the nominal beam current. Whe the beam current is decreased, an increasing mismatch is obtained, as discussed in /13/. The power needed to maintain the field amplitude, is lowered simultaneously. Reflection of the rf power during the pulse is shown in Fig. A 1.7-4. In addition to these regular reflections, statistical events (e.g. rf-arcing in the transmission line or in the resonator) may occur, causing total reflection almost instantaneously.

The reflection during the pulse course may overload the klystron. In particular, overvoltages are hazardous for the output cavity and the rf window. More details on this problem are given in /14, 15/. The following precautions may be considered to prevent damage of components.

A circulator in the transmission line leads the reverse power into an absorber and thus protects the klystron output. Circulators of the phase shifter type are in operation at DESY, e.g. /16, 17/ with positive experience. Disadvantages are, however, considerable cost and space requirements. For the SNQ, the more compact and less expensive type of a junction circulator is feasible /18-20/.

Severe reflections during the filling process can be mitigated by slowing down the procedure. According to /13/, the stationary mismatch of the resonator without beam loading remains tolerable. Protection of the klystron against irregular reflections (i.e. arcing) may be obtained by fast switching of the rf drive. Positive experiences with klystron operated without circulators under comparable circumstances are reported by LANL /1/.

For operation of the SNQ klystrons no circulators are proposed. Development of specific operational procedures and of protecting circuits without a penalty of efficiency is anticipated. Verification of reliable operation has to be shown by prototypes. Space for circulators was considered in the layout of the SNQ-buildings.

1.7.8 The Control System

The stability requirement of $\pm 10^{-3}$ for the amplitude and of $\pm 0.2^{o}$ for the phase of the accelerating voltage in pulsed operation and the necessity to economize the operational costs lead to the following strategy:

1. Optimized filling time of the resonator by separate control of amplitude and phase.

2. Optimized recovery time of the control loops by a small initial error and by predetermining the controller.

3. Optimized control error during the beam pulse by an adaptive forward control, compensating for repetitive disturbances.

The pulse traces of the control signals are shown in fig. A 1.7-6. An ideal rectangular beam pulse was assumed. For the discussion of the layout for the control system, the step function at the beginning of the beam pulse is the most universal test signal, considering the different pulse courses for different tasks (see ch. A 1.6). In the following paragraphs, the control system will be described in detail.

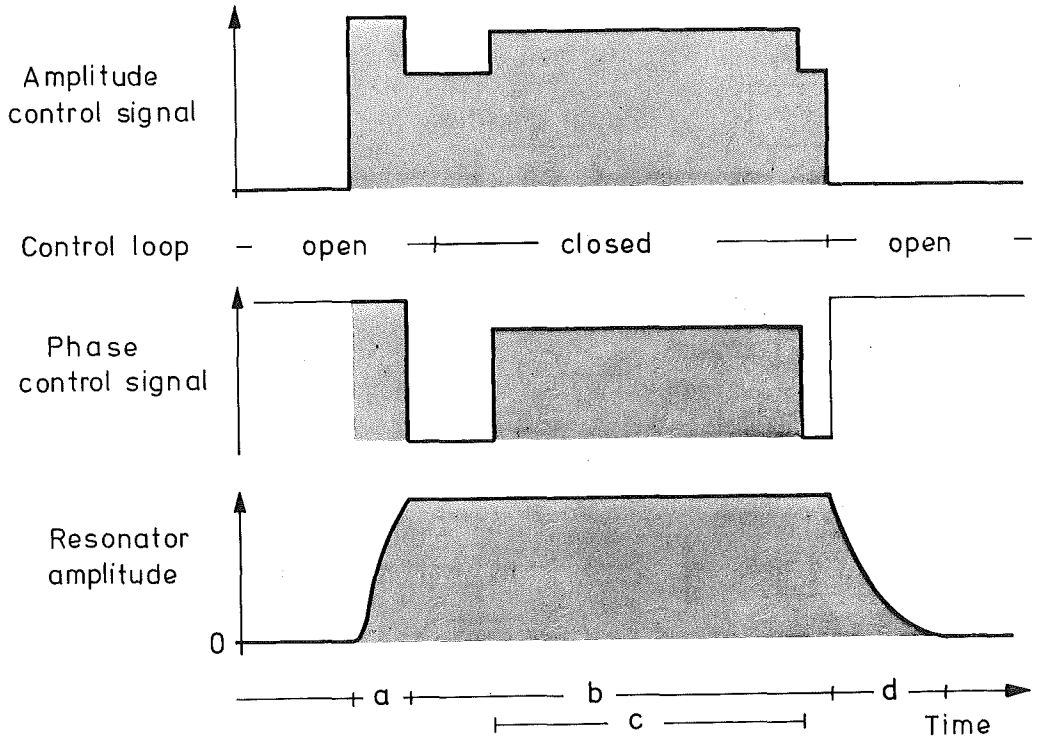

Fig. A 1.7-6: Pulse course of the control signals

a - filling process

b - nominal field operation

c - particle beam pulse

d - field decay

1.7.9 Amplitude and Phase Control System

For the stabilization of the complex accelerating voltage two control loops are required, which have to control either two orthogonal amplitudes or amplitude and phase corresponding to a cartesian or a polar vector representation /21, 22/. Both alternatives are tested and are of equivalent effect Because of grid modulation (amplitude control) of the 324 MHz klystron, which is essential for a high efficiency, the polar method was applied, which, for simplification, was also used for the 108 MHz system. The basic circuit diagram of this control system is shown in fig. A 1.7-7. A rough layout of the controller starts from an analysis of the loop constituents (e.g. rf amplifier, resonator) and leads to a synthesis of the controller based on stability considerations

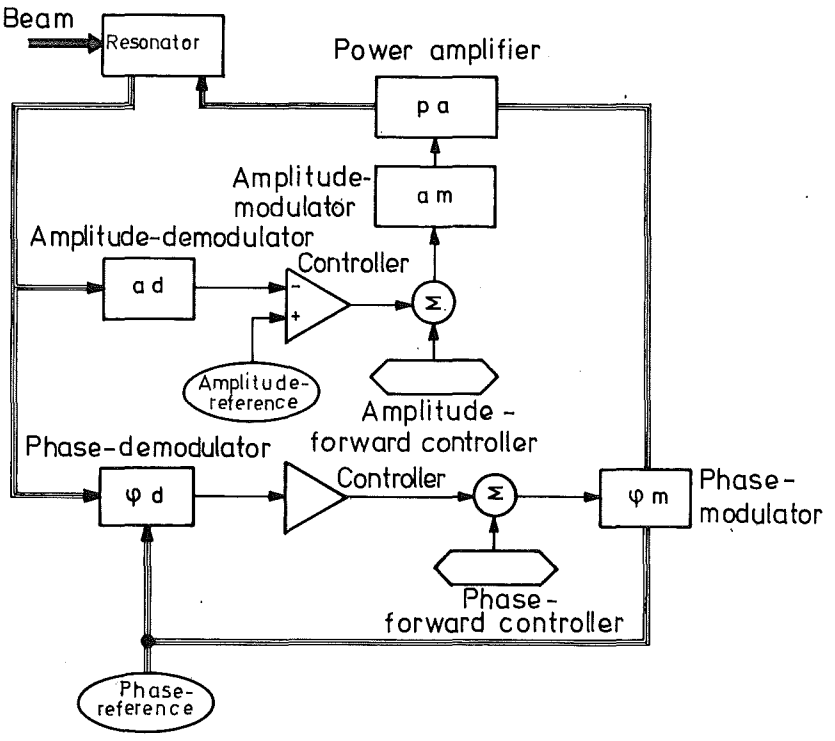

Fig. A 1.7-7: Basic circuit diagram of the control system

In the time domain the resonator is represented by a lag having a cutoff frequency of 10 kHz. The rf transmission and measurement lines form a delay of τ=300 ns. The power amplifiers (klystrons or tetrode amplifiers can be represented by several lags with cut-off frequencies in the 1 to 5 MHz range. With a safety morgin from the stability limit included for the phase, a unity-gain frequency of 200 kHz results. The frequency response of this control loop is shown in fig. A 1.7-8a as a Bode-plot. The limit for a sinusoidal disturbation causing the highest tolerable error ($\pm$ 0.1 % or $\pm$ o.2°) is shown in fig. A 1.7-8b. This frequency dependence is likewise valid for random disturbances (noise of the beam current or amplifier gain fluctuations, e.g.). Because of the equal behaviour of the amplitude and the phase control loops, the following error consideration can be restricted to the amplitude loop.

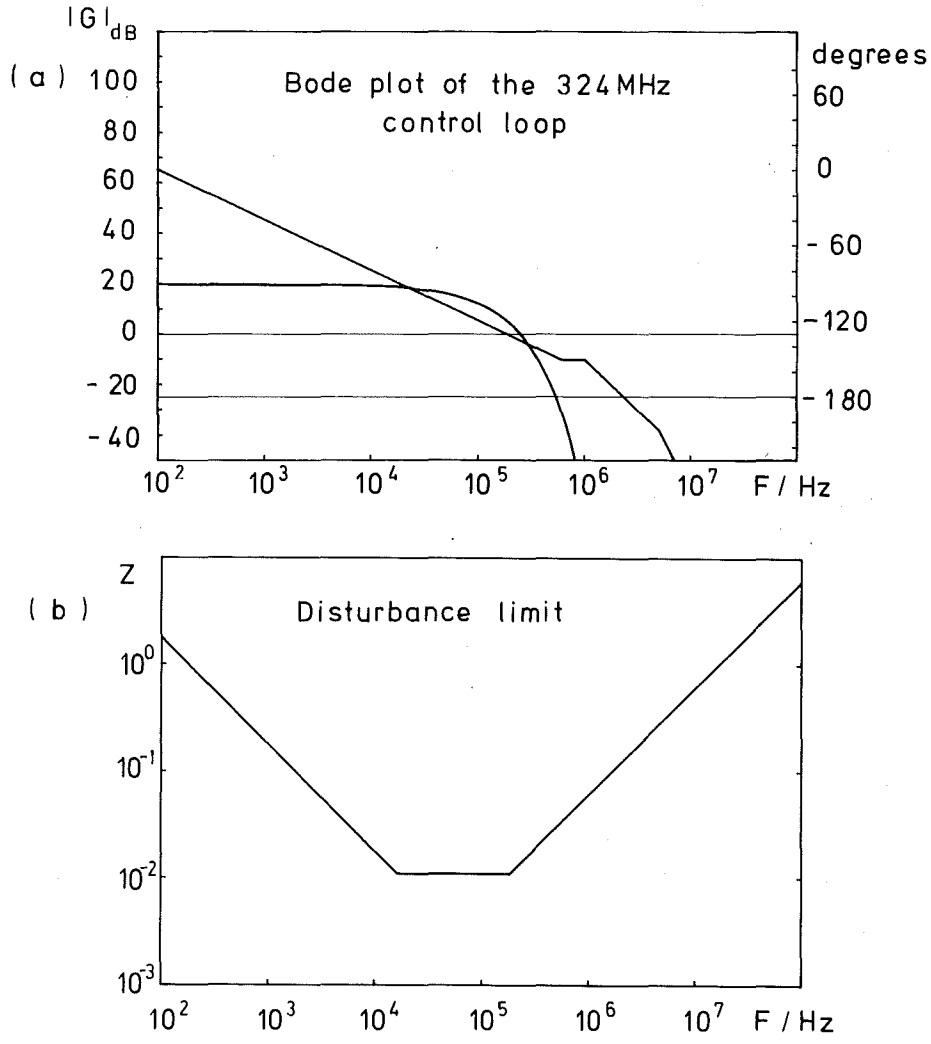

Fig. A 1.7-8: Bode plot (a) and disturbance limit (b)

Between pulses the rf generators are inactive. The control loops are therefore interrupted. However, each beam pulse must be preceded by the filling process for the resonator and by the recovery time for the control system. A short recovery time is achievable by forcing the controller, before switching on, into a state close to the later steady state. An auxiliary loop, which is active between pulses, allows for this function.

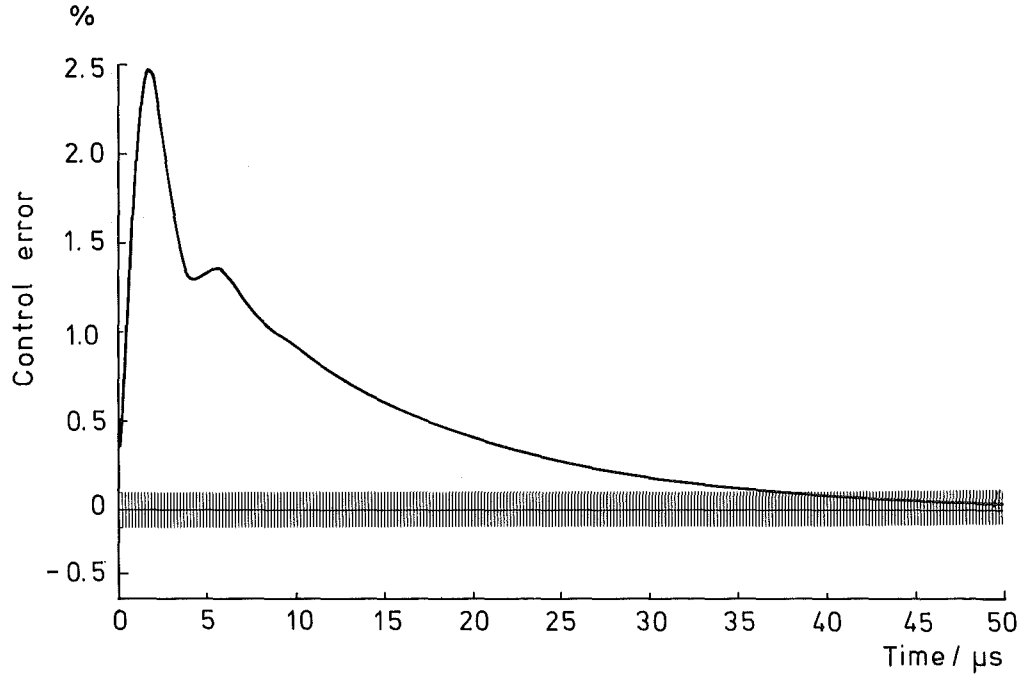

Fig. A 1.7-9: Control error response to the beam pulse (without forward control)

1.7.10 Fast Filling Process

Considerations of the filling process start from the stationary beam loaded resonator, which is matched for optimum utilization of the available generator power. This requires resonant tuning and matching of the coupling for the beam loaded case. Since the beam is a complex load related to the accelerating field by the synchronous phase angle ($\varphi_s \simeq 30^o$),

without beam, the resonator is detuned and overcoupled. In absence of the beam, the excess power of the generator can be used to speed up the filling of the resonator.
An optimized filling speed is obtained at saturation of the generator power. When the nominal amplitude is achieved, the generator has to be switched down instantaneously, as shown in fig. A 1.7-4. As the cavity is still unloaded and therefore detuned, the field amplitude would start to oscillate. This can be completely eliminated by stepping off the generator phase /25/.

Parameters of the rf system may fluctuate, which would cause excessive initial errors for the control system. Automatic setting andrepeated correction by a computer is therefore applied.

Calculations of the filling procedure have shown, that an optimum filling time of 150 μs for the Alvarez- and 50 μs for the DAW-part of the accelerator can be obtained /26/.

1.7.11 Adaptive Forward Control

In general, the response on disturbances can be greatly improved by forward control /27/. Disturbances, which can be measured directly, are used to drive the modulator, thus bypassing the controller. In the system discussed here, a signal is derived from a nearby beam pick-up, conditioned and summed up with the output of the controller at the input of the phase or amplitude modulators. The slower path via the resonator is thus avoided.

The effect of this system, involving a proportional forward control, is demonstrated in fig. A 1.7-10. Without forward control, the amplitude error in response to a step function for the beam transient was reduced by normal control to 2.5 % (fig. a). With the proportional forward control, a further reduction factor of 4 can be gained (fig. b). At the same time, the recovery time is shortened from 40 μs to 4 μs.

As the course of the pulse is known in advance, a preceding forward control may be applied, which realizes a final reduction of the vontrol error to 0.12 %, provided that the lead time is optimized (fig. c). The information required can be derived from the preceding pulse.

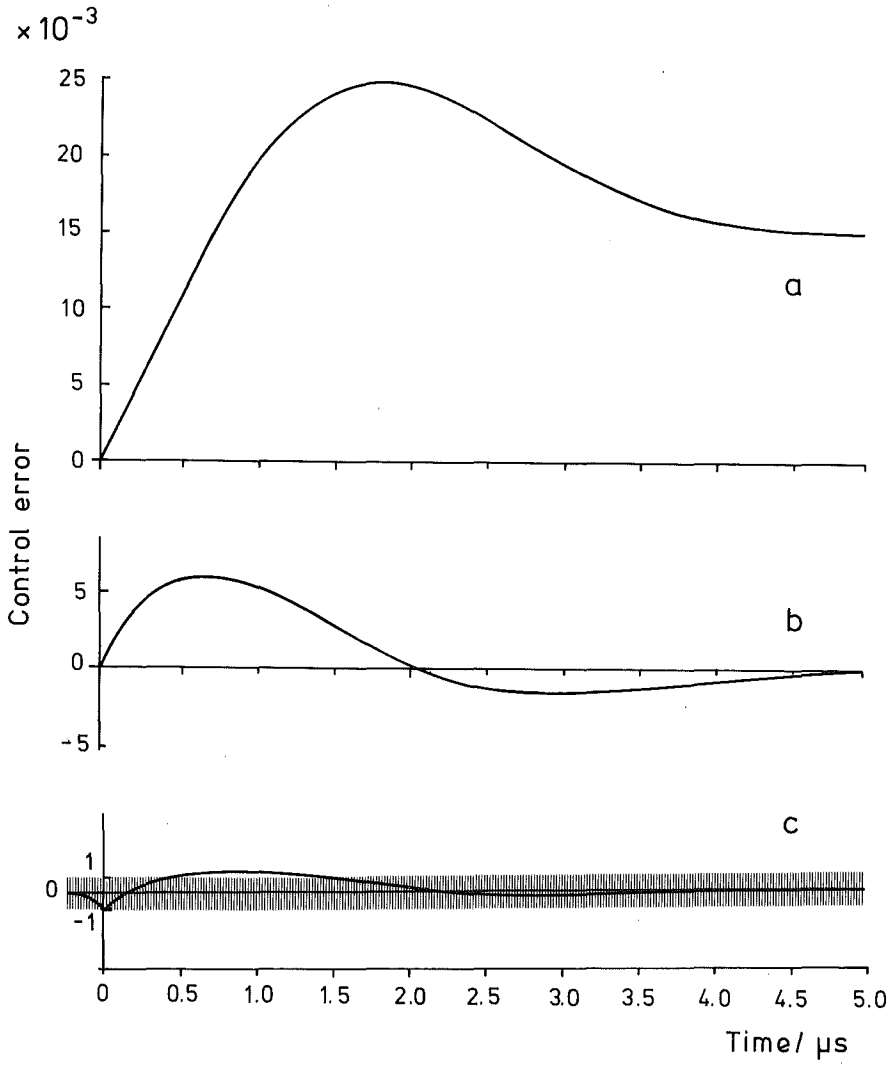

Fig. A 1.7-10: The control error in response to the beam transient a without, b with proportional and c with preceding forward control

Theoretically, by introducing a differentiating element, complete compensation of the beam induced control error could be obtained /28/. The transfer characteristics of the modulator and the rf amplifier could be compensated by this measure. For a step function of the beam current, infinite generator power would, however, be needed. For the system discussed here, an excess power of 10 % over the nominal value is available. Full compensation of beam loading can therefore be only obtained, if the rise time of the beam pulse is longer than 1 µs/29/.

Any repetitivexdisturbances can be suppressed, if the control signal is derived from the control signals of the preceding pulses, rather than from a beam current monitor.

Random disturbances, such as noise of the generator or noise of the beam current can, however, not be cured by the forward control system. They have, on the contrary, to be removed from the stored pulse course by averaging over several pulse cycles. The suppression of noise remains to be done by the normal control loops.

Forward control systems previously applied to linear accelerators /27/ suffered from parameter fluctuations. A small control error could be adjusted at short notice, but fluctuations in long-term operation and in numerous individual systems involved, could not be corrected on-line.

The concept of the forward control for SNQ is based on digital storage of the measured values, correction by computer and, finally, conversion to an analogue control signal (fig. A 1.7-11). The computer correction uses a strategy of error minimization and enables a continous fit to slowly fluctuating system parameters /29/.

The adaptive forward control system automatically compensates for non-linearities in the loop. The polar control system, as proposed here, has from its principle a non-linear response /30/. Non-linearities are also found in modulators and amplifiers of the control loop. Non-linearities are different in the amplitude and phase control loops. Two independent systems must, however, be used for phase and amplitude, but by time multiplexing, several components can be used in common.

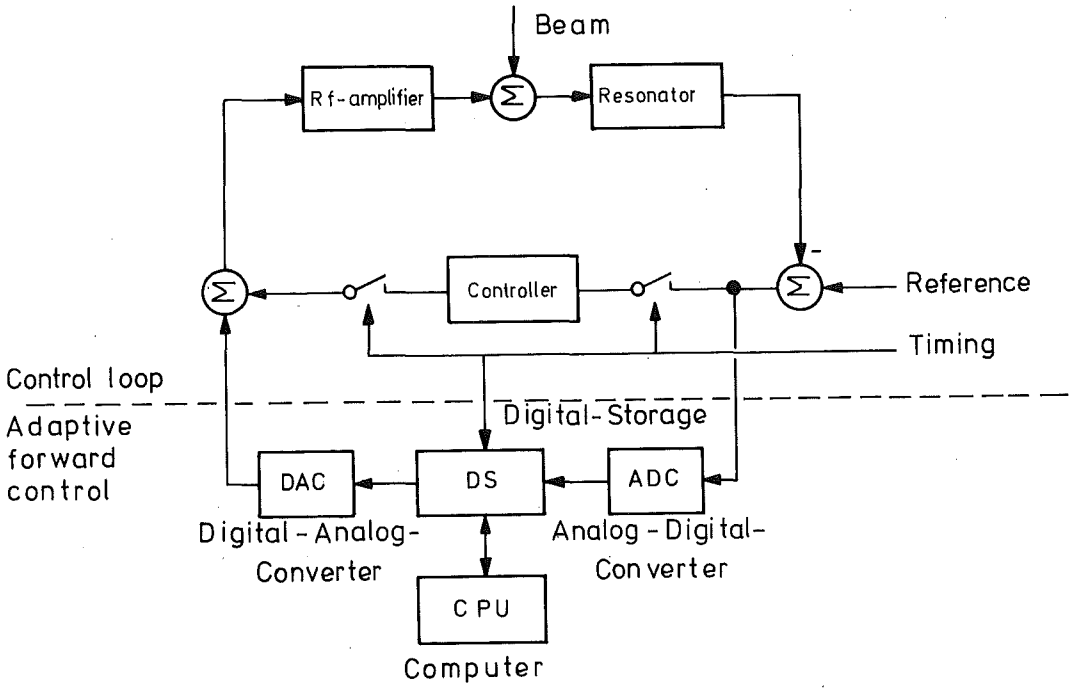

Fig. A 1.7-11: Circuit diagram of the adaptive forward control

The forward control circuit discussed above, can be used in addition to control the filling process (ch.A 1.7.9)

1.7.12 Tank Frequency Control

The resonant frequency of the accelerating tank varies depending on the temperature of the mechanical structure and on the atmospheric pressure by a few bandwidths and in consequence must be corrected by a motor driven tuning piston /31/. A coarse correction is achieved by control in relation to the cooling water temperature and to the atmospheric pressure, whereas, within the bandwidth, a fine correction is done by transmission phase control. The resonant tuning refers to the beam loaded tank but is also achievable with the unloaded tank by a specific phase offset simulating the beam induced detuning.

Contributors: R. Hietschold (KfK), G. Hochschild (KfK),
A. Hornung (University of Karlsruhe), D. Schulze (KfK)

References

/ 1/ D.C. Hagerman: "LAMPF Operations at 500 μA", Proc. 1979 Lin. Acc. Conf., Montauk, NY, Sept. 1979, BNL 51 134

/ 2/ K. Batchelor: "Linear Accelerator Development at Brookhaven National Laboratory", AECL-5677, 1976

/ 3/ J. Cuperus, F. James, W. Pirkl: "The rf-System of the CERN "New Linac", Proc. 1979 Lin. Acc. Conf., Montauk, N.Y., Sept. 1979, BNL 51 134

/ 4/ R. Hietschold: "Koaxiale Hochfrequenzfenster für SNQ", this study, part III A, vol. 1, unpublished

/ 5/ Valvo, data sheet YK 1300

/ 6/ E. Demmel: "Testergebnisse zum SNQ-Studienklystron V 107 SK" this study, part III A, vol. 1, unpublished

/ 7/ G.T. Konrad: "High Efficiency, cw, High Power Klystrons for Storage Ring Applications", IEEE, Trans.Nucl.Sci. NS-22, No. 3, pp. 1249-1252, June 1975

/ 8/ G.T. Konrad: "Performance of a High Efficiency High Power VHF Klystron" IEEE, Trans.Nucl.Sci. NS-24, No. 3, pp. 1689-1691, June 1977

/ 9/ P.J. Tallerico: "Low-Frequency Klystron for Accelerator Applications", IEEE, Trans.Nucl.Sci. NS-24, No. 3, pp. 1692-1694, June 1977

/10/ E.L. Lien: "High-efficiency Klystron Amplifiers", Proceedings MOGA 70 (Kluwer, Deventer, The Netherlands, 1970), pp. 11.21-11.27

/11/ G. Hochschild: "Optimierung des Betriebswirkungsgrades der SNQ-Hf-Versorgung bei 324 MHz", Kernforschungszentrum Karlsruhe, unpublished report

/12/ P.J. Tallerico, R.L. Cady, J.D. Doss: "Design and Performance of the LAMPF 1-1/4 MW Klystron Modulator", 11. Modulator Symposium, New York, Sept. 1973

/13/ G. Hochschild: "Lastbeschreibung eines Hochstrom-Beschleunigungs-resonators", July 1978; this study, part III A, vol. 1, unpublished

/14/ M.J. Lee: "Some Design Considerations of the PEP rf System", Aug. 1977, private communication

/15/ H. Bohlen: "Zum Verhalten eines Klystronverstärkers bei Lastreflexion", this study, part III A, vol. 1, unpublished

/16/ E. Pievit: "Ein Hochleistungszirkulator für das deutsche Elektronen-Synchroton DESY", Internationale Elektronische Rundschau 1971, No. 4, pp. 101-103

/17/ Raytheon: "1.2 MW cw WR 2300 waveguide Circulator for CERN 85 GeV/ 120 GEV Collision Beam Machine", unpublished report

/18/ F. Pötzl: "Hohlleiter-Verzweigungszirkulator für das Kernforschungs-zentrum Karlsruhe", unpublished report

/19/ S. Anami et al.: "High Power Isolator for the KEK Proton Linac", Proc. 1979 Linear Accelerator Conference, Montauk, N.Y., Sept. 1979, BNL 51 134

/20/ Raytheon: "High Power 324 MHz Junction Circulator for a Proton Accelerator", unpublished report

/21/ F.R. Delayen, G.J. Dick, J.E. Mercereau: "A Microprocessor based feedback System for Phase and Amplitude Stabilisation of Super-conducting Resonators", IEEE-NS 24, No. 3, June 1977

/22/ R.A. Jameson: "Analysis of a Proton Linear Accelerator rf-System and Application to rf Phase Control", LA-3372, Los Alamos, N.M., June 1965

/23/ A. Hornung: "Entwurf eines Amplitudenreglers für die 324 MHz-Tanks des SNQ-Beschleunigers", this study, part III A, vol. 1, unpublished

/24/ D. Schulze: "Analyse des SNQ-Hf-Regelungssystems und Simulation des zeitlichen Störverhaltens", this study, part III A, vol. 1, unpublished

/25/ D. Schulze: "Zeitoptimales Anfahren der Hf-Resonatoren für eine Spallationsneutronenquelle", this study, part III A, vol. 1, unpublished

/26/ D. Schulze: "Anfahrzeiten der Disk-and-Washer-Struktur", Kernforschungszentrum Karlsruhe, February 1980, unpublished report

/27/ R.A. Jameson, D.J. Wallace: "Feedforward Control of Accelerator rf Fields", IEEE, Trans.Nucl.Sci. NS-18, No. 3, pp. 598-600, June 1971

/28/ O. Föllinger: "Regelungstechnik", Elitera-Verlag, Berlin, 1972, p. 156

/29/ D. Schulze: "Rechnergestützte adaptive Störaufschaltung für das SNQ-Hf-Regelungssystem", Kernforschungszentrum Karlsruhe, unpublished report

/30/ D. Schulze: "Störaufschaltung in Polar- oder karthesischen Koordinaten", Kernforschungszentrum Karlsruhe, unpublished report

/31/ D. Böhne, M. Emmerling, A. Casper: "Recent Improvements of Accelerator Components at the Unilac", Proc. 1979 Lin. Acc. Conf., Montauk, N.Y., Sept. 1979, BNL 51 134

/32/ H. Brand: Schaltungslehre linearer Mikrowellennetze, S. Hirzel Verlag, Stuttgart 1970

A 1.8 Accelerator Parameters

1.8.1 Basic Parameters of the Linear Accelerator

Particle	Protons (H^-) *
Final energy / MeV	350 / 1100
Total length / m (Including intertank spaces and matching sections)	548
Accelerating structures and rf-frequencies	Alvarez (108 MHz) / Disk-and-Washer (324 MHz)
Peak beam current / mA	100
Time averaged beam current / mA	5 (10)
Max. repetition frequency / Hz	100
Beam pulse duration / μs	500 (1000)*
Mains power / MVA	44.3

* Brackets refer to options

1.8.2 Injection Parameters

Ion Source and Extraction	
Type of ion source	Magnetic multipole ion source
Total ion beam current extracted / mA	250
Pulse duration / μs	700 to 1000
Proton content / %	$\geq$ 60
Normalized 100 % emittance at extraction / π mm mrad	0.2
Extraction voltage / kV	50
Stability of ion current	10^{-2}
Stability of extraction voltage	10^{-2}
Electrostatic Preacceleration	
Type of preaccelerator	Cockcroft Walton
Accelerating voltage / kV	400
Stability of the acc. voltage	$\pm$ 2.5 x 10^{-4}
Max. Proton current / mA	135
Accelerator tube:	
- Aperture diameter / cm	10
- Number of electrodes	4
- Max. field strength / kV cm^{-1}	34
Normalized 100% emittance at the exit of the accelerator tube / π mm mrad	0.5

1.8.3 Beam Dynamics and Beam Properties

	Alvarez-Acc.		Disk-and-Washer-Acc.		
Energy / MeV	0.45	105	105	350	1 100
Av. accelerating field strength / MV m^{-1}	2	2	3.4	3.9	4.2
Transit-time-factor	0.7	0.87	0.89	0.87	0.84
Synchronous phase / °	- 35	- 35	- 30	- 25	- 25
Longitudinal tune (100 mA) / °	28	2.5			
Transverse tune (100 mA) /°	40	40	45	45	30
Transverse tune (0 mA) / °	83	65	55^+	50^+	32^+
Phase width /° (full width)					
- 100 % of the particles	150	18	44^+	30^+	20^+
- 95 % of the particles	74	11			
- rms-value	41	6	15^+	10^+	7^+
Energy spread / MeV (full width)					
- 100 % of the particles	0.12	1.4	1.7^+	2.5^+	3.7^+
- 95 % of the particles	0.10	0.8			
- rms-value	0.05	0.35	0.4^+	0.6^+	1^+
Beam diameter in the quadrupoles / cm					
- 100 % of the particles	1.8	4.0	3^+	3^+	3^+
- 95 % of the particles	1.4	1.5			
- rms-value	0.6	0.7	0.7^+	0.7^+	0.7^+
Aperture diameter / cm	2.8	6.6	7.0	8.0	8.0
Normalized transv. emittance / π mm mrad					
- 100 % of the particles	3	6	6^+	10^+	15^+
- rms-value	0.6	1.2	1.2^+	2^+	3^+

$^+$ estimated from analytical calculations

1.8.4 Parameters of the Alvarez Accelerating Structure

Tank no.	1	2	3	4	5	6	7	total
Injection energy / MeV	0.45	15.7	31.8	47.3	62.4	77.4	91.7	
El. length of tanks / m	11.20	11.48	11.67	11.80	12.16	12.14	11.79	82.24
El. diameter of tanks / m	1.76	1.68	1.60	1.60	1.60	1.60	1.60	
Intertank length / cm		25.0	35.0	42.5	42.5	42.5	42.5	230
No. of cells	39	19	15	13	12	11	10	119
Length of drift tubes / cm								
min.:	7.37	39.29	52.52	59.26	63.92	67.38	69.95	
max.:	32.36	49.02	58.46	63.26	66.85	59.52	71.52	
Diameter of drift tubes / cm	33.8	30.0	30.0	30.0	30.0	30.0	30.0	
Gap / cell length								
min.:	0.28	0.31	0.36	0.45	0.52	0.59	0.65	
max.:	0.52	0.42	0.44	0.51	0.58	0.64	0.69	
Aperture diameter / cm	2.8..4.6	5.6	6.6	6.6	6.6	6.6	6.6	
Accelerating gradient / $MeVm^{-1}$	1.36	1.4	1.33	1.28	1.23	1.18	1.13	
Eff. shunt impedance / $M\,\Omega\,m^{-1}$	25.9	32.0	27.9	25	22.5	20.2	18.2	
Theor. Q-value / 10^3	110	97	97	95	94	93	92	
Cavity loss / MW	1.50	1.30	1.38	1.43	1.52	1.55	1.55	10.23
Beam power / MW	1.53	1.6	1.56	1.51	1.49	1.43	1.34	10.46

1.8.5 Parameters of the DAW Accelerating Structure

Tank geometries

Injection energy / MeV	105.0	167.6	298.5	350.0	487.9	753.9	tot.
No. of tanks	7	13	5	6	11	15	57
Eff. accelerating rate / MeV m^{-1}	2.6	2.8	3.1	3.1	3.0	3.2	
El. tank length / m	3.1..3.6	3.2..3.8	3.4	7.2..7.5+	7.8..8.3+	7.2+	328
El. tank diameter / m	1.35	1.35	1.35	1.35	1.35	1.35	
No. of cells/tank	15	13	11	22	22	18	
Diameter of aperture / cm	7.0	7.0	7.0	8.0	8.0	8.0	
Cavity loss / MW	2.05	1.97	1.85	3.64+	3.6+	3.5+	
Increase of beam power/MW	0.81	0.92	1.07	2.24	2.34	2.2	
Intertank length / m	1.3	1.3	1.3	1.3	1.3	1.3	72.8

+ Tanks consist of two resonators, separately fed with rf from 350 MeV on.

1.8.6 Cell Parameters of the DAW Structure

Energy / MeV	109	117	325	376	533	901
Rel. Proton velocity v/c	0.44	0.54	0.67	0.70	0.77	0.86
Gap / cell length	0.300	0.353	0.425	0.461	0.499	0.535
Tank diameter / cm	134.8	134.8	134.8	134.8	134.8	134.8
Diameters of aperture / cm	7.0	7.0	7.0	8.0	8.0	8.0
Diameters of disks / cm	96.22	99.04	103.28	104.3	106.9	110.6
Diameters of washers / cm	90.12	87.72	85.00	84.4	82.6	79.66
Thickness of disks / cm	3.95	6.12	9.94	10.75	13.2	16.42
Thickness of washers / cm	3.0	3.0	3.0	3.0	3.0	3.0
Cell length / cm	20.58	24.98	31.00	32.4	35.62	39.8
Eff. shunt impedance / M Ω m^{-1}	22.9	29	35.9	35.2	38.25	41.8
Transit-time-factor	0.89	0.89	0.88	0.86	0.85	0.84
Q-value / 10^3	40	54	68.7	72.5	82	95
Peak to acc. field ratio Ep/Eo	5.38	5.07	4.76	4.2	4.38	4.29

1.8.7 Focusing Parameters of the rf-Linac

Focusing elements	Electromagnetic quadrupoles				
Supplies	100 % duty cycle				
Field stability	10^{-3}				
	Alvarez-accelerator		DAW-accelerator		
Configuration	singulets		dublets		
Periodicity	F-Hf-D		FD-Hf		
Energy / MeV	0.45	105	105	350	1 100
Length of foc. element / cm	5	38	40	50	60
Diameter of aperture / cm	3.2	7.0	8.0	9.0	9.0
Gradient / TM^{-1}	47	4.0	23^{+}	17.8^{+}	15.6^{+}
Pole Tip field strength / T	0.8	0.1	0.9^{+}	0.8^{+}	0.7^{+}

$^{+}$ estimated from analytical calculations

1.8.8 Parameters of the rf-System

Stability of acc. field amplitude	± 0.1 %	
~ Phase	± 0.2 °	
Total peak power / MW	288	
Mains power / MVA	34 (54)	
	Alvarez-accelerator	Disk-and-Washer-accelerator
Frequency / MHz	108	324
No. of power amplifiers	2 x 7	89
Peak power at amplifier exit / MW	2 x 1.8	3.5
Total rf power, time av. / MW	1.62	16.9
Operational efficiency+) / %	39 (46)	52 (60)
No. of power feeds per resonator	2	1
Type of power amplifier	Tetrode	Klystron
Type of tube	8973 (Eimac)	V116SK (Valvo)
Amplitude modulation, type	via rf control	grid
Max. filling time / µs +)	150	50
Max. rise time / µs +)	100	50
Max. start-up time for operation / min.	20	20

+) for definition see ch. A 1.7